UNIVERSIDAD CARLOS III DE MADRID

DOCTORAL THESIS

Sliding Mode Control in Grid-Connected Wind Farms for Stability Enhancement

Author:
Diana Marcela Flórez Rodríguez

Supervisors:
Hortensia Amarís Duarte Universidad Carlos III de Madrid
Enrique Acha Tampere University of Technology

DEPARTMENT OF ELECTRICAL ENGINEERING

Leganés, 2012

TESIS DOCTORAL

SLIDING MODE CONTROL IN GRID-CONNECTED WIND FARMS FOR STABILITY ENHANCEMENT

Autora: Diana Marcela Flórez Rodríguez

Directores: Hortensia Amarís Duarte, Universidad Carlos III de Madrid

Enrique Acha , Tampere University of Technology

Firma del Tribunal Calificador:

Firma

Presidente:

Vocal:

Vocal:

Vocal:

Secretario:

Calificación:

Leganés, de de

Abstract

Aiming at reducing the rather high percentage of CO2 emissions attributed to the electrical energy production industry, a new generation of power plants has been introduced which produce electricity by using primary energy resources which are said to be renewable, such as wind, solar, geothermal and biomass. This has had not only the benefit of reducing CO2 emissions into the atmosphere to a trickle, by the new power plants but to also encourage a great deal of technological advance in both the manufacturing sector and in research institutions. Wind power is arguably the most advanced form of renewable energy generation today, from the bulk energy production and economic vantages.

This doctoral thesis rigorously deals with the analysis, assessment and description of the impact of double-fed variable speed wind turbine on the dynamic behaviour of both, the wind farm itself and its interconnection with the conventional power generation system.

Analytical analysis of the results published in the open literature is used as a tool to gain a solid understanding of the dynamic behaviour of power systems with wind generation.

The influence of the characteristics of the electrical system and wind turbines or external parameters on stability is assessed using modal analysis. Studies conducted have focused on the analysis of transient stability and small signal stability for the damping of oscillations in power systems and its enhancement. Analysis of small signal stability

and transient stability analysis are carried out using modal analysis and dynamic simulations in the time domain.

This thesis proposes the implementation of sliding mode control techniques for the DFIG WT converters, both the Machine-Side Converter (MSC) and the Grid-Side Converter (GSC). The proposed control system is assessed on conventional dynamic power systems with wind power generation under different test case scenarios.

The newly developed SMC control scheme demonstrates the importance of employing non-linear control algorithms since they yield good operational performances and network support. This is of the utmost important since in power systems with wind power generation is critically important to ensure the robust operation of the whole system with no interaction of controllers.

Sliding Mode Control shows to be more robust and flexible than the classical controller, opening the door for a more widespread future participation of DFIG-WECS in the damping of power system oscillations.

Resumen

Con el objetivo de reducir el elevado porcentaje de las emisiones de CO2 atribuidas al sector de la generación de energía eléctrica, se ha introducido una nueva generación de centrales eléctricas cuya fuente primaria de energía es de naturaleza renovable como las eólicas, solares, geotérmicas y de biomasa. Esto no sólo beneficia la reducción de las emisiones de CO2 a la atmósfera sino que también estimula e impulsa el avance tecnológico, tanto en el sector manufacturero como en los centros de investigación. En la actualidad la energía eólica es probablemente la fuente de energía renovable más avanzada, desde la producción de energía hasta las ventajas económicas.

La presente Tesis Doctoral se ha centrado en analizar, evaluar y describir rigurosamente el impacto de los aerogeneradores de velocidad variable doblemente alimentados en el comportamiento dinámico tanto del propio sistema eólico como de su interconexión con el sistema síncrono convencional de generación de energía eléctrica.

El análisis analítico de los resultados publicados en la literatura es utilizado como herramienta para una mejor comprensión del comportamiento dinámico de los sistemas de potencia con generación eólica.

La influencia de las características del sistema eléctrico y de los aerogeneradores o parámetros externos sobre la estabilidad es evaluada empleando análisis modal. Los estudios realizados se han enfocado en el análisis de estabilidad transitoria y de pequeña señal para la evaluación de la amortiguación de oscilaciones en las redes eléctricas de

potencia. Análisis de estabilidad de pequeña señal y análisis de estabilidad transitoria son llevados a cabo usando análisis modal y simulaciones dinámicas en el dominio del tiempo.

En esta tesis se propone la aplicación de técnicas de control en modo deslizante en los convertidores de los aerogeneradores doblemente alimentados, tanto en el convertidor de la máquina como en el convertidor de la red. El sistema de control propuesto es evaluado en redes dinámicas de generación convencional con generación eólica, considerando diferentes escenarios.

El recientemente sistema de control CMD desarrollado demuestra la importancia de implementar algoritmos de control no lineales, ya que producen un buen rendimiento y dan soporte a la red. Esto es sumamente importante ya que en los sistemas de potencia con generación de energía eólica es vital asegurar el funcionamiento eficiente de todo el sistema sin interacción de los controladores.

El Control en modo deslizante demuestra ser más robusto y flexible que el controlador clásico, abriendo la puerta a un futuro con una mayor participación de generación eólica en la amortiguación de las oscilaciones de potencia.

Agradecimientos

Esta tesis doctoral, aunque resultado del esfuerzo, sacrificio y dedicación personal, no hubiera sido posible sin la confianza, ayuda, tiempo y motivación de personas e instituciones involucradas durante todo su desarrollo y a quienes es preciso decir: "Gracias".

En primer lugar, sin duda, mi más profundo y sincero agradecimiento a la Dra. Hortensia Amarís y al Dr. Enrique Acha, con quienes no habría podido trabajar más a gusto y quienes se convirtieron en más que mis tutores académicos. Ha sido un gran honor realizar este trabajo bajo su dirección.

Hortensia, gracias por haber confiado en mí desde el primer momento y haber continuado guiándome en mi formación como investigadora. He aprendido tanto de ti que sería demasiado pretensioso intentar enumerarlo, me has apoyado incondicionalmente y has adoptado sin reserva el papel de amiga, confidente e incluso de madre. Gracias por tu tiempo, entrega, dedicación y paciencia.

Profesor Acha, ha sido una gran bendición trabajar contigo, por tu excelente prestigio y experiencia y por tu gran corazón. Gracias por tu buena disposición, generosidad, por tus oportunas indicaciones, por todo el tiempo que has dedicado a este trabajo, por las revisiones y apoyo constante. Gracias por haber hecho realidad mis estancias de investigación en Escocia y en Finlandia y contribuir a que fuesen tan agradables, productivas e inolvidables.

Agradezco de manera muy especial a dos prestigiosas instituciones en Escocia y Finlandia: *University of Glasgow - Department of Electronics and Electrical Engineering* y *Tampere University of Technology - Department of Electrical Energy Engineering* por permitirme realizar mis estancias de investigación. En Glasgow: A Mr Douglas Irons, por facilitarme el uso de los recursos de la universidad, a Julie Mitchell, Glenn Moffat, Nagisa Okada por toda la ayuda y paciencia con mi inglés y por hacer más especiales los días en Escocia. En Tampere, al director de departamento Dr. Seppo Valkealahti por su amabilidad, colaboración y total disposición, a Terhi, Merja y Mirva, por su amabilidad, voluntad e interés para ayudarme con toda las formalidades y facilitarme el uso de las instalaciones de la universidad.

A todos y cada uno de mis compañeros del Departamento de Ingeniería Eléctrica de la Universidad Carlos III de Madrid, gracias por todos los buenos momentos y por todas las enseñanzas.

Julio Usaola, gracias por tu confianza y las acertadas recomendaciones, Javier Sanz, Juan Carlos Burgos, Jorge Martinez, gracias por las entretenidas conversaciones y el buen sentido del humor con que siempre me han contagiado, Guillermo, gracias por tu apoyo, tu cordialidad y siempre buena disposición. Eva, por tu eficiencia en todas las gestiones y por tu invaluable ayuda, siempre dispuesta con una gran sonrisa.

Un especial agradecimiento a quienes se convirtieron en más que mis compañeros de trabajo: Johann, por tu disposición desde antes de mi llegada a España; te convertiste en mi mejor amigo y posibilitaste grandiosas oportunidades, nunca podré retribuir tanto cariño, preocupación y apoyo, Yimy, Quino, por toda la ayuda desde mi llegada a la universidad, Luchía, amiga, gracias por darme un espacio en tu corazón, has sido mi soporte en muchos momentos difíciles, gracias por permitirme compartir tantas cosas contigo, que increíbles momentos hemos vivido, gracias también a tu hermano Antonio por haber sido

cómplice en tantos momentos, Mónica Alonso gracias por tu apoyo incondicional, confianza, ayuda y cariño, Carlos Álvarez, por tu asombrosa cordialidad y buena voluntad.

A mis amigos de Sta. Bea, por su paciencia, comprensión, ayuda, ánimo, cariño y alegría: un millón de gracias. Ahora tengo una gran familia.

A mi madre, por condescender siempre a la locura de mis sueños y luchar por contribuir a su realización, gracias por todos los sacrificios. A Chuchín y a Nico por toda la ayuda y siempre buena voluntad en Madrid.

A toda mi familia en Colombia, en especial a mi hermana Ángela, gracias por todo el ánimo, apoyo y compañía a pesar de la distancia, a mis niños, Samuel y Juanfe, cómo pagar tantos momentos de compañía, tantas sonrisas, abrazos y besos "virtuales", gracias por ser parte de mi motivación y alegría, a mi Abue, gracias por todas las oraciones y preocupaciones, a Sigi, gracias por todo el apoyo y por creer en mi.

Gracias a todos mis amigos en Colombia por entender mi ausencia y encomendarme en sus oraciones.

Gracias Señor por darme la gracia de terminar este trabajo y por bendecirme todos los días a través de tantas personas y oportunidades maravillosas.

Muchas gracias a todos!!
Thank you very much!!
Kiitos paljon!!

Contents

List of Figures

List of Tables

Nomenclature

	Variable	Unit
A	rotor swept area	m^2
B	susceptance	
c	damping coefficient	pu . s/el.rad
C_p	performance coefficient	
e , $\underline{e}$	induced voltage, e.m.f	V, pu
f	frequency; generic function	Hz $= 1/s$
G	conductance	
g	generic function	
H	inertia constant	s
i	current	A, pu
k	shaft stiffness	pu/el.rad
K	proportional gain	
L	inductance	H, pu
n_{gb}	gearbox ratio	
n_{pp}	generator pole pairs number	
P	active power, mechanic power	W, pu
Q	reactive power	VA, pu
R	resistance	Ω,pu
s	slip	pu
T	time constant	s
v, $\underline{v}$	voltage	V, pu

v_w	wind speed	m/s
Y	admittance matrix	
β	pitch angle	rad
λ	tip speed ratio; eigenvalue	
ψ	flux linkage	Wb, pu
ρ_{air}	mass density of air	
ρ	angle of space vector	rad
σ	leakage factor	
τ	torque	N.m, pu
θ_{tw}	shaft twist angle (mechanical)	rad
ω	angular frequency , angular velocity	rad/s, pu

Subscripts

d	d-axis
dc	direct current
$eleB$	electrical base
f	filter
g	generator
GSC	grid-side converter
l	leakage
mB	mechanical base
o	mutual
q	q-axis
R	rotor
Ref	reference
sh	shaft
S	stator
t	turbine
$\_$	vector

Abbreviations

dc	Direct Current
DFIG	Double Fed Induction Generator
FACTS	Flexible Alternating Current Transmission System
FRC	Fully Rated Converter
FSWT	Fixed Speed Wind Turbines
G	Generator
GSC	Grid-Side Converter
MIMO	Multiple Input Multiple Output
PCC	Point of Common Coupling
PWM	Pulse Width Modulation
SCIG	Squirrel Cage Induction Generator
SG	Synchronous Generator
VSC	Voltage Source Converter System
WECS	Wind Energy Converter System
WT	Wind Turbine

Chapter 1

Introduction

Electrical energy demand continuous to grow unabated fuelled by rapid technological change and economic development. However, the increases in energy consumption have been met, to a larger extent, by building new power plants of the conventional kind, particularly those that burn fossil fuels. This has resolved the pressing issue of electrical energy demand but has led to excessive and dangerous levels of carbon (CO2) emissions into the atmosphere. Recent estimates of CO2 emissions put the contribution of the electrical energy production industry at more than 40% of the total global. This is followed by 22% contribution of the transport sector and 20% of the manufacturing sector.

Aiming at reducing the rather high percentage of CO2 emissions attributed to the electrical energy production industry, a new generation of power plants has been introduced which produce electricity by using primary energy resources which are said to be renewable, such as wind, solar, geothermal and biomass. This has had not only the benefit of reducing CO2 emissions into the atmosphere to a trickle, by the new power plants but to also encourage a great deal of technological advance in both the manufacturing sector and in research institutions.

Wind power is arguably the most advanced form of renewable energy generation today, from the bulk energy production and economic

vantages. It is fair to say that the central status that the wind power generation has reached within the global electricity supply industry has been the result of far-sighted public energy policies pursued by individual governments and international organizations, where economic incentives figure prominently. For instance, in the United States of America, Production Tax Credits (PTC) or Investment Tax Credits (ITC) were introduced to promote the development of new technologies in the renewable energy sector and to bring down the competitive barrier with respect to the conventional forms of electricity generation [1]. In contrast, wind energy projects in Europe have been supported mainly from the profits side by feed-in premium and fee-in tariffs (FIT) which are over electricity market prices [2]. The past decade has witnessed rather impressive developments in wind power technology, particularly in Europe, where the individual wind turbines have grown in size and the number of wind power installations has multiplied rapidly. However, as reported in [3], in developing countries and emerging economies, more wind power capacity was installed in 2010 for the first time.

1.1 Motivation

There is a general agreement that the increasing penetration of wind power will impact quite significantly power system operation and system stability [4, 5]. The dynamic behaviour of power systems with large wind energy plants require careful examination and a full system characterization in order to evaluate the operating parameters of the system, operating regions and control strategies to follow. Likewise, it is essential to identify both benefits and drawbacks relating to location, the technologies employed and power penetration levels as well as to consider the new requirements regarding the integration of wind power into the power system.

This research project explores one key aspect relating to stability threats concerning the impact of increasing wind power penetrations,

more specifically, it researches on the damping of electromechanical oscillations.

The double fed induction generator (DFIG) is today one of the most popular schemes for variable-speed wind turbines which has been introduced to replace the fixed-speed, squirrel-cage induction generators. This variable speed technology offers advantages such as four quadrant power capabilities, maximum aerodynamic efficiency, reduced mechanical stress and a relatively small converter size.

The DFIG control capabilities have been researched quite amply by other researchers and it has been shown that wind power can increase the damping of inter-area oscillations and that advanced controls may be used to enhance even further their damping performance.

Technological advances have lead to the development of more efficient strategies based on advanced and modern control techniques such as Fuzzy Logic Control, Robust Control, Adaptive Control and Sliding Mode Control (SMC). Among all these control techniques, SMC emerges as a particularly suitable option to deal with electronically controlled variable speed operating WECS, owing to its potential to eliminate the undesirable effects of parameter variations with minimum complexity of implementation [6], [7].

To push further the boundaries of power system stability investigations with particular reference of multi-machine systems with significant content of WECS, the research reported in this thesis looks at applying a robust and flexible solution to the control capabilities of the double fed wind generators that yields an improvement to the stability of power systems with a high penetration of DFIGs. The solution put forward is based on the SMC method and the analysis is geared towards the assessment of network oscillations damping.

1.2 Objectives and approach of the thesis

This thesis aims to study the dynamic performance of grid connected wind energy conversion systems (WECS) with double-fed induction generators (DFIG) and its impact on power system stability. The focus is on evaluating the stability of the DFIG control system itself and on assessing the stability of the system to which it is connected, for different wind power penetration levels using both, small-signal and time domain based analyse. These studies complement each other rather well and they are widely accepted amongst the power systems engineering community [8] to be an entirely suitable approach to evaluate power system oscillations.

A single-machine infinite bus system is assessed with the sole aim of investigating local modes in a rather exhaustive manner. It is argue that this kind of system is the best test bed available to study such modes in a robust manner, without the interference of external noise. A multi-machine framework is developed to lend further credence to the above assertion but more importance to study inter-area oscillations. The developed multi-machine frame work enables de investigations of combined power systems with conventional synchronous generation systems and DFIG-based wind turbines controlled by two different approaches: one of them is the most widely employed classical control technique which is based on Field Oriented Control (FOC); the second one is a new control method based on non-linear Sliding Mode Control. In this research work the role of FOC is to form a basis for comparison for the results obtained with SMC.

It should be brought to attention that the non-linear SMC technique has been applied in variable-speed WECS but that it has been applied to the mechanical circuits as opposed to the electrical ones, i.e., the focuses has been on mechanical power maximization and pitch control. Research work on SMC applied to the electrical control of

WECS is very limited, for instance, no modal analysis has not been reported.

In this thesis SMC is applied to the machine side converter to control the supplied rotor voltage and to the grid side converter to control the reactive power generated by the wind turbine. The common objective is to ameliorate electromechanical oscillations.

The specific objectives of the research can be outlined as follows.

- To assess the dynamic performance of a DFIG when connected to a very strong equivalent grid.
- To assess the dynamic performance of a power system when synchronous conventional generators are replaced by DFIG-based wind farms.
- To analyse the correlation between the damping of electromechanical oscillations, the DFIG-based wind turbine control systems and wind power penetration levels.
- To put forward a control strategy to improve on the damping of electromechanical oscillations of combined power systems with wind power generation.

1.3 Contributions

- A critical assessment of parameters variation of a DFIG-based wind turbine led to the identification of the critical variables that affect most the frequency and damping of the dominant oscillation modes.
- A non-linear control strategy based on sliding mode control has been put forward. The dynamic performance of the DFIG-based wind turbine with such a controller is evaluated under a wide range of operation conditions.

- A better understanding of the dynamic performance of the DFIG-based wind turbine has been achieved by implementation of the proposed controller and its comparison with a classical control implementation based on the decoupled field oriented control using dq components.

- The development of an analytical tool for eigenvalue analysis of a grid connected DFIG, suitable for both, an equivalent grid and a multi-machine power system.

- A comparative analysis of the dynamic behaviour of DFIG-based wind turbines is performed. To this end, small signal stability and transient stability analyse are carried out for different wind power scenarios drawing special attention to the phenomena of power oscillations.

- A critical assessment of the impact of wind integration into the power grid, is carried out with emphasis on the nature of power oscillations of electrical systems. This is carried out by replacing conventional synchronous generation with wind generation of the DFIG type,employing different network topologies and, in each case, starting from its power flow solution.

1.4 Thesis organization

The thesis is organized in seven chapters. Chapter 1 is the introductory chapter where a background to the research study is presented. It includes a succinct review of wind power together with the objectives, motivation and contributions of this research.

Chapter 2 presents a review of power system stability concepts and provides current definitions of transient stability and small signal stability. The chapter further reviews the state-of-the-art in wind power engineering, with particular regard to power system stability and the

analysis mechanisms used to assess the effect of DFIG-based wind farms on the electrical network.

Chapter 3 presents models of variable-speed wind turbines with DFIG systems and the non-linear sliding mode control put forward in this research as applied to the DFIG.

Chapter 4 analyse the dynamic behaviour of the DFIG-based wind turbine with the proposed control system by drawing comparisons with a conventional controller based on the modal analysis approach. Computer simulation results are presented to show the effectiveness of the proposed controller.

Chapter 5 assesses the impact of wind generation and the DFIG control system on the dynamic characteristics of different power network topologies. The assessment is geared towards small-signal stability analysis.

Chapter 6 addresses the transient performance of the DFIG-based wind turbines relaying on simulations results to assess the impact of reactive power control under increasing wind penetration levels and subjected to grid disturbances.

Chapter 7 bring the thesis to a close stating the overall conclusions and key findings of the research work carried, as well as directions and recommendations for further research work.

Chapter 2

Power System Stability Concepts

The present chapter includes a review of general concepts relating to power system stability in order to contextualize this research. The classification of stability problems in the power grid along with the methods that have been proposed for its analysis are summarized. An overview of variable-speed wind turbines performance in this framework is also presented.

2.1 Power System Stability

The continuing growth in power systems interconnections as well as the introduction of new technologies and control equipment, and the increasing number of operation actions carried out under highly stressed operating conditions explain the fact that power systems stability remains a topic of paramount importance in power system operation. Some challenging problems in power system management are vindicate because power systems are operated closer to security limits, environmental constraints restrict the expansion of transmission network and the necessity of power transfers over long distances has increased. Rising energy consumption, attention on environmental concerns and de-

velopment in renewable technologies have encouraged the installation of renewable energies. Within the renewable energies, wind energy plays today a potential role; it has developed to a mature stage and is becoming widely used all over the world. However, better power exchange capabilities over long distances is one of essential characteristics of transmission systems to achieve a higher penetration level of wind power.

In order to contextualize the subject, a definition of power system is quoted from IEEE task force on terms and definitions [9]:

"A network of one or more electrical generating units, loads, and/or power transmission lines, including the associated equipment electrically or mechanically connected to the network."

It should be remarked that this definition is made solely from the vantage of engineering with no consideration to either political, geographical or any other jurisdictional boundary.

Over the years, several definitions of power systems stability have been formulated aiming at clarifying technical and physical aspects of the problem from the system theory perspective. The stability concert more consistent with the emphasis placed in this research project is the one relating to the system's ability to ride-through disturbances arising the system itself and its capacity to settle down to a new stable operating state after the effects of such disturbance disappears.

A formal definition of power system stability is provided by [10],

"Power system stability is the ability of an electric power system, for a given initial operating condition, to regain a state of operating equilibrium after being subjected to a physical disturbance, with most system variables bounded so that practically the entire system remains intact."

To a greater or lesser extent, all possible disturbances may fall into two categories: small and large signal disturbances. In a small disturbance the equations that describe the dynamics of the power system may be linearised around a base operating point for the purpose of analysis. Small load or generation changes may be designated to be small disturbances whilst sudden voltage changes resulting from short-circuit faults, switching operations, loss of generation or transmission circuits will come under the category of large disturbances.

For the purposes of system analysis, power system stability is divided into two broad classes [9, 11].

1. **Small signal stability or steady-state stability.** A power system is said to be stable, for a given steady-state operating condition, if following a small disturbance, it reaches a steady-state operating condition which is identical or close to the pre-disturbed operating condition. This is also known in some quarters as small disturbance stability of a power system [9].

2. **Transient stability.** A power system is said to be transiently stable at a given steady-state operating condition if following a large disturbance it reaches an acceptable new steady-state operating condition.

It should be emphasized that transient stability is a function of both, the operating condition and the disturbance, whereas small-signal stability is a function only the operating condition.

Although power system stability is essentially a single problem, the phenomenon can take different forms. Therefore a classification into more manageable categories is essential for meaningful practical analysis and for the resolution of power system stability problems. The different forms of stability phenomena, according to the root cause of instability, or otherwise are categorized into three main subclasses: rotor angle stability, voltage stability, and frequency stability; even

though these three issues are not widely disjointed when a major disturbance arises in utility-size power systems. A brief description of each form is given as follows:

Rotor angle stability

For a power system to remain stable, it is a pre-condition that there is sufficient synchronizing torque as well as sufficient damping torque for each one of the synchronous machines in operation. These are the two components of the net electrical torque acting on a generator. The synchronizing torque is the component of the torque incremental change which is in phase with the rotor angle perturbation. On the other hand, damping torque is the component of torque which is in phase with the speed deviation. Lack of sufficient synchronizing torque results in a *periodic* or *non-oscillatory instability*, whereas lack of damping torque results in an *oscillatory instability* [12, 13].

Solution of the differential equations representing the system will yield at least one positive real root, or one pair of complex roots with real parts. In cases of small disturbances, this class of stability can be assessed by analysing the roots of the linearised system, whilst in cases of large disturbances, because of the non-linearities involved, the difference between the torque components (synchronizing and damping torque) can only be estimated from the nature of the trajectories [9].

Voltage Stability

Insufficient reactive power support may induce voltage instability problems leading to a wide-area voltage collapse. When one or more generators reach their reactive power limits the ability to transfer power becomes severely restricted restricted. It may be argued that loads are the driving force of voltage instability; the tendency of distribution voltage regulators, tap changing transformers, and thermostats is to re-establish the consumed power by the loads, following a disturbance

[14]. Such a response increases the stress on the high voltage network owing to the rising power consumption; exceeding the capacity of the network and causing, in turn, a further voltage reduction. [15, 16].

Unlike rotor angle stability, the distinction between small-signal and large is blurred. Voltage stability can be seen as a single problem where a combination of both, linearised and non-linear analytical tools is applied.

Frequency Stability

Frequency stability is a phenomenon that involves the whole system. It is the ability of the power system to maintain the steady-state frequency within acceptable limits following a severe system contingency. The system frequency will decrease following an event that reduces the total active power output; system frequency is a key indicator of mismatch between generation and demand.

All things considered, frequency stability depends primarily on the overall system response to a contingency and on the availability of system power reserve. In general, apart from insufficient generation reserve, frequency stability problems concern deficiencies in equipment responses, poor control coordination and protection equipment [10].

Although power system stability is classified according to causes of instability with suitable analysis tools and property corrective measures, any one instability form (rotor-angle stability, voltage stability, frequency stability) may not occur in its pure form, particularly in highly stressed power systems and for cascading events, and one instability form may, in the end, lead to another one. Thus, the differentiation between them is important to understand the causes of the problem in order to develop appropriate design operating procedures.

In general, keeping in mind that stability is an integral property of a system, quite independently from its classification, the solution of a

specific problem should not be at the expense of creating a different kind of stability problem. Therefore, a comprehensive assessment of the stability phenomenon, involving different aspects of the problem, is essential.

In modern power systems where conventional synchronous generation is replaced by wind generation the stability impact evaluation must to be considered. In power systems with a large wind power penetration there will be large asynchronous active power flows that can help to preserve rotor angle stability of the system. However, angular stability support of the synchronous units may depend on the manner in which reactive power is injected from wind systems. Insufficient reactive power support from wind generation can lead to voltage stability issues [17, 18]. Also, the frequency stability of the system will be impacted if synchronous generation is displaced by wind generation [19, 20]. Power system stability assessment with large-scale wind power integration is restricted due to the lack of appropriate dynamic models.

2.2 Small Signal Stability

2.2.1 Characteristics of the Small Signal Stability Problems

Interactions amongst system components bring about the phenomena associated with small signal stability. For instance, diverse oscillations modes are caused by the generators' rotors swing against each other. The two kinds of electromechanical oscillation modes most widely spoken of are:

1. *Local mode* involves a small portion of the system. Oscillations of one or two remotely located power stations swinging against the rest of the power system are called local mode oscillations. These are amongst the most commonly found problems. Oscillations of

electrically close machines swinging against each other are called inter-machine or inter-plant mode oscillations.

The local mode oscillations have frequencies typically in the range of 1 to 3 Hz.

There are other possible local modes associated with control modes, such as those involving the inadequate tuning of control systems (generator excitation systems, HVDC converters, FACTS equipment) [21] and the turbine-generator rotational (mechanical) components [22]. These are the so-called torsional mode oscillations and involve the interaction of the turbine shaft dynamics with these controls.

2. *Inter-area oscillations* relates to oscillations of a group of generators in one area against those in another area, usually across a long or a weak tie-line. If the oscillation frequency is very low, in the range of 0.1 to 0.3 Hz, the system is breaking up into two parts, each one swinging against the other. Modes of higher oscillation frequencies, in the range of 0.4 to 1 Hz, involve subgroups of generators swinging against each other.

The duration of these two modes will depend on their relative damping, which is, in many systems, a critical factor to operate in a secure mode.

2.2.2 Modal Analysis

The behaviour of a dynamic system, such as a WT-DFIG, may be described by a set of n first-order, non-linear, ordinary algebraic-differential equations (DAE) of the following form [21, 23, 24]:

$$\frac{dx_i}{dt} = f_i(x_1, x_2, ..., x_n;\ z_1, z_2, ..., z_m;\ u_1, u_2, ..., u_r) \tag{2.1}$$

$$0 = g_i(x_1, x_2, ..., x_n;\ z_1, z_2, ..., z_m;\ u_1, u_2, ..., u_r) \tag{2.2}$$

where $i = 1, 2, ..., n$.

Using vector-matrix notation, the system can be expressed by

$$\dot{\mathbf{x}} = \mathbf{f}(\mathbf{x}, \mathbf{z}, \mathbf{u}) \tag{2.3}$$

$$0 = \mathbf{g}(\mathbf{x}, \mathbf{z}, \mathbf{u}) \tag{2.4}$$

with

$$\mathbf{x} = \begin{bmatrix} x_1 \\ x_2 \\ \vdots \\ x_n \end{bmatrix} \quad \mathbf{z} = \begin{bmatrix} z_1 \\ z_2 \\ \vdots \\ z_m \end{bmatrix} \quad \mathbf{u} = \begin{bmatrix} u_1 \\ u_2 \\ \vdots \\ u_r \end{bmatrix} \quad \mathbf{f} = \begin{bmatrix} f_1 \\ f_2 \\ \vdots \\ f_n \end{bmatrix} \quad \mathbf{g} = \begin{bmatrix} g_1 \\ g_2 \\ \vdots \\ g_n \end{bmatrix} \tag{2.5}$$

where $\mathbf{x}$, $\mathbf{z}$, and $\mathbf{u}$ are the column-vectors of the states, algebraic, and input variables, respectively; n is the order of the system, m is the number of algebraic variables, r is the number of inputs. f and g are vectors of non-linear functions relating state, algebraic and input variables to derivatives of the state variables and to algebraic equations, respectively.

The system output can be expressed in terms of the state variables, algebraic variables and input variables in the following form:

$$\mathbf{y} = \mathbf{h}(\mathbf{x}, \mathbf{z}, \mathbf{u}) \tag{2.6}$$

where $\mathbf{y}$ is the column vector of outputs and $\mathbf{h}$ is a vector of non-linear algebraic output equation.

The system's state is an important concept in state-space representations. It encapsulates all the necessary information to describe the system at any instant in time. A set of linearly independent system variables, referred to as the *state variables*, along with the inputs to the system yield a complete description of the system's behaviour [21].

Either physical quantities (such as voltage, torque, angle, speed) or mathematical variables associated with the differential equations de-

scribing the system dynamics may be chosen as state variables. However, the state variables are not unique and whatever the set of state variables selected, it will provide the essentially same information about the system.

Modal analysis starts from a power flow solution corresponding to a particular loading condition (initialisation procedure) to determine an operating point (x_0, z_0, y_0). The differential-algebraic equations are linearised around the operating point by applying Taylor Series Expansion. The Taylor series represents a non-linear function as an infinite sum of terms calculated from the values of its derivatives evaluated at a single point.

Neglecting terms of order two and above and eliminating the algebraic variables $\mathbf{z}$, a procedure for small perturbations is established,

$$\begin{aligned} \dot{x_i} &= \dot{x_{i0}} + \Delta\dot{x_i} = f_i\left[(\mathbf{x_0} + \Delta\mathbf{x_0}), (\mathbf{u_0} + \Delta\mathbf{u_0})\right] \\ &= f_i(\mathbf{x_0}, \mathbf{u_0}) + \frac{\partial f_i}{\partial x_1}\Delta x_1 + \ ... \ + \frac{\partial f_i}{\partial x_n}\Delta x_n \\ &\quad + \frac{\partial f_i}{\partial u_1}\Delta u_1 + \ ... \ + \frac{\partial f_i}{\partial u_r}\Delta u_r \end{aligned} \tag{2.7}$$

Since $\dot{x}_{i0} = f_i(\mathbf{x_0}, \mathbf{u_0})$,

$$\Delta\dot{x_i} = \frac{\partial f_i}{\partial x_1}\Delta x_1 + \ ... \frac{\partial f_i}{\partial x_n}\Delta x_n + \frac{\partial f_i}{\partial u_1}\Delta u_1 + \ ... \frac{\partial f_i}{\partial u_r}\Delta u_r$$

with $i = 1, 2, ..., n$

In a likewise manner, and with reference to (2.6),

$$\Delta y_j = \frac{\partial g_j}{\partial x_1}\Delta x_1 + \ ... \frac{\partial g_j}{\partial x_n}\Delta x_n + \frac{\partial g_j}{\partial u_1}\Delta u_1 + \ ... \frac{\partial g_j}{\partial u_r}\Delta u_r$$

with $j = 1, 2, ..., n$.

The prefix Δ denotes a small deviation, thus

$$\Delta x = x - x_0 \qquad \Delta y = y - y_0 \qquad \Delta u = u - u_0$$

The linearised system model is of the form

$$\Delta \dot{\mathbf{x}} = \mathbf{A}\,\Delta \mathbf{x} + \mathbf{B}\,\Delta \mathbf{u} \tag{2.8}$$

$$\Delta \mathbf{y} = \mathbf{C}\,\Delta \mathbf{x} + \mathbf{D}\,\Delta \mathbf{u} \tag{2.9}$$

where

$$\mathbf{A} = \begin{bmatrix} \frac{\partial f_1}{\partial x_1} & \cdots & \frac{\partial f_1}{\partial x_n} \\ \vdots & \ddots & \vdots \\ \frac{\partial f_n}{\partial x_1} & \cdots & \frac{\partial f_n}{\partial x_n} \end{bmatrix} \qquad \mathbf{B} = \begin{bmatrix} \frac{\partial f_1}{\partial u_1} & \cdots & \frac{\partial f_1}{\partial u_r} \\ \vdots & \ddots & \vdots \\ \frac{\partial f_n}{\partial u_1} & \cdots & \frac{\partial f_n}{\partial u_r} \end{bmatrix}$$

$$\mathbf{C} = \begin{bmatrix} \frac{\partial h_1}{\partial x_1} & \cdots & \frac{\partial h_1}{\partial x_n} \\ \vdots & \ddots & \vdots \\ \frac{\partial h_m}{\partial x_1} & \cdots & \frac{\partial h_m}{\partial x_n} \end{bmatrix} \qquad \mathbf{D} = \begin{bmatrix} \frac{\partial h_1}{\partial u_1} & \cdots & \frac{\partial h_1}{\partial u_r} \\ \vdots & \ddots & \vdots \\ \frac{\partial h_m}{\partial u_1} & \cdots & \frac{\partial h_m}{\partial u_r} \end{bmatrix}$$

The partial derivatives are evaluated at the equilibrium point corresponding to where the small perturbation are being analyzed. An equilibrium point is a point where all the derivatives $\dot{x_1}, \dot{x_2}, ..., \dot{x_n}$ are simultaneously zero and defines the points on the trajectory with zero velocity.

In Equations (2.8) and (2.9),

$\Delta \mathbf{x}$ is the state vector of dimension n

$\Delta \mathbf{y}$ is the output vector of dimension m

$\Delta\mathbf{u}$ is the input vector of dimension r

A is the state or plant matrix of size nxn

B is the control or input matrix of size nxr

C is the output matrix of size mxn

D is the (feed-forward) matrix which defines the proportion of inputs appearing directly in the outputs, size mxr

Eigenvalues and eigenvalue properties

Small signal stability analysis studies the properties of the system ((2.8), (2.9)) around (x_0, z_0, y_0) through an eigenvalue analysis of the state matrix **A**. Each eigenvalue, denoted by λ, describes one special dynamic behaviour of the system called a *mode* which is obtained from **A** matrix.

For an operating point to be stable, the real parts of all eigenvalues of **A** must lie in the left half-plane of the complex plane (i.e, with negative real parts). This ensures that oscillations will decay with time and will return to a steady state following a small disturbance. The opposite will occur if an eigenvalue has a positive real part. The amplitude of the modes will increase exponentially and the power system will be unstable at that operating point.

If **A** is real, complex eigenvalue occur in conjugate pairs, and each pair would correspond to an oscillatory mode. Fig. 2.1 shows the possible natural modes of a system.

The eigenvalues of **A** contain essential information about the mode's frequencies and their damping after a small disturbance. The real part component gives the damping and the imaginary component gives the frequency of oscillation.

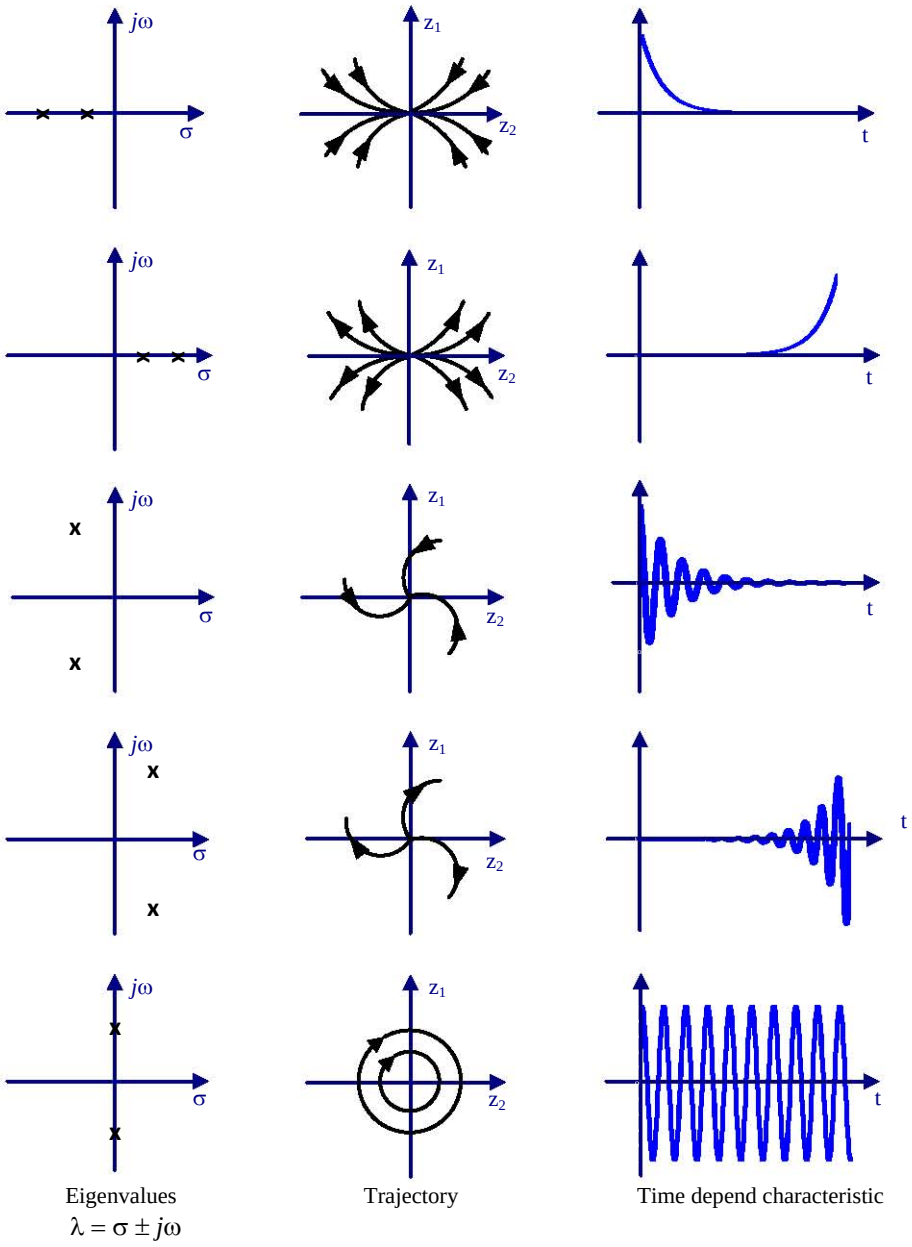

Figure 2.1: Possible combination of eigenvalues pairs (left). Their trajectories (middle) and time responses (right).

For a complex eigenvalue $\lambda_i = \sigma_i \pm j\omega_i$, the damping ratio ζ is defined as:

$$\zeta_i = -\frac{\sigma_i}{\sqrt{\sigma_i^2 + \omega_i^2}} \tag{2.10}$$

with $\zeta \in [-1, 1]$.

The damping ratio ζ determines the rate of decay of the amplitude of the oscillation. The time constant τ of the amplitude decay is $\tau = {}^{1}/_{|\sigma|}$ [21].

The damping is an important measure of the quality of the system's transient response. A poorly damped system oscillates for a relatively long time following a disturbance, an undesirable characteristic which ought to be minimized.

Several researchers have addressed the issue of small signal security, which is strongly related to the damping of system oscillations [25, 26, 27, 28]. Minimum admissible dampings have been defined to be in the range 3 to 5%.

The oscillation frequency f of the i^{th} mode, in Hz, is defined as:

$$f_i = \frac{\omega_i}{2\,\pi} \tag{2.11}$$

Mode shape and eigenvectors

The shape of a mode that corresponds to a certain eigenvalue is described by its associated *right eigenvector*, which defines the relative activity of the system's dynamic states on each mode.

The eigenvectors are determined regarding the chosen states for the formulation of the power system model, but it is not a good indicator of the importance of states to a mode, since eigenvectors are not unique.

The *left eigenvector* weighs the contribution of the states within a mode.

The right eigenvector $\mathbf{\Phi_i}$ and the left eigenvector $\mathbf{\Psi_i}$ associated with the i^{th} eigenvalue $\lambda_\mathbf{i}$ satisfy

$$\mathbf{A}\mathbf{\Phi_i} = \lambda_\mathbf{i}\mathbf{\Phi_i} \tag{2.12}$$

$$\mathbf{\Psi_i}^t\mathbf{A} = \mathbf{\Psi_i}^t\lambda_\mathbf{i} \tag{2.13}$$

Eigenvalue sensitivity

Differentiating equation (2.12) with respect to a_{kj} the element of $\mathbf{A}$ in k^{th} row and j^{th} column yields

$$\frac{\partial \mathbf{A}}{\partial a_{kj}}\mathbf{\Phi_i} + \mathbf{A}\frac{\partial \mathbf{\Phi_i}}{\partial a_{kj}} = \frac{\partial \lambda_i}{\partial a_{kj}}\mathbf{\Phi_i} + \lambda_\mathbf{i}\frac{\partial \mathbf{\Phi_i}}{\partial a_{kj}}$$

Pre-multiplying by Ψ_i

$$\mathbf{\Psi_i}\frac{\partial \mathbf{A}}{\partial a_{kj}}\mathbf{\Phi_i} + \mathbf{\Psi_i}(\mathbf{A} - \lambda_i\mathbf{I})\frac{\partial \mathbf{\Phi_i}}{\partial a_{kj}} = \mathbf{\Psi_i}\frac{\partial \lambda_\mathbf{i}}{\partial a_{kj}}\mathbf{\Phi_i}$$

and knowing that $\mathbf{\Psi_i}\mathbf{\Phi_i} = 1$ and $\mathbf{\Psi_i}(\mathbf{A} - \lambda_i\mathbf{I}) = 0$, the above equation simplifies to

$$\mathbf{\Psi_i}\frac{\partial \mathbf{A}}{\partial a_{kj}}\mathbf{\Phi_i} = \frac{\partial \lambda_i}{\partial a_{kj}}$$

Since the only non-zero partial derivatives of A with respect to a_{kj} are equal to 1 (corresponding to element in the k^{th} row and j^{th} column),

$$\frac{\partial \lambda_i}{\partial a_{kj}} = \Psi_{ik}\,\Phi_{ji} \tag{2.14}$$

Therefore the sensitivity of the eigenvalue λ_i to the element a_{kj} of the state matrix is equal to the product of the left eigenvector element Ψ_{ik} and the right eigenvector element Φ_{ji} [21] .

Participation Factors

Participation factor represents a measure of the contribution of each dynamic state in a given mode or eigenvalue.

In terms of eigenvectors, the participation factor may be defined by:

$$p_{f_{ki}} = \frac{\Psi_{ki}\Phi_{ik}}{\mathbf{\Psi_i^t \Phi_i}} \tag{2.15}$$

where Ψ_{ki} and Φ_{ik} are the k^{th} entries in the left and right eigenvectors associated with the i^{th} eigenvalue.

The participation matrix $\mathbf{P_f}$, proposed in [29, 30], is defined as:

$$\mathbf{P_f} = \begin{bmatrix} \mathbf{p_{f_1}} & \mathbf{p_{f_2}} & \dots & \mathbf{p_{f_n}} \end{bmatrix} \tag{2.16}$$

with

$$\mathbf{p_{f_i}} = \begin{bmatrix} p_{f_{1i}} \\ p_{f_{2i}} \\ \vdots \\ p_{f_{ni}} \end{bmatrix} = \begin{bmatrix} \Phi_{1i}\Psi_{i1} \\ \Phi_{2i}\Psi_{i2} \\ \vdots \\ \Phi_{ni}\Psi_{in} \end{bmatrix} \tag{2.17}$$

By using the scale property of an eigenvector it is possible to choose a scaling that simplifies the use of participation factors. Thus, by choosing eigenvectors such $\mathbf{\Psi_i}^t \mathbf{\Phi_i} = 1$, a normalised form of the participation factor is defined as:

$$p_{f_{ni}} = \frac{|\Phi_{ni}|\,|\Psi_{in}|}{\sum_{i=1}^{n} |\Phi_{ni}|\,|\Psi_{in}|} \tag{2.18}$$

where n is the number of state variables, $p_{f_{ni}}$ is the participation factor of the system. The $p_{f_{ni}}$ magnitude represents a measure of the relative participation of the n^{th} state variable into mode i, and vice versa. A further normalization can be done by making the highest of the participation factors equal to unity. From equation (2.14), it can be observed that the participation factor $p_{f_{ki}}$ is equal to the sensitivity of the eigenvalue λ_i to the diagonal element a_{kk} of $\mathbf{A}$,

$$p_{f_{ki}} = \frac{\partial \lambda_i}{\partial a_{kk}} \tag{2.19}$$

In power systems, participation factors can be used as a complementary measure to the suitability of power system stabilizers (PSS) placement.

Transfer Function

Although eigenvalue analysis of the system state matrix is carried out to examine small signal stability of power systems, modal analysis is very useful when it comes to control design, addressing the open-loop transfer function and its relationship to the state matrix and its eigenproperties.

The transfer function has the general form of:

$$G(s) = K\frac{N(s)}{D(s)} \tag{2.20}$$

By applying the method used in [21], it can be seen that $G(s)$ may be written as:

$$G(s) = \sum_{i=1}^{n} \frac{R_i}{s - \lambda_i} \tag{2.21}$$

where the residues, R_i, in terms of the eigenvectors

$$R_i = \mathbf{c}\,\mathbf{\Phi_i}\mathbf{\Psi_i}\,\mathbf{b} \tag{2.22}$$

It can be seen that the poles of $G(s)$ are given by the eigenvalues of $\mathbf{A}$.

2.2.3 Methods for Modal analysis

The eigenvalues of the system state matrix can be computed by solving the characteristic equation of first and second order systems. For higher-order systems a method that has been widely used is the QR transformation method [31, 32].

In this method, a tridiagonal matrix Q is constructed from a set of orthogonal transformations applied to A matrix. A good description of the method can be found in [33].

Application of the QR method is confined to small size power systems with up to approximately 80 generators. Due to computer limitations it has only used in systems containing up to about 800 modes [28].

For larger power systems, special techniques have been developed, in which partial modal analysis is used. The first algorithm was the Analysis of Essentially Spontaneous Oscillations in Power Systems (AESOPS), originally presented in [34], which uses the quasi-Newton iteration method to find eigenvalues associated with rotor angle modes close to initial value set. It is able of handle up to about 2000 states.

Other more efficient methods such as the *Inverse Iteration, Generalized Rayleigh Quotient Iteration*, *Modified Arnoldi* [35] and, *Simultaneous Inverse Iteration* [35] have been proposed. All these methods are based on iterative multiplication of a vector by the system state matrix **A**. The *Program for Eigenvalue Analysis of Large Systems* (PEALS) combines the AESOPS and the modified Arnoldi method. It is presented in [36].

On the other hand, *Selective Modal Analysis* (SMA) focuses on the relevant eigenvalues in a specific area and therefore, storage and computer requirements are heavily reduced. This method is described in [30] and [37].

2.3 Transient Stability Analysis

The so-called *transient stability analysis* aims to assess the dynamic response of a power system when subjected to a contingency, such as line outage or a short circuit of different types: phase-to-ground, phase-to-phase-to-ground, or three-phase. Although they are commonly assumed to occur in transmission lines, occurrences in buses or transformer should also be considered. Of course, as the transient analysis pertains to stability under large disturbances, the non-linearities of the

model have to be taken into account and, hence, linearization of the power system is deemed as not valid.

In contrast to the small signal stability analysis, the system commonly presents a stable pre and post-disturbance equilibrium. The point in question is whether or not the trajectory of the system following the contingency is unstable and reaches a new stable equilibrium operating point. Caution needs to be exercised though, because although the system may reach a stable operating point from the mathematical vantage, it cannot be considered transiently stable if the mode of operation is not an acceptable one. From a mathematical viewpoint, *"transient stability implies that an acceptable post-disturbance steady-state operating condition of the power system is asymptotically stable and the response to the given disturbance is such that the trajectories of the operating quantities tend to this operating condition as time increase"* [38].

The study's period of interest may be cover 3 to 5 seconds and perhaps extended to go up to 10 seconds in some special cases.

With regards to the simulation method some of the most important techniques that have been used thus far are *a*) carrying out numerical integrationof the differential equations that describe the system and observe the power system response; *b*) using Lyapunov-based approaches based on energy functions of the power system; and *c*) carrying out probabilistic solutions.

The stability or otherwise of the first solution *a*), is determined by the convergence (divergence) of the time domain simulation. The accuracy of this approach depends only on the numerical integration method and on the system model. In a complete contingency analysis this is applied in off-line environments, but for on-line applications the computational burden of the method is an important issue to be considered.

The second approach is known as the transient energy function (TEF), a method in which a stability criterion substitutes the numerical integration. TEF is based on an analytical representation of the system to determinate the transient kinetic and the potential energy for the post-contingency system. The energy responsible for the deviation from synchronous operation is quantified by the transient kinetic energy, whereas the integral of the instantaneous real power mismatch between electrical and mechanical power at generator buses defines the potential energy [39].

In the last method, stability is assessed by examining probability distribution functions resulting from initiating factors such as fault type, fault location, system conditions, (loading and configuration) which are probabilistic in nature. This seems to be a tool more suitable for planning purposes; statistically meaningful results require a large amount of computation time [40].

2.4 Wind Power Generation Systems

Although many wind turbine designs have been proposed over the years, the horizontal axis, three-blades, upwind turbines have prevailed because they have proved to offer an efficient configuration.

Fixed-speed and variable speed are the two types used for wind energy conversion; fixed- speed operation is generally associated with smaller turbines whereas variable speed operation is associated with the largest machines.

2.4.1 Fixed-speed Wind Turbines

The fixed-speed or constant speed generator is based on a directly coupled conventional squirrel-cage induction generator whose slip, and hence the rotor speed, vary depending on the amount of generated power.

However, the rotor speed variation is generally 1 or 2 percent [5, 41]. The configuration of a FRC is illustrated in Fig. 2.2.

Squirrel-cage induction generators always consume reactive power and therefore, the factor power correction is provided by capacitors at each wind turbine. The power control is done by stall and pitch control which allow reducing the aerodynamic efficiency of the rotor. The first one (stall) corresponding to the design of the rotor blades reduces the efficiency of wind speed above nominal value. With pitch control the efficiency is reduced by turning the blades out of the wind using hydraulic mechanisms or electric motors [41].

Both, advantages and drawbacks of this generation system can be summarizes as follows [41, 42]:

- This is a relatively simple generation system and less expensive.
- FSIG-based wind farms can contribute to network damping but their ability to survive network faults is poor.
- The fluctuations of the drive train torque produced by fluctuations in wind speed could lead to high structural loads due to the lack of capability to vary the rotor speed. This requires a more mechanically robust turbine.

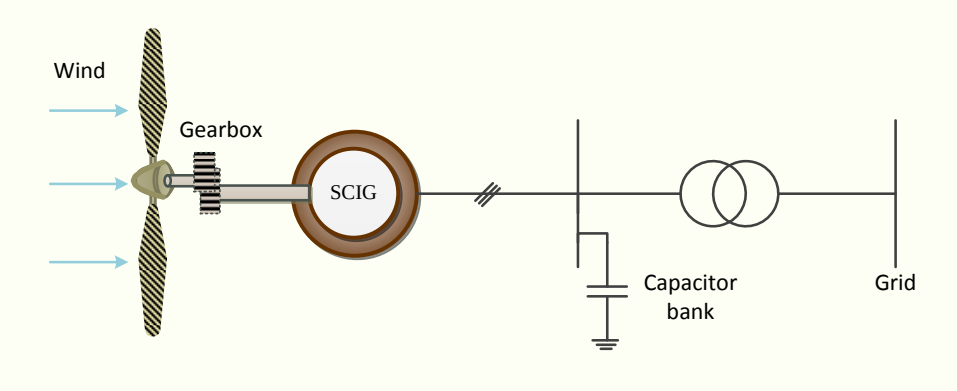

Figure 2.2: Configuration of a fixed-speed wind turbine.

2.4.2 Variable-speed Wind Turbines

The two most common variable-speed wind turbines configurations are the double fed induction generator (DFIG) wind turbine and the fully rated converter wind turbine. The double fed induction generator wind turbine is essentially a wound rotor induction generator with slip rings and a back-to-back converter between the rotor slip rings and the grid, and with the stator directly connected to the grid. Fully rated converter (FRC) wind turbine may employ induction generator or wound-rotor or permanent-magnet synchronous generator and the power electronic converter is directly connected to the generator's stator. The typical configuration of a FRC is shown in Fig. 2.3.

FRC with permanent magnet synchronous offers a better performance due to higher efficiency and less maintenance because of the fact that it does not have rotor current. No gearbox, high power density and easy to control are some advantages of this configuration. The main drawbacks are the cost of the machine which is incremented by permanent magnets and, on the other side, there are no methods to control the strength of the magnetic field and hence, the power factor [43].

The variable-speed wind turbine equipped with a double fed induction generator and controlled by the back-to-back converter is the concept of electricity-producing wind turbine examined in this work.

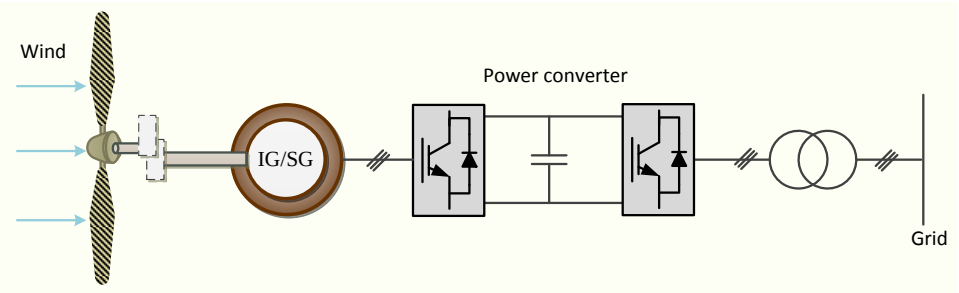

Figure 2.3: Typical configuration of a FRC-connected wind turbine.

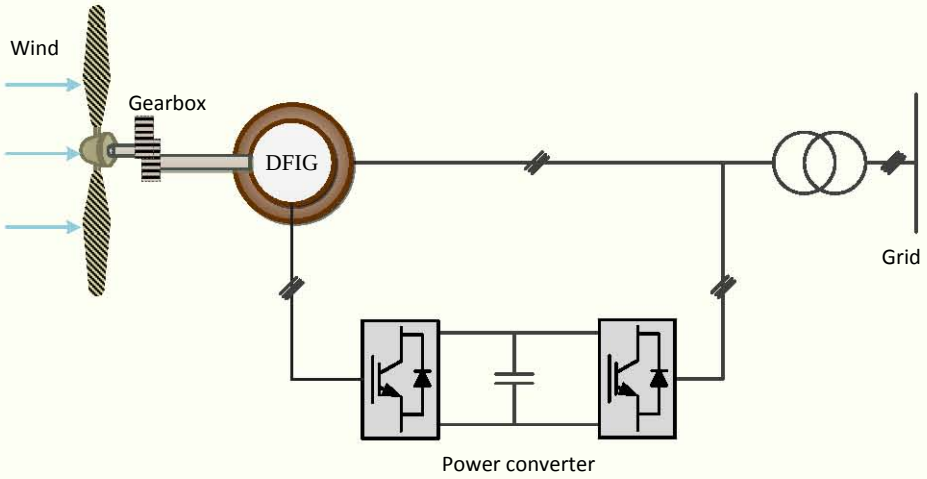

Figure 2.4: Typical configuration of a DFIG-based wind turbine.

A typical configuration is shown in Fig. 2.4. It consists of an induction wound rotor generator with slip rings to take current into and out of the rotor. The variable-speed operation is obtained by injecting a controllable voltage into the rotor through a variable frequency converter [44, 45]. The frequency converter is regularly based on AC/DC IGBT-based voltage source converter (VSC) linked by a DC bus [41, 5]. It is rated at approximately 30% of the generator's power [46, 47]. The stator of the DFIG is directly connected to the power grid.

The configuration of this variable-speed wind turbine concept allows the decoupling of the grid frequency (electrical) and the rotor speed (mechanical) [48, 49]. The power is supplied from the stator to the power network and provided or absorbed from the grid through the rotor circuit. For normal operating conditions, the converter control can be set to provide the minimum amount of reactive power output.

The most prominent benefit of this concept is the output power maximization by the possibility of changing rotational speed. The range of rotational speed can be -40% up to $+30\%$ of the synchronous speed [46]. However a disadvantage of this topology is that both, generator (related to slips rings and brushes) and gearbox require maintenance and periodic checkups.

2.5 Variable-speed Wind Turbine Systems Integrated in Power Systems

Technical aspects, such as the use of converter utility interfaces, the inherent uncontrollability of the wind, and the existence of machines of smaller size make a distinction between wind power system generation and conventional synchronous generation systems and their interaction with power networks. Impacts both, local (power flows, busbar voltages, protection schemes, power quality) and system-wide (system dynamics, system stability, reactive power, voltage and frequency support) affect the system's behaviour either in the vicinity or as a whole.

As described above, fixed-speed and variable-speed wind turbines are the two main categories used at wind power systems. However thanks to the development of power electronics and their cost reduction, the variable-speed wind technology becomes a competitive candidate for the wind energy system operation. This is the addressed technology in this thesis.

Variable-speed turbines can affect their terminal voltage by modifying the exchange of reactive power. The use of power electronic converters in this kind of wind turbine is an important subject. Regarding power quality the attention is focused on harmonic distortion.

In case of faults, the wind turbine may be disconnected from the grid by intervention of the converter control system: in FRC wind turbine by blocking the turn-on pulses for the converter; in DFIG-based wind turbines, in case of too high rotor voltages, the rotor windings are short-circuited by a crowbar protection system.

This is an important issue concerning the power system stability. The consequences of disconnecting the wind turbines in a high wind penetration scenario, i.e., above 10% [46], can lead to voltage drops which degrade the power generation performance. Thus, nowadays,

new technical requirements for the reliable operation of large wind energy systems interconnected to the power grid are imposed by grid codes [50, 51].

Dynamic advantages of the variable-speed DFIG wind turbines include enhancement of machine stability margin and damping of system oscillations. However, under transient conditions, as the ones me above mentioned, the generator works as a traditional squirrel cage induction generator due to the fact that the protection scheme acts to short circuit the rotor.

Comparative studies between this concept with synchronous generators (SG) and squirrel cage induction generators (SCIG) have been considered to analyze how the dynamic behaviour of the DFIG itself affects stability of the power system. The studies have been carried out by considering both frequency domain and time domain approach.

An analysis using a frequency-domain approach based on eigenvalue analysis has been performed to examine the impact of the DFIG-based wind turbine on the low-frequency oscillatory modes of the synchronous machines [52, 53, 54, 55, 56]. The time domain approach has been extensively used throughout the literature to investigate voltage dynamics of power systems subject to large disturbances [57, 58, 59, 60, 61].

The decoupled controllability of the d-axis and q-axis component of the DFIG rotor voltage vector confers greater flexibility. It is a significant difference between DFIG and both, SG and SCIG. In case of SG, developed excitation systems use additional control such as power system stabilizer to control the field voltage, to damp system oscillations, and, in general, to enhance the whole system dynamic performance. In case of SCIG, additional components, e.g. power electronic-based compensator, are inherent associated with any dynamic control [62, 63, 64, 65].

Otherwise, in recent years a growing interest in studying the DFIG frequency support is justified because the DFIG does not contribute to any inertial response to frequency events (as a fixed-speed wind turbine with induction machine does) [66]. Although it has not been studied extensively, some papers deal with the impact of DFIG frequency response [19, 67, 68], but because of their assumptions, there are some discrepancies between the pointed out conclusions. None of these papers discusses the limiting factors of DFIG frequency support.

The interest on this topic also increases along with the risk of occurrence of frequency variations because of interactions between large active power variations, an installed high wind power capacity, and the existence of frequency controllers in the conventional power stations.

In order to quantify the extra active power support provided from a variable-speed wind turbine at a certain wind speed, it is calculated the amount of energy that can be extracted from the wind turbine with along the extra energy from the stored rotational energy in the turbine-generator [69]. As expected, the capability of providing an extra active power support of the wind turbine is reduced at high wind speed conditions (above medium wind speed) and hence, the dimensions of the turbine mechanical design and the power rating of the generator side converter need to be suitably adjusted. In [70], a variable proportional controller to facilitate a temporary extra wind turbine active power support in high wind speed conditions is proposed, in which a maximum delivery of 5% and 10% extra active power was reported.

Implementation of primary frequency regulation in wind turbines can be found in [20, 71, 72, 73, 74, 75].

Acknowledging the control capabilities of the DFIG, the authors in [55], brought forward a power system stabilizer for a wind turbine employing a DFIG and showed that this PSS could significantly influence the contribution of a DFIG-based wind farm to network damping. The power system stabilizer was designed to operate with a flux magnitude

and an angle controller (FMAC) scheme, by which the terminal voltage and the stator power output can be controlled via the magnitude of the rotor flux vector and its angular position.

The control strategies usually adopted are those one based on inertial control, using the kinetic energy stored in the rotating masses and the proportional control implemented in conventional units. The possibility of releasing kinetic energy from a DFIG-based wind turbine system by adding an extra control loop, sensitive to the network frequency, has also been applied in works as [76, 19] and compared to fixed-speed wind turbines [42, 67].

Considering the published results it can be concluded that variable speed DFIG farms with frequency control managed to increase the eigenvalues damping, improving as well the dynamic response of the frequency. This improvement is more significant in DFIG-based wind farms with frequency control than in the fixed-speed SCIG.

Chapter 3

Variable-Speed Wind Power Generation Systems

Some basic considerations concerning the performance of wind turbines in electrical power systems are presented in this chapter. To this end, an introduction to aerodynamic aspects of wind turbines is presented, followed by a brief overview of the concept of modelling, simulation aspects, and the main elements of a variable-speed wind turbine model in connection with the type of studies addressed in this work.

3.1 Introduction

Computer simulations of complex systems, as it is the case of wind turbines, make possible to investigate a wide range of properties of key technology aspects such as design, construction and applications.

It is fair to say that investigation has its own requirements concerning its necessary level of modelling detail and the model data requirements all of which need to be agreed on before simulation can start. This is strongly related to the accuracy and reliability of the obtained results.

In this way, an overview of the wind turbine generation system is first presented aimed at having a good understanding of the technology with a view to assess the relevance of each one of its components within the scope of this thesis.

3.2 Wind Speed

The modelling of power fluctuations of wind farms in continuous operation may be a key requirement to obtain realistic results in most studies. Wind speed is one of the most difficult variables to predict in order to estimate the wind farms energy production and to get an acceptable analysis of its behaviour when connected to the electrical network.

Theoretical estimations can be collected by means of statistical data related to wind variations at a particular location, although these are better suited for planning stage in terms cost, electricity output per unit and area. To ensure that all design limits are satisfied, the performance evaluation of wind power generation system schemes has be considered in the full range of wind speed variations. Stochastic and deterministic effects (caused by turbulences, the tower shadow, etc.) have been taken into account by means of various wind functions.

For power output of a wind turbine the long-term variations of the mean wind velocity are of great importance while short-term fluctuations determine the fatigue loading on the wind turbine structure.

The wind, in time, can be regarded as having a quasi-static mean speed which fluctuations superimposed on the average value. Random variations of the instantaneous speed from the mean wind speed in periods below 10 minutes are considered as termed turbulences [77]. Turbulences are caused by the airflow over the earth's surface and are influenced by orography characteristics, soil surfaces or by the presence of obstacles such as buildings.

The mean wind speed $\bar{v}_w$ (generally over a period of ten minutes), ignoring short-term fluctuations, is determined by the level of wind speed. Thus, the instantaneous wind speed can be expressed as a function of a steady mean wind speed $\bar{v}_w(y,z)$ and a field of turbulence $v_T(y,z,t)$ corresponding to the superimposed fluctuating part of the wind speed

$$v(y,z,t) = \bar{v}_w(y,z) + v_T(y,z,t) \tag{3.1}$$

A more common measure of the wind variability is the turbulence intensity index, which is defined as the relation of the standard wind speed deviation to the mean wind speed

$$I_{vT} = \frac{\sigma_w}{\bar{v}_w} \tag{3.2}$$

This index can be up to 20% over forest or urban areas [78].

Other kind of wind fluctuations denominated gusts, also exist and may vary from a few to several tens of seconds. The average wind speed is often modelled by a Weibull distribution function whose density function is given by

$$p(v) = \left(\frac{a}{b}\right)\left(\frac{v}{b}\right)^{a-1} \exp\left[-\left(\frac{v}{b}\right)^{a}\right] \tag{3.3}$$

where $p(v)$ is the probability related to wind speed v, b is the scale factor, and a is the form factor.

The so-called Rayleigh distribution is a special case of Weibull distribution, in which the a parameter is assumed to be equal to 2 [79, 80]. Both distributions fit quite well to most wind histograms and b and a can be determined by applying common estimation methods such as the standard deviation method (SD), the maximum likelihood method (MLM), and the least squares method (LSM) [81]. Wind speed increases with height because of friction at the earth surface [82]. The increase rate of wind speed is given by

$$v(z) = v_0 \left(\frac{z}{z_0}\right)^{\alpha} \tag{3.4}$$

where v is the predicted wind speed at height z and v_0 is the wind speed at height z_0. This results in a significant increase in power greater heights. At the same time, α is an empirical parameter of the wind shear and it can take a value of either $1/7$ (during the day) and $1/5$ (during the night) [83]. For more specialised information on wind speed in wind turbines the following references [84, 85], are particularly useful.

3.3 Mechanical System of a Wind Turbine

The wind mechanical turbine model represents essentially the shaft dynamics of the wind turbine and its control system. The main mechanical turbine components are the blades, hub, shafts and depending on the wind turbine technology, the gearbox.

In this section, the energy conversion process is addressed to explain the role that the drive train elements play in the wind power extraction process. Afterwards the shaft system model is presented.

3.3.1 Principles of wind energy conversion

Elementary momentum theory

The elementary "momentum theory" provides a common physical basis for the understanding and operation of wind energy conversion. The analysis considers a control volume bordered by a surface of a stream tube and two cross-sections of the stream tube, as shown in Fig 3.1. An uniform 'actuator disc' represents the turbine.

This theory states that the kinetic energy of an air mass m, moving at a velocity v can be expressed as

$$E = \frac{1}{2}mv^2 \tag{3.5}$$

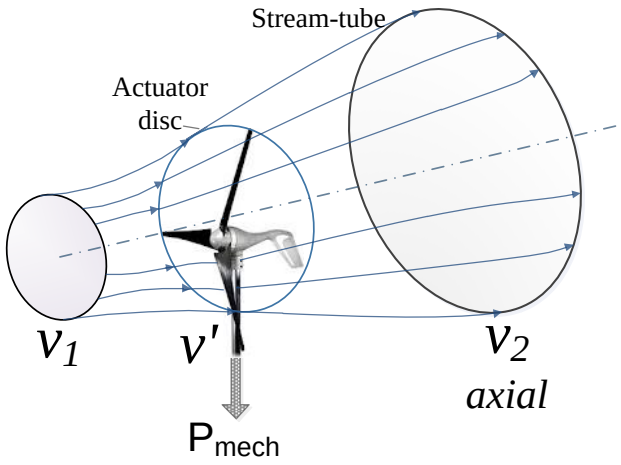

Figure 3.1: Flow model of momentum theory

The volume V flowing through a certain cross-sectional area A, through which the air passes at velocity v, is

$$\dot{V} = vA \tag{3.6}$$

and the mass flow with air density ρ is

$$\dot{m} = \rho vA \tag{3.7}$$

The energy passing through the cross-section A per second, which has been produced by the kinetic energy of the moving air and the mass flow, is identical to the power P

$$P = \frac{1}{2}\rho v^3 A \tag{3.8}$$

The mass flow through the stream-tube must remain unchanged everywhere. Therefore, the flow velocity increases due to its narrow cross-sectional area.

The power difference of the air flow upstream and downstream of the converter yields the mechanical energy that has been previously

extracted from the airflow

$$P = \frac{1}{2}\rho A_1 v_1^3 = \frac{1}{2}\rho A_2 v_2^3 = \frac{1}{2}\dot{m}(v_1^2 - v_2^2) \tag{3.9}$$

Downstream v_1 is the wind velocity before it gets to the converter, whereas v_2 is the flow velocity behind the converter. In theory, the power would reach its maximum level when the downstream velocity is zero. However, the wind speed cannot be reduced to zero in practice. This equation is of great importance since it reveals that the power increases with the cube of wind speed and only linearly with air density and swept area.

Conservation of momentum provides the relationship between the converter thrust, T, and the rate of change of momentum of the airflow,

$$T = \dot{m}(v_1 - v_2) \tag{3.10}$$

The net force on the control volume must be equal and opposite to the converter thrust, which is an equal force exerted by the converter on the air stream. In this sense the required power is

$$P = Fv' = \dot{m}(v_1 - v_2)v' \tag{3.11}$$

Thus the mechanical power extracted from the air stream can be deduced from both, the power difference between the upstream and downstream of the converter and the thrust and the flow velocity. By equating (3.9) and (3.11)

$$\frac{1}{2}\dot{m}(v_1^2 - v_2^2) = \dot{m}(v_1 - v_2)v' \tag{3.12}$$

The power coefficient C_p is defined as the ratio of the wind power and the mechanical power output of the converter,

$$C_p = \frac{P_{\text{wind turbine}}}{P_{\text{air}}} \tag{3.13}$$

A theoretical ideal maximum coefficient C_p, which was derived by Betz [78], is $C_p = \frac{16}{27} = 0.593$ [1]

The dependency of the power coefficient on such a relationship, when looked at from the energy vantage, is what it is termed tip-speed ratio λ, which is determined by the ratio of the rotor blade's tangential velocity in the undisturbed axial airflow and the wind speed. It is commonly referenced to the tangential velocity of the rotor blade tip, u_T.

$$\lambda = \frac{u_T}{v_w} = \frac{\text{tangential velocity of the rotor blade tip}}{\text{wind speed}} \tag{3.14}$$

or

$$\lambda = \frac{\omega R}{v} \tag{3.15}$$

where

ω = rotational speed of rotor

R = radius to tip of rotor

v = upwind free wind speed, $\mathrm{m\,s^{-1}}$

The tip-speed ratio λ, and the power coefficient C_p are dimensionless and are well suited to characterize the performance of any size of wind turbine rotor, as it will be described later in the chapter.

Blade element momentum

The physical framework from which the analysis of conversion of kinetic energy to mechanical energy is developed, should not be separated from the actual capabilities of the energy converter. Under real conditions, the power output depends on the aerodynamic forces that have been employed to produce it.

[1] It is frequently called the Betz factor or Betz limit. Modern wind turbines, operate close to the power coefficient limit, with C_p up to 0.5 and are therefore optimized because of this.

Such forces, expressed as a function of the local aerodynamic lift and drag coefficients, can be derived by using the blade element theory, which divides the rotor blade into a number of elements. Both, the velocity component in the span-wise direction and three-dimensional effects are ignored.

Fig. 3.2 shows all the forces and velocities relative to the blade chord line at radius r. The blade elements are formed by the local rotor blade chord and the radial extension of the element δr. The incident resultant velocity, v_r, is obtained from the combination of the axial flow velocity in the rotor plane and the tangential speed at the radius of the blade cross-section. The angle of attack is an aerodynamic parameter formed from v_r in the cross-sectional plane of the blade. The blade pitch angle is a geometrical parameter (design parameter) referring to the plane of rotation.

The lift force, L, is perpendicular to the flow direction, and the drag force, D, is parallel to the flow direction. These forces are defined by following relations

$$L = \frac{1}{2}\rho_{air} v_r^2 \, c \, C_L \tag{3.16}$$

$$D = \frac{1}{2}\rho_{air} v_r^2 \, c \, C_D \tag{3.17}$$

where c is the chord of the blade section and C_L and C_D are the lift and the drag coefficients, respectively, which can be determined by using the airfoil data catalogues.

The normal and tangential forces, F_N and F_T, acting on the blade sections are

$$F_N = L\cos\phi + D\sin\phi \tag{3.18}$$

$$F_T = L\sin\phi + D\cos\phi \tag{3.19}$$

with ϕ being the angle between the relative velocity and the rotor plane,

$$\phi = \arctan\left(\frac{v_{axial}}{r\omega}\right)$$

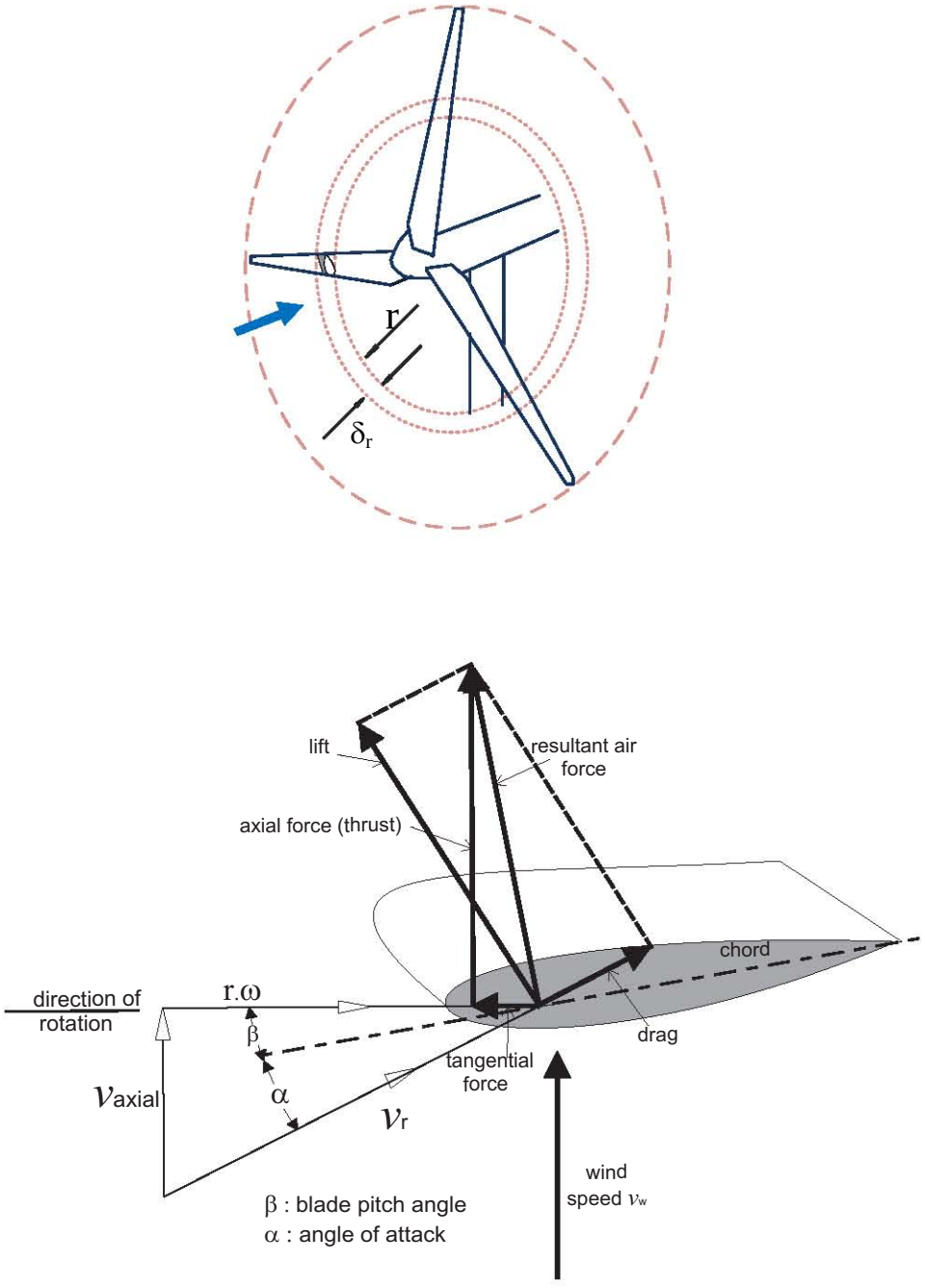

Figure 3.2: Flow velocities and aerodynamics forces at a blade element

On this basis, the exerted forces on the blade element moving though the stream tube-strip can be calculated. Assuming that there is no aerodynamic interference between the strips, the forces on the blade elements distributed over the blade length can be added, and hence the aerodynamic force distribution over the blade length is obtained.

The rotor torque is obtained by the integration of the tangential force distribution and the power coefficient C_p or the rotor power with the rotor speed.

The rotor thrust is obtained from the axial force distribution. Thus, both the rotor performance and the aerodynamic loading for a given rotor geometry can be determined by applying the blade theory.

Further details on theoretical modelling concepts are available in the literature [78, 86, 87].

3.3.2 Wind turbine rotor performance and model for power system studies

The power, torque and rotor thrust are the three main indicators used to assess the performance of a wind turbine, depending on how these vary with wind speed.

The amount of energy taken from the wind and the gearbox size are defined by the power and the developed torque, respectively. The wind turbine tower design is strongly linked to the rotor thrust.

For power system studies the wind turbine is represented by a non-linear wind power model relating power output P_t to wind speed v_w and power coefficient C_p. Since the interest is mainly focused on the input torque, the complex airflow dynamics and their associated mechanical vibrations and deformations are ignored.

The available shaft power Pt is calculated as, [5]

$$P_t = \frac{1}{2}\rho_{air}\, v_w^3\, A_{wt}\, C_p\,(\lambda, \beta) \tag{3.20}$$

where ρ_{air} is the mass density of air, A_{wt} is the wind turbine rotor swept area, the power coefficient C_p, is a function of the tip speed ratio λ_{tip} and the pitch angle β.

Fig. 3.3 illustrates a power coefficient curve with the pitch angle, β as parameter. The power coefficient is maximum for a unique tip-speed ratio. For a fixed-speed wind turbine, operation at maximum power coefficient corresponds to a particular wind speed; however in variable-speed wind turbines it is possible to cover a wide range of wind speeds.

$C_p - \lambda$ curves are obtained from field measurements and are generally provided by manufacturers. Numerical approximations have been used to obtain the $C_p - \lambda$ curves for academic purposes. Using a generic equation developed in reference [49], C_p can be calculated as

$$C_p = c_1 \left(\frac{c_2}{\lambda_i} - c_3\beta - c_4\beta^{c_5} - c_6 \right) \exp \frac{-c_7}{\lambda_i} + c_{10}\lambda \tag{3.21}$$

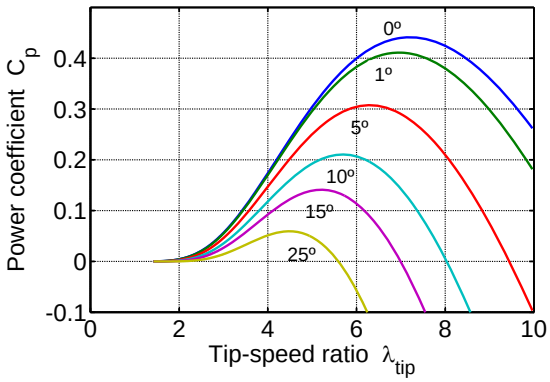

Figure 3.3: Power Coefficient as a function of tip speed ratio and the pitch angle.

where

$$\lambda_i^{-1} = \left[\left(\frac{1}{\lambda + c_8\,\beta}\right) - \left(\frac{c_9}{\beta_3 + 1}\right)\right]^{-1}$$

The C_p parameters c_i, are given in Table 3.1.

A straightforward and convenient way to obtain the dynamic performance relating to the operating point is by means of power and torque coefficients curves resulting from the theoretical analysis mentioned above.

Power curves of wind turbines give the steady-state relationship between the net electrical power output and the wind speed at hub height. These are normally given by the turbine manufacturer.

Fig. 3.4 shows an example of a typical power curve for a wind turbine.

Table 3.1: Approximation of power curve for a variable-speed wind turbine

c_1	c_2	c_3	c_4	c_5	c_6	c_7	c_8	c_9	c_{10}
0.73	151	0.58	0.002	2.14	13.2	18.4	-0.02	-0.003	0

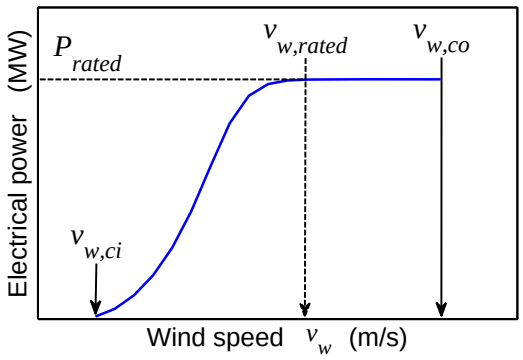

Figure 3.4: Typical Power curve for a wind turbine

The points corresponding to cut-in wind speed, $v_{w,ci}$, and rated wind speed, $v_{w,rated}$, represent the wind speed value at which the machine will deliver the minimum useful power and the rated power, P_{rated}, respectively. Due to safety restrictions, the delivery electrical power is limited at a maximum wind speed, termed cut-out wind speed, $v_{w,co}$. The cut-in and the cut-out wind speed are given by the wind designer. All wind velocities are measured at hub height.

Approximated values for an average annual wind speed of 8 m/s are [5]:

- cut-in wind speed: $5\mathrm{m\,s^{-1}}$
- rated wind speed: $12 - 14\mathrm{m\,s^{-1}}$
- cut-in wind speed: $25\mathrm{m\,s^{-1}}$

In small network disturbance studies a simple turbine model with constant input power or torque (constant wind speed, rotor speed and pitch angle) can be used, since the variation in rotor speed, and hence pitch angle are small.

3.3.3 Shaft system

The shaft system represents the coupling between mechanical and electrical parameters of a wind turbine. For small-signal stability studies of wind turbines with DFIG's, a multi-mass drive train must be considered.

A complete shaft system of a turbine-generator unit can be modelled as three masses connected by two shafts, as shown in Fig. 3.5. It consists of turbine, low-speed shaft, gearbox, high-speed shaft, and generator.

High turbine inertia and low stiffness between the turbine and generator rotor are distinctive characteristics of wind turbines in contrast with conventional steam and hydro turbines [88]. Low mechanical shaft stiffness, viewed from the high-speed shaft, is a result of the gearbox.

A simplified two-mass model, shown in Fig 3.6, can be obtained by comparing the shaft stiffness and the masses of the same speed reference. If $k^*_{LS} = k_{LS}/n^2_{gb}$ is the low-speed shaft stiffness referred to the high-speed side, the high-speed side can be considered rigid respect to the low-speed shaft, since the gear ratio for machines rated between 300 kW and 2000 kW (with higher rotational speeds between 48 and 17 r.p.m.) is between about 1:31 and 1:88 [86].

Thus, one of the masses is related to the wind turbine (low-speed shaft) representing the lumped-mass of hub and blades, while the second mass represents the equivalent shaft, the high-speed shaft, in which gearbox and generator inertia are lumped together. The shaft stiffness in Fig 3.6 is represented by k_{sh}.

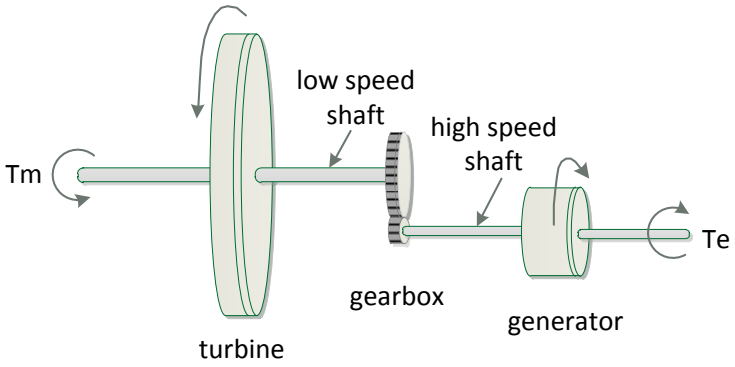

Figure 3.5: Three-mass model of drive train

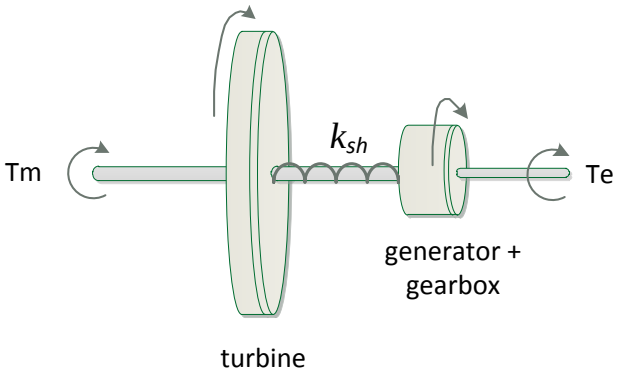

Figure 3.6: Two-mass model of drive train

The two-mass approach is recommended for power system stability studies because the flexibility (or softness) of the shafts are correctly represented [89]. It should be emphasised that the gearbox of the wind turbine represents a low mechanical stiffness, k_{sh}, hence, the two-mass model is used to preserve correctly the drive train dynamics [90].

The resonance frequency of the low speed shaft is in the range between 1 and 2 Hz for multi-megawatt wind turbine generators, and therefore within the frequency band of interest (0.1-10 Hz). The resonance frequencies of the gearbox and the high speed shaft are above this band, hence, these are considered to be infinitely stiff [41].

Moreover, the modes associated with the blades and the hubs are either well damped or their frequencies are out of the range of interest [90].

The dynamics equations for the shaft system can be obtained from Newton's equations of motion for each mass,

$$J_t^* \frac{d\omega_t^*}{dt} = (T_t^* - T_{sh}) \tag{3.22}$$

$$J_g \frac{d\omega_g}{dt} = (T_{sh} - T_e) \tag{3.23}$$

$$\frac{d\theta_{\omega t}}{dt} = \omega_{eleB} \left(\omega_t^* - \omega_g\right) \tag{3.24}$$

with shaft mechanical torque given by:

$$T_{sh} = k_{sh}\, \theta_{\omega_t} + c\, \frac{d\theta_{\omega t}}{dt} \tag{3.25}$$

where J_t and J_g are the inertia of the turbine and generator; ω_t and ω_R are the turbine and generator speed; T_t and T_g are the torques of the turbine and generator; $\omega_{\omega t}$ is the shaft torsional angle; and k_{sh} and c are the equivalent shaft stiffness and damping coefficient. All turbine variables (angular speed and torque) are referred to the generator side of the gearbox and are denoted by a superscripted asterisk.

In power systems it is helpful to normalize all variables and parameters using per unit notation, in order to make all variables dimensionless and simplify the computation and the system analysis. For that, appropriate reference bases should be chosen, and thus the per unit value is given by the ratio between the actual value and the base value,

$$per\ unit\ value = \frac{actual\ value}{base\ value} \tag{3.26}$$

The following base speed and base torque are defined to express the drive train system in per unit values

$$\omega_{tB} = \frac{\omega_{RB}}{n_{gb}} \tag{3.27}$$

$$T_{tB} = T_{eB}\, n_{gb} \tag{3.28}$$

where $\omega_{RB} = \omega_{elB}/n_{pp}$ is the base speed of the generator with ω_{elB} the electrical speed equal to $2\pi f$, and n_{pp} the generator's pole-pair number, $T_{eB} = P_{rated}/\omega_{RB}$ is the base of the generator electrical torque and, n_{gb} is the gearbox ratio.

With the turbine speed inertia and torque referred to the high-speed shaft by $\omega_t^* = n_{gb}\omega_t$, $J_t^* = J_t/n_{gb}^2$ and $T_t^* = T_t/n_{gb}$, respectively, and the turbine bases (ω_{tB}, T_{tB}), equation (3.22) in per unit can be written as

$$\frac{J_t}{n_{gb}^2}\omega_{RB}\frac{\omega_{t_{pu}}}{dt} = T_{eB}(T_{t_{pu}} - T_{sh_{pu}}) \tag{3.29}$$

and together with the inertia constant of the turbine (in seconds),

$$H_t = \frac{1}{2}\frac{J_t\,\omega_{RB}}{n_{gb}^2\,T_{eB}} \tag{3.30}$$

yields to the turbine speed equation,

$$\frac{d\omega_{t_{pu}}}{dt} = \frac{1}{2\,H_t}(T_{t_{pu}} - T_{sh_{pu}}) \tag{3.31}$$

Similarly, the rotor generator speed equation ((3.23)) in per unit form is obtained

$$\frac{d\omega_{g_{pu}}}{dt} = \frac{1}{2\,H_g}(T_{sh_{pu}} - T_{e_{pu}}) \tag{3.32}$$

where the electromagnetic torque, T_e, in per unit, as presented in next section, is calculated as

$$T_e = i_{Sd}\,\Psi_{Sq} - i_{Sq}\,\Psi_{Sd} \tag{3.33}$$

The shaft torque from (3.25) can be expressed in per unit by applying the per unit definition (equation (3.26)) with the stiffness base as $k_B = T_{eB}/(1\,\text{el.rad})$ and the base damping coefficient as $c_B = T_{eB}/(1\,\text{el.rad}/1\,\text{s})$

$$T_{sh_{pu}} = k_{sh_{pu}}\,\theta_{\omega t} + c_{pu}\,\frac{d\theta_{\omega t}}{dt} \tag{3.34}$$

The equation (3.24) for the equivalent twist angle is expressed in actual units (radians). The equations for the drive train system are summarized as below. The system model in this document is assumed to be expressed in per unit notation, therefore the subscript '$_{pu}$' and superscript '*' are omitted, from now on,

$$\frac{d\omega_t}{dt} = \frac{1}{2\,H_t}(T_t - T_{sh}) \tag{3.35}$$

$$\frac{d\omega_g}{dt} = \frac{1}{2\,H_g}(T_{sh} - T_e) \tag{3.36}$$

$$T_{sh} = k_{sh}\,\theta_{\omega t} + c\,\frac{d\theta_{\omega t}}{dt} \tag{3.37}$$

$$\frac{d\theta_{\omega t}}{dt} = \omega_{eleB}\,(\omega_t - \omega_g) \tag{3.38}$$

3.4 Electrical System of a Wind Turbine Equipped with DFIG

Along with the mechanical drive train, the electrical system is a fundamental part of a wind turbine. The electrical system comprises the

components necessary to convert the mechanical energy into electric power, including electrical auxiliaries and control systems.

The electrical generator is the central component for the mechanical/electrical energy conversion process in a wind turbine. Nowadays, wind turbines equipped with double fed induction generators are the most widely used variable speed wind turbine technology for large wind turbines (above 1 MW). It consists essentially of a wound rotor induction generator with slip rings and a back-to-back converter between the rotor slip rings and the grid, and with the stator directly connected to the grid. A typical configuration is shown in Fig. 2.4.

The main features of this generator are:

- The range of rotational speed can be -40% up to $+30\%$ of the synchronous speed [46].
- The frequency converter is rated at approximately 30% of the rated generator power [46, 47].
- The grid frequency (electrical) and the rotor speed (mechanical) are decoupled [48, 49].
- The power is supplied from the stator to the power network and provided or absorbed from the grid through the rotor circuit.

Likewise, the controllability of the electrical system is an important aspect linked to the energy quality of the power system and plays an important role to ensure its security and stability.

3.4.1 Generator Model

The induction generator comprises three-phase windings in the stator $_{S_a}$, $_{S_b}$, $_{S_c}$ and three-phase windings in the rotor $_{R_a}$, $_{R_b}$, $_{R_c}$ distributed 120° as shown Fig. 3.7.

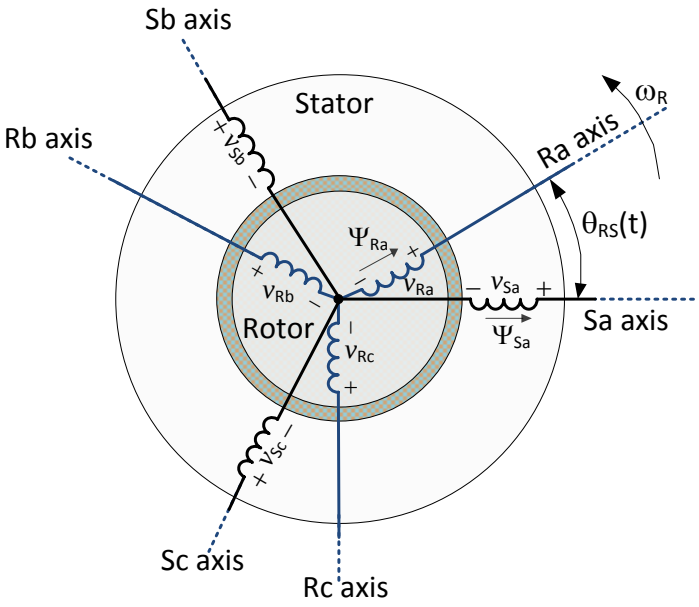

Figure 3.7: Stator and rotor circuits of an induction machine

The angle θ_{SR} corresponds to the angular displacement between the phase $_{S_a}$ of the stator winding and $_{R_a}$ of the rotor winding.

The stator and rotor angular velocity are represented by ω_S and ω_R in electrical radians per second, respectively. The synchronous speed ω_{syn} is given by the ratio of the electrical frequency of the applied stator voltage f_S and the number of pole pairs n_{pp} as

$$\omega_{syn} = \frac{f}{n_{pp}} \tag{3.39}$$

where f is in Hz and, ω_{syn} in rad/s.

When the rotor operates either below or above the synchronous speed, rotor voltages are induced in the rotor windings with a frequency f_R equal to the slip frequency

$$f_R = s\, f_S \tag{3.40}$$

where the slip s is given by

$$s = \frac{\omega_{syn} - \omega_R}{\omega_{syn}} \tag{3.41}$$

Stable state performance

The equivalent circuit of at double fed induction generator is shown in Fig. 3.8. In this, $\underline{\boldsymbol{V}}_S$ and $\underline{\boldsymbol{I}}_S$ represent the phase stator voltage and current, $\underline{\boldsymbol{V}}_R$ and $\underline{\boldsymbol{I}}_R$ the rotor voltage and current, R_S and R_R the stator and rotor resistances, L_{sl} and L_{rl} are the stator and rotor leakage inductances and L_o the magnetizing inductance.

From Fig. 3.8 stator and rotor voltage (referred to the stator) are expressed as

$$\underline{\boldsymbol{V}}_S \;=\; -R_S\,\underline{\boldsymbol{I}}_S + j\omega_S\,L_{sl}\,\underline{\boldsymbol{I}}_S + j\omega_S\,L_o\,(\underline{\boldsymbol{I}}_S + \underline{\boldsymbol{I}}_R) \tag{3.42}$$

$$\frac{\underline{\boldsymbol{V}}_R}{s} \;=\; -\frac{R_R}{s}\,\underline{\boldsymbol{I}}_R + j\omega_S\,L_{rl}\,\underline{\boldsymbol{I}}_R + j\omega_S\,L_o\,(\underline{\boldsymbol{I}}_S + \underline{\boldsymbol{I}}_R) \tag{3.43}$$

The electromechanical torque is given by

$$Te \;=\; 3|\underline{\boldsymbol{I}}_R|^2 R_R \frac{n_{pp}}{s\omega_S} - 3\,\Re\,[\underline{\boldsymbol{V}}_R\,\underline{\boldsymbol{I}}_R^*]\,\frac{n_{pp}}{s\omega_S} \tag{3.44}$$

Then, the torque is slip dependent.

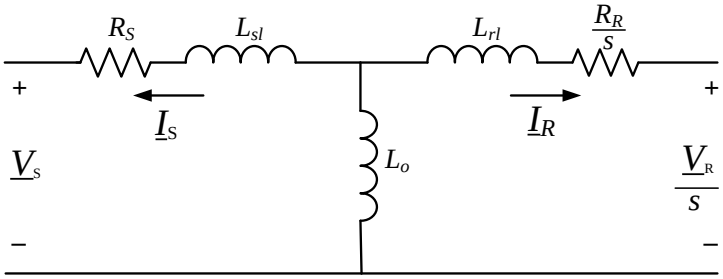

Figure 3.8: Steady-state equivalent circuit of the DFIG

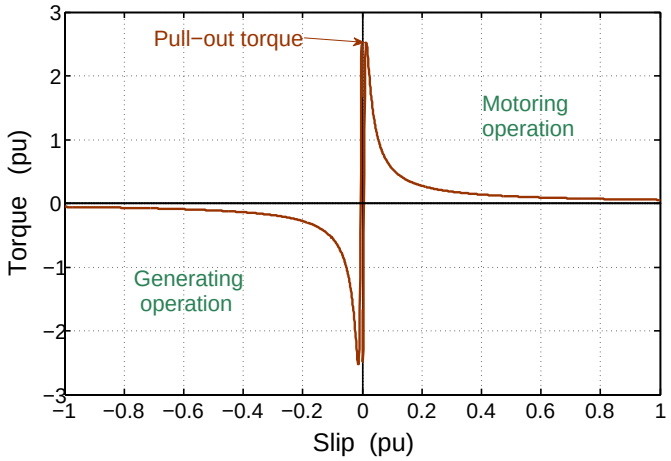

Figure 3.9: Typical torque-slip characteristic of an induction machine

Fig. 3.9 illustrates the relationship between torque and slip. When rotor operates below the synchronous speed (i.e., slip increases) the machine operates in motoring mode; if rotor speed is greater than synchronous speed (negative slip) the machine operates in generating mode.

Dynamic analysis

Depending on stator and rotor windings, the voltage dynamics of the machine can be described by

$$v_{S_a}(t) = -R_S\, i_{S_a}(t) - \frac{d\Psi_{S_a}(t)}{dt} \tag{3.45}$$

$$v_{S_b}(t) = -R_S\, i_{S_b}(t) - \frac{d\Psi_{S_b}(t)}{dt} \tag{3.46}$$

$$v_{S_c}(t) = -R_S\, i_{S_c}(t) - \frac{d\Psi_{S_c}(t)}{dt} \tag{3.47}$$

$$v_{R_a}(t) = -R_R\, i_{R_a}(t) - \frac{d\Psi_{R_a}(t)}{dt} \tag{3.48}$$

$$v_{R_b}(t) = -R_R\, i_{R_b}(t) - \frac{d\Psi_{R_b}(t)}{dt} \tag{3.49}$$

$$v_{R_c}(t) = -R_R\, i_{R_c}(t) - \frac{d\Psi_{R_c}(t)}{dt} \tag{3.50}$$

where $v_{S_a}(t)$, $v_{S_b}(t)$, $v_{S_c}(t)$ are the instantaneous stator voltages of phases a, b, c; $i_{S_a}(t)$, $i_{S_b}(t)$, $i_{S_c}(t)$ are the stator phase currents ; $\Psi_{S_a}(t)$, $\Psi_{S_b}(t)$, $\Psi_{S_c}(t)$ are the stator flux linkages and, R_S is the stator resistance. Similar definitions are applied to the rotor.

Stator and rotor flux linkages are produced by the currents flowing through the windings. By assuming symmetrical stator, and rotor structures and a balanced system ($i_{Sa}+i_{Sb}+i_{Sc}=0$), the flux linkages are given by

$$\begin{pmatrix}\Psi_{Sa}\\ \Psi_{Sb}\\ \Psi_{Sc}\end{pmatrix} = \begin{pmatrix}L_S & L_{S_m} & L_{S_m}\\ L_{S_m} & L_S & L_{S_m}\\ L_{S_m} & L_{S_m} & L_S\end{pmatrix}\begin{pmatrix}i_{S_a}\\ i_{S_b}\\ i_{S_c}\end{pmatrix} + \begin{pmatrix}L_{RS_{aa}} & L_{RS_{ab}} & L_{RS_{ac}}\\ L_{RS_{ba}} & L_{RS_{bb}} & L_{RS_{bc}}\\ L_{RS_{ca}} & L_{RS_{cb}} & L_{RS_{cc}}\end{pmatrix}\begin{pmatrix}i_{R_a}\\ i_{R_b}\\ i_{R_c}\end{pmatrix}$$
$$\begin{pmatrix}\Psi_{Ra}\\ \Psi_{Rb}\\ \Psi_{Rc}\end{pmatrix} = \begin{pmatrix}L_R & L_{R_m} & L_{R_m}\\ L_{R_m} & L_R & L_{R_m}\\ L_{R_m} & L_{R_m} & L_R\end{pmatrix}\begin{pmatrix}i_{R_a}\\ i_{R_b}\\ i_{R_c}\end{pmatrix} + \begin{pmatrix}L_{SR_{aa}} & L_{SR_{ab}} & L_{SR_{ac}}\\ L_{SR_{ba}} & L_{SR_{bb}} & L_{SR_{bc}}\\ L_{SR_{ca}} & L_{SR_{cb}} & L_{SR_{cc}}\end{pmatrix}\begin{pmatrix}i_{S_a}\\ i_{S_b}\\ i_{S_c}\end{pmatrix} \tag{3.51}$$

with

$$\begin{aligned} L_S &= L_{S_{self}} - L_{S_o}\\ L_R &= L_{R_{self}} - L_{R_o}\end{aligned}$$

L_S, L_R are the stator and rotor inductances representing the total self inductance of the winding as the sum of a magnetizing inductance ($L_{S_{self}}$, $L_{R_{self}}$) and a mutual inductance between two windings (L_{S_o}, L_{R_o}).

All other inductances $L_{SR_{aa}}$, $L_{SR_{ba}}$, $L_{SR_{ca}}$, $L_{RS_{aa}}$, $L_{RS_{ab}}$, $L_{RS_{ac}}$, etc., are the mutual inductances between stator and rotor windings. Mutual inductances depend on the angle between the two windings; then for the phase a of stator and rotor windings

$$L_{SR_{aa}} = L_{SR}\cos\theta_{SR} \tag{3.52}$$

where L_{SR} is the peak value of the mutual inductance between stator and rotor windings. Similarly all other mutual inductances are obtained.

Equations (3.45)-(3.51) can be written in the general matrix form as

$$\begin{aligned} \boldsymbol{v}_S &= -\frac{d\boldsymbol{\Psi}_S}{dt} - R_S\,\boldsymbol{i}_S \\ \boldsymbol{v}_R &= -\frac{d\boldsymbol{\Psi}_S}{dt} - R_R\,\boldsymbol{i}_R \qquad (3.53) \\ \boldsymbol{\Psi}_S &= L_S\,\boldsymbol{i_S} + \mathcal{L}_{\mathcal{SR}}\,\boldsymbol{i_R} \\ \boldsymbol{\Psi}_R &= L_R\,\boldsymbol{i_R} + \mathcal{L}_{\mathcal{RS}}\,\boldsymbol{i_S} \qquad (3.54) \end{aligned}$$

where $\boldsymbol{v}_S$, $\boldsymbol{v}_R$, $\boldsymbol{i}_S$, $\boldsymbol{i}_R$ are the three-phase voltage and current vectors, and the matrices $\mathcal{L}_{\mathcal{SR}} = \mathcal{L}_{\mathcal{SR}}$ are

$$\mathcal{L}_{\mathcal{SR}} = L_{SR}\begin{pmatrix} \cos\theta_{SR} & \cos\left(\theta_{SR}+\frac{2\pi}{3}\right) & \cos\left(\theta_{SR}-\frac{2\pi}{3}\right) \\ \cos\left(\theta_{SR}-\frac{2\pi}{3}\right) & \cos\theta_{SR} & \cos\left(\theta_{SR}+\frac{2\pi}{3}\right) \\ \cos\left(\theta_{SR}+\frac{2\pi}{3}\right) & \cos\left(\theta_{SR}-\frac{2\pi}{3}\right) & \cos\theta_{SR} \end{pmatrix} \qquad (3.55)$$

d-q Model

The dynamic equation of a three-phase DFIG can be represented in the *d-q* frame since the resultant equations are especially suited for control and simulation purposes.

The Park transformation can be written as

$$\boldsymbol{x}_{dq} = \begin{bmatrix} x_d \\ x_q \end{bmatrix} = \mathbf{T}(\theta)\ \begin{bmatrix} x_a \\ x_b \\ x_c \end{bmatrix} \qquad (3.56)$$

with

$$\mathbf{T}(\theta) = K\begin{bmatrix} \sin\theta & \sin(\theta-\frac{2\pi}{3}) & \sin(\theta+\frac{2\pi}{3}) \\ \cos\theta & \cos(\theta-\frac{2\pi}{3}) & \cos(\theta+\frac{2\pi}{3}) \\ \frac{1}{\sqrt{2}} & \frac{1}{\sqrt{2}} & \frac{1}{\sqrt{2}} \end{bmatrix} \qquad (3.57)$$

where θ is the rotation angle and the factor K is taken as usually $\sqrt{\frac{2}{3}}$ for power invariant transformations.

By applying the transformation to equations (3.45)-(3.50)

$$v_{Sd} = -R_S\, i_{Sd} - \frac{d\Psi_{Sd}}{dt} - \omega_S \Psi_{Sq} \tag{3.58}$$

$$v_{Sq} = -R_S\, i_{Sq} - \frac{d\Psi_{Sq}}{dt} + \omega_S \Psi_{Sd} \tag{3.59}$$

$$v_{Rd} = R_R\, i_{Rd} - \frac{d\Psi_{Rd}}{dt} - s\,\omega_S \Psi_{Rq} \tag{3.60}$$

$$v_{Rq} = -R_R\, i_{Rq} - \frac{d\Psi_{Rq}}{dt} + s\,\omega_S \Psi_{Rd} \tag{3.61}$$

with rotor and stator d-q fluxes given by

$$\Psi_{Sd} = L_S\, i_{Sd} + L_o\, i_{Rd} \tag{3.62}$$

$$\Psi_{Sq} = L_S\, i_{Sq} + L_o\, i_{Rq} \tag{3.63}$$

$$\Psi_{Rd} = L_R\, i_{Rd} + L_o\, i_{Sd} \tag{3.64}$$

$$\Psi_{Rq} = L_R\, i_{Rq} + L_o\, i_{Sq} \tag{3.65}$$

Per unit

In order to normalize the electrical system, the power and the voltage are usually chosen as base quantities; that is to say, equal to one per unit under rated condition.

The wind turbine electrical system in dq-axis reference frame ((3.58)-(3.61)) is described in per unit (pu) values based on nominal voltage, on the three-phase nominal power of the generator, and on the electrical speed of the generator,

$$V_B = \sqrt{3} V_{LL_{rated}} \quad [\,\mathrm{V}\,] \tag{3.66}$$

$$S_B = S_{3\phi,rated} \quad [\,\mathrm{VA}\,] \tag{3.67}$$

$$\omega_{elB} = 2\pi f \quad \left[\frac{\text{el.rad}}{\text{s}}\right] \tag{3.68}$$

where f is the electrical grid frequency in Hz.

Thus, the base current and impedance are defined as

$$I_B = \frac{S_B}{V_B} \quad [\mathrm{A}]\,, \qquad Z_B = 3\frac{V_B^2}{S_B} \quad [\,\Omega\,]$$

The base voltage of low and high voltage side are referred to the same side by the turns ratio of the transformer. The mechanical and electrical speeds are related by the pole-pair number as

$$\omega_{RB} = \frac{\omega_{elB}}{n_{pp}} \quad \left[\frac{\text{mech.rad}}{\text{s}}\right] \tag{3.69}$$

The bases of the electromagnetic and turbine torque are given by $T_{eB} = S_B/\omega_{RB}$ and $T_{tB} = S_B/\omega_{tB}$, respectively, with $\omega_{tB} = \omega_{RB}/n_{gb}$ as defined in the previous section. The base torque is in [Nm].

With the per-unit definition in (3.26), stator and rotor voltage equations in *d-q* reference frame ((3.58)-(3.61)) in per-unit notation can be rewritten as

$$v_{Sd} = -R_S\, i_{Sd} - \frac{1}{\omega_{elB}}\frac{d\Psi_{Sd}}{dt} - \omega_S \Psi_{Sq} \tag{3.70}$$

$$v_{Sq} = -R_S\, i_{Sq} - \frac{1}{\omega_{elB}}\frac{d\Psi_{Sq}}{dt} + \omega_S \Psi_{Sd} \tag{3.71}$$

$$v_{Rd} = -R_R\, i_{Rd} - \frac{1}{\omega_{elB}}\frac{d\Psi_{Rd}}{dt} - s\,\omega_S \Psi_{Rq} \tag{3.72}$$

$$v_{Rq} = -R_R\, i_{Rq} - \frac{1}{\omega_{elB}}\frac{d\Psi_{Rq}}{dt} + s\,\omega_S \Psi_{Rd} \tag{3.73}$$

$$\Psi_{Sd} = L_S\, i_{Sd} + L_o\, i_{Rd} \tag{3.74}$$

$$\Psi_{Sq} = L_S\, i_{Sq} + L_o\, i_{Rq} \tag{3.75}$$

$$\Psi_{Rd} = L_R\, i_{Rd} + L_o\, i_{Sd} \tag{3.76}$$

$$\Psi_{Rq} = L_R\, i_{Rq} + L_o\, i_{Sq} \tag{3.77}$$

Notice that subscript "*pu*" is not indicated in the previous equations as the model used in the remainder of this text is expressed in per-unit (unless otherwise stated).

The electromagnetic torque expression in per-unit can be written in terms of stator and rotor flux as

$$T_e = \frac{L_o}{L_S L_R - L_o^2} \left(\Psi_{Rd}\Psi_{Sq} - \Psi_{Rq}\Psi_{Sd}\right) \tag{3.78}$$

3.5 Converter System and Control Strategies

The DFIG is connected to the grid by two power converters to form a back-to-back HVDC-link as shown schematically in Fig. 3.10. The link consists of two VSCs, one connected to the rotor of the DFIG and the other to the grid-side. The two VSCs share a common capacitor on their dc-sides.

The range of rotor speed variation is dependent on the rating of the rotor VSC. The grid-side VSC is used to regulate the active and reactive power exchange between the generator and the grid. This is represented as a controlled current source injecting an ac current at grid frequency to the network. The machine-side converter (MSC) is related to the active power flow control. The MSC is controlled such that maximum wind power is extracted at sub-synchronous regimes and constant torque is tracked at synchronous regime.

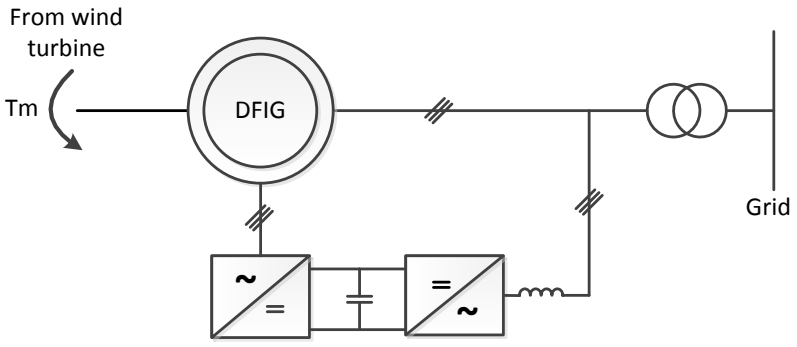

Figure 3.10: Schematic of a DFIG-based wind turbine.

The DFIG converter control has been generally dealt with classical methods. The most widely employed control techniques are based on field oriented control (FOC) [91] and direct control techniques like the direct control torque (DTC), direct self control (DSC) and direct power control (DPC) [92, 93, 94]. The direct control techniques, as applied to the DFIG, are based on rotor flux regulation as opposed to stator flux regulation which applies to squirrel cage induction machine.

Technological advances have lead to develop more efficient strategies based on advanced and modern control techniques such as Fuzzy Logic Control, Robust Control, Adaptive Control, etc. Among them, Sliding Mode Control (SMC) emerges as a particularly suitable option to deal with electronically controlled variable speed operating WECS. Interest in this control approach has emerged due to its potential to eliminate the effects of parameter variations with minimum complexity of implementation [6], [7]. The non-linear SMC technique has been widely applied in variable-speed wind systems but it has been applied at only the mechanical system, i.e., the thrust has been on power maximization and on the pitch controller.

In this thesis a non-linear technique based on Sliding Mode Control (SMC) is put forward as an alternative approach to control the converter of a DFIG-based wind system. A FOC based scheme is also applied as a basis of comparison with the new results obtained with the proposed SMC.

3.5.1 Machine Side Converter

3.5.2 Field Oriented Control (FOC)

The control of the MSC has been generally carried out by the classical field-oriented control to carry out a decoupled regulation of active and reactive power delivery through the stator. In the FOC method, the active and reactive powers are controlled separately by means of d-q components of the rotor currents using PI controllers [95].

The block diagram of the FOC in a DFIG application is shown in Fig. 3.11. In this control scheme, the dq-axis frame of reference is linked to the stator voltages, with the stator flux vector in the direction of the d-axis. Hence, the components of the stator voltage vectors are $v_{Sd} = 0$ and $v_{Sq} = |\underline{v}_S|$.

Using the current-dependent flux expressions (3.74)-(3.77),

$$i_{Sq} = -\frac{L_o}{L_R} i_{Rq} \tag{3.79}$$

Neglecting the stator resistances, the active and reactive powers generated by the machine may be written down as:

$$P_S = v_{Sq}\, i_{Sq} = -v_{Sq} \frac{L_o}{L_R} i_{Rq} \tag{3.80}$$

$$Q_S = -v_{Sq}\, i_{Sd} = \omega_S \left(L_S\, i_{Sd} + L_o\, i_{Rd}\right) i_{Sd} \tag{3.81}$$

The size of the rotor-side converter is determined bearing in mind the power distribution in both circuits of the machine and, at the same time, being capable of controlling the supplied power to the rotor circuit.

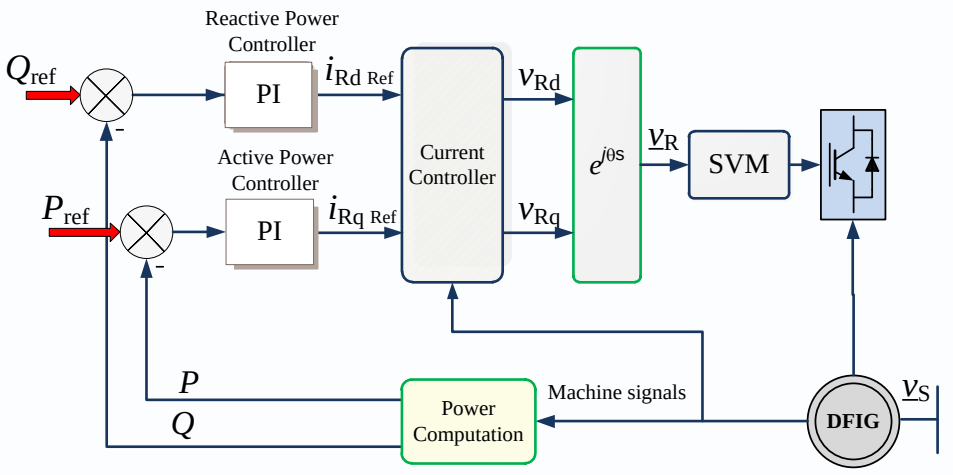

Figure 3.11: Block diagram of a vectorial control of a DFIG.

The reference values for the rotor currents are determined from the steady-state relationship between the rotor and stator currents, with the stator resistance neglected,

$$\underline{i}_R = \frac{\underline{v}_S}{\omega_S L_o} - \frac{L_S}{L_o}\underline{i}_S \tag{3.82}$$

Assuming known values of the stator reference active and reactive powers, the corresponding reference currents referring to the rotor are

$$i_{Rd_{Ref}} = \frac{|\underline{v}_S|}{\omega_S L_o} + \frac{L_S}{|\underline{v}_S| L_o} Q_{S_{Ref}} \tag{3.83}$$

$$i_{Rq_{Ref}} = -\frac{L_S}{L_o} i_{Sq} P_{S_{Ref}} \tag{3.84}$$

The rotor voltage components are obtained from the dynamic equations of the machine-side controller as follows.

For the d-axis control loop

$$\frac{dX_{Q_S}}{dt} = Q_{S_{Ref}} - Q_S = Q_{S_{err}} \tag{3.85}$$

$$\frac{dX_{id}}{dt} = K_{Q_S} Q_{S_{err}} + \frac{K_{Q_S}}{T_{Q_S}} X_{Q_S} - i_{Rd} \tag{3.86}$$

$$u_{Rd} = K_{id} \frac{dX_{id}}{dt} + \frac{K_{id}}{T_{id}} X_{id} \tag{3.87}$$

For the q-axis control loop

$$\frac{dX_P}{dt} = P_{Ref} - P = P_{err} \tag{3.88}$$

$$\frac{dX_{iq}}{dt} = K_P P_{err} + \frac{K_P}{T_P} X_P - i_{Rq} \tag{3.89}$$

$$u_{Rq} = K_{iq} \frac{dX_{iq}}{dt} + \frac{K_{iq}}{T_{iq}} X_{iq} \tag{3.90}$$

where $Q_{S_{err}}$ is the reactive power error; X_{Q_S} is the state variable of the outer controller; X_{i_d} is the state variable of the inner controller, P_{err} is the active power error; X_P and X_{i_q} are the state variables of the outer and inner controllers. The parameters K_{id}, K_{iq}, K_P, K_{Q_S} are the

controller proportional gains (P-gains). The parameters T_{i_d}, T_{i_q}, T_P, T_{Q_S} are the controller reset times or integral times (I-times).

3.5.3 Sliding Mode Control (SMC)

The design of the rotor controller is developed through a theoretical framework based on the combination of a geometric approach and sliding mode techniques, as put forward in [96]. The key idea of sliding-mode control (SMC) is to allow a desired performance of the system to follow a specified sliding surface. Interest in this control approach has emerged due to its potential to eliminate the effects of parameter variations with minimum complexity of implementation [6, 7].

Design method

The sliding mode control design consists of two steps:

- First Step: selection of an equilibrium sliding surfaces (x), such that the internal zero-dynamics is stable and the enforcing sliding mode in this manifold $(x) = 0$. Considering the non-linear system

$$\begin{aligned} \dot{x} &= A\,x + B\,u + h \\ y &= s(s) \end{aligned} \tag{3.91}$$

  where $x \in \Re^n$, $u(x) \in \Re^m$, $B(x) \in \Re^{nxm}$, and $y \in \Re$.

  x, u, and B, represent the state, control vectors and control input matrix, h represents the external uncertainties and disturbances. The disturbances are assumed to be bounded as follows: $|h_1| \leq H_1$, $|h_2| \leq H_2$.

  The system (3.91) is transformed to the regular form [6]

$$\dot{x_1} = A_{11}\,x_1 + A_{12}\,x_2 + h \tag{3.92}$$

$$\dot{x_2} = A_{21}\,x_1 + A_{22}\,x_2 + B_2\,u + h \tag{3.93}$$

where $x_1 \in \Re^{n-m}$, $x_2 \in \Re^m$, and B_2 is an mxm non-singular matrix.

Let the tracking error $e = x^* - x$ where x^* is the commanded value. The system can be expressed as

$$\frac{de}{dt} = \dot{e} = A\,e + B\,u + \hat{h} \tag{3.94}$$

where $\hat{h} = h - (A - I)x^*$.

The sliding mode manifold can be defined as

$$s = Ce = \begin{bmatrix} F & b_2 \end{bmatrix} \begin{bmatrix} e_1 \\ e_2 \end{bmatrix} = Fe_1 + e_2 \tag{3.95}$$

with $F \in \Re^{mxn}$ The state vector e_2 is selected as a function of the state vector e_2 as

$$e_2 = -F\,e_1 \tag{3.96}$$

Shaping the desired dynamics of the system

$$\dot{e_1} = (A_{11} - A_{12}F)e_1 \tag{3.97}$$

where matrix F is chosen such that $A_{sys_{SM}} = A_{11} - A_{12}F$ has stable eigenvalues and the system response has the desired behaviour while the system is in sliding mode.

- Second Step: After switching surface design, the next important aspect is guaranteeing the existence of a sliding mode. These conditions may be derived from a Lyapunov function

$$\begin{aligned} V(x) &> 0 \\ V(x) &= \frac{1}{2}s^T\,s \end{aligned} \tag{3.98}$$

The time derivative of $V(x)$ is given by

$$\dot{V}(x) = \frac{1}{2}s^T\frac{\partial s}{\partial x}\dot{x} = s^T\frac{\partial s}{\partial x}\left(f(x) + B(x)u\right) \tag{3.99}$$

where $s = \left[s_1, s_2, ..., s_m\right]^T$ and $\dfrac{\partial s}{\partial x} = \left[\dfrac{\partial s_1}{\partial x}, \dfrac{\partial s_2}{\partial x}, ..., \dfrac{\partial s_m}{\partial x}\right]^T_{mxn}$

In order to design a sliding mode control scheme to drive the system trajectories onto the sliding mode $s = 0$ for $t > 0$, it may be assumed that $\dot{s}(x) = 0$ too, and then the equivalent control law is obtained. From (3.95)

$$u(x) = -\left[\frac{\partial s}{\partial x}B\right]^{-1}\left[\frac{\partial s}{\partial x}A\right] \tag{3.100}$$

and substituting $u(x)$ into (3.91) to yield the sliding mode dynamics as

$$\dot{x} = A + B\left(-\left[\frac{\partial s}{\partial x}B\right]^{-1}\left[\frac{\partial s}{\partial x}A\right]\right) \tag{3.101}$$

Sliding surfaces of a DFIG

In a wind turbine DFIG is necessary to regulate both, the active and the reactive power to a set point ordered by the wind farm control system. This is so in order to meet the demanded generation control capability by the grid connection requirements [97, 98].

The block diagram of the SMC in a variable speed wind turbine application in this research project is shown in Fig. 3.12.

The reference value for the stator active power is determined from the electromagnetic torque expression given by (3.78) and by the flux-currents relationship between the rotor and the stator ((3.74)-(3.77)).

The objective of active power control can be set through the individual sliding manifold determined by

$$s_1 = P_{S_{Ref}} - \left(\frac{-\omega_S\, L_o\, \Psi_{Sd}\, \Psi_{Rq}}{\sigma\, L_S\, L_R}\right) \tag{3.102}$$

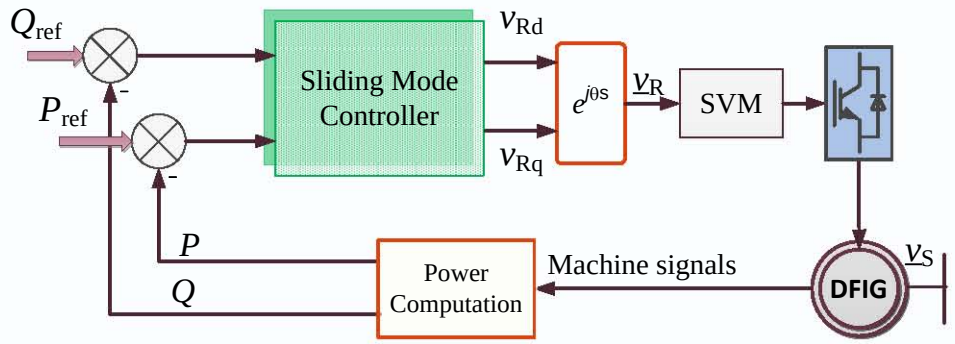

Figure 3.12: Block diagram of a sliding mode control of a DFIG.

The second objective control is the reactive power tracking, defined by considering the minimization of the DFIG's copper losses. It can be expressed through the following sliding variable:

$$s_2 = Q_{Ref} - \left(-\frac{L_o \, |\underline{v}_S| \, i_{Rd}}{\omega_S \, (L_S + L_o)} - \frac{|\underline{v}_S|^2}{\omega_S \, L_o} \right) \tag{3.103}$$

3.5.4 Grid Side Converter

Since the DFIG-based wind system is particularly sensitive to voltage variations, disturbed grid voltage conditions have to be considered in the GSC control design. The dc-link voltage is kept constant by the control of the grid-side converter and ensures steady active power output from the whole system. As GSC controls affect primarily the dynamics of dc-link, they are not specifically applied to wind driven DFIG applications. These dynamic characteristics of the dc link can be well encapsulated by representing their impact on the DFIG's rotor by a dynamic equivalent voltage source, which is a function of the power balance at the dc bus,

$$P_{dc} = P_g + P_R \tag{3.104}$$

$$P_{dc} = v_{dc} \, i_{dc} = C \, v_{dc} \, \frac{dv_{dc}}{dt} \tag{3.105}$$

According to the DFIG-converter configuration, it can be stated that

$$P_R = P_{output} - P_S \tag{3.106}$$

Moreover, in accordance with (3.104) and (3.105),

$$P_g = P_{output} - P_S \tag{3.107}$$

the dc link voltage will be kept around its reference value. An exhaustive literature search indicates that the GSC controls employ PI controllers where the dc link voltage and the reactive power are commanded by different loop controls.

Regarding reactive power flow control, different operating strategies may be pursued depending on the sharing of reactive power production between the DFIG stator and the grid-side converter [91, 99, 100].

Control of the DFIG based on SMC has been addressed both under ideal [101, 102] and unbalanced grid voltage conditions [103, 104]. In [101] a non-linear sliding-mode control scheme was employed in a direct active and reactive power control (DPC) of a grid-connected DFIG-based wind turbine system. In [104] a DFIG-based wind turbine operating under unbalanced and/or harmonically distorted grid voltage conditions was addressed.

In this work, the control of the GSC is carried out using SMC under grid disturbances to assess the dynamical control performance of the DFIG.

3.6 Conclusions

In this chapter a wind turbine system model with double fed induction generator was presented. The turbine performance was described by means of the energy conversion theory and general considerations regarding simulations for wind turbines in electrical power systems were

presented. Simple turbine model assuming constant wind speed, rotor speed and pitch angle can be used in studies in which the variation in rotor speed is small as in the case of small disturbance studies with constant wind speed. However it is not suitable for studies with changing wind speed or significant rotor speed variation.

Non-linear algebraic models in which power output is obtained from the wind speed were used in power system stability analysis. The drive train was modelled by the two-mass model approach in order to represent correctly the shaft dynamics. The electrical system model was expressed in per-unit notation and d-q reference frame. The converter configuration was described and the machine side controller was detailed. The rotor voltage was determined either applying FOC-based or SMC-based algorithm. In the scheme put forward, the grid-side converter controls regulate the reactive power which flows through converter to grid and influence mainly the dc-link dynamics by maintaining the voltage of dc-capacitor into a fixed value.

Chapter 4

Double-fed Induction Generator Grid Connected applying Sliding Mode Control

The small-signal stability assessment of a wind turbine with doubly-fed induction generator under sliding mode control is carried out in this chapter. The Double-fed Induction Generator is represented by its seventh order model and subjected to a wide range parameter variation aiming at carrying out a rather comprehensive dynamic stability assessment of the system. In order to evaluate the impact that controllers have on the system modes of a Double-fed Induction Generator-based wind system, the sliding mode control (SMC) algorithm is used and compared to the classical field-oriented control (FOC).

4.1 Background

Wind energy has shown to be one of the most competitive and efficient renewable energy sources and, as a result, its use is continuously increasing. It has been reported that in June 2010, the total installed

wind energy capacity around the world stood at 175,000 MW [105]. However, incorporation of wind energy units into power networks not only modifies power flows but may also induce under-voltages or over-voltages at specific points of the network [106], as well as in certain cases introduce dynamic stability problems. Doubly-Fed Induction Generators (DFIG) are the most widespread technology around the world and they offer the ability of a decoupled PQ control and the possibility of maintaining their steady state under small perturbations. The increase of wind energy penetration based on power converters is reducing the effective inertia of power networks [107], increasing thus the need to improve the dynamic behaviour of WTs under disturbances.

When performing small signal and transient stability analysis, models of generators, shafts and their controls must be accurate within the range of oscillation modes. The use of inaccurate models of equipment and controls will yield erroneous results in most cases [108]. In [109], a two-axis model with constant lumped parameters is used for transient stability analysis in which the mechanical part of the turbine is all but omitted. Also it is customary to neglect the stator dynamics [55, 110, 111]. However, the associated modes could have significant effects on DFIG transient behaviour, as it has been shown in [112].

Classic controllers of DFIGs are usually based on Field Oriented Control (FOC), where its performance relies on the tuning of the PI parameters according to the adopted model of the wound induction machine, the flexible shaft coupling and the converters. Very little research has been done on analyzing the effect of non-linear control on the improvement of the stability assessment. Technology break-throughs have allowed the incorporation of advanced control systems into wind energy generation systems (WECS) and the development of more efficient strategies based on modern control techniques such as: Fuzzy Logic Control, Robust Control, Adaptive Control, etc. Among them, Sliding Mode Control (SMC) emerges as a particularly suitable option

to deal with electronically controlled variable speed operating WECS. Interest in this control approach has emerged due to its potential to eliminate the effects of parameter variations with minimum complexity of implementation [6], [7]. In recent years, the application of SMC techniques to electrical drives and wind-energy generation [113], [114] has been studied.

The small-signal stability of a wind turbine with DFIG has been assessed under different operating modes and control tuning [115]. However, the study was carried out using the 5^{th} reduced order model (ROM) of the induction generator and the control representation was simplified and based on decoupled vector control principles.

To overcome these limitations, this study uses a full 7^{th} order DFIG model. The model comprises the wind turbine, the DFIG and its associated back-to-back HVDC link and its associated controls. Connection of the DFIG to a strong equivalent grid is assumed at this stage of development. This study is particularly useful to check the stability of the DFIG itself and its controls.

The dynamic stability of the system is investigated by eigenvalue assessment for a wide range of parameter variations. The modal analysis carried out elucidates the main effects existing on system modes of a DFIG-based wind system by applying the classical FOC control and the SMC techniques. This study may form basis on which to establish guidelines to improve the small-signal stability of DFIG wind turbines by applying non-linear controls such as the SMC. The results were obtained with a computer program written in MATLAB.

4.2 Simulation and Results

The small-signal stability of a DFIG directly connected to an equivalent grid is studied by examining the eigenvalues, eigenvalue properties and participation factors for a number of different system conditions.

The simulation used for this analysis contains models of the turbine, drive train, generator, electrical network and controllers.

It is important to emphasize how the dynamic behaviour of the DFIG-based WT system changes under different modes of operation.

First, modal analysis (analysis of eigenvalue locations, eigenvalue properties and participation factors) of the open-loop DFIG is carried out to gain a solid understanding of the inherent strengths and weaknesses of the system with no control.

From the linearised DAE model (2.8), the system state matrix, A_{sys} can be obtained:

$$\Delta\dot{x} = A_{sys}\,\Delta x \tag{4.1}$$

The state vector is defined by

$$x = \begin{bmatrix} i_{Sd} & i_{Sq} & e_{Sd} & e_{Sq} & \omega_t & \omega_R & \theta_{\omega t} \end{bmatrix}^T \tag{4.2}$$

The terminal voltage is 1 pu and remains constant throughout the simulation. The reactive power output is zero. The parameters of the DFIG wind turbine system are listed in Table 4.1.

The linearised model (4.1) is used for the small-signal stability analysis. For the given case of the DFIG-based WT system, the charac-

Table 4.1: DFIG-WT DATA

DFIG parameters

$\boldsymbol{R_S}$ (pu)	$\boldsymbol{R_R}$ (pu)	$\boldsymbol{L_o}$ (pu)	$\boldsymbol{L_{sl}}$ (pu)	$\boldsymbol{L_{rl}}$ (pu)	$\boldsymbol{H_g}$ (s)	$\boldsymbol{n_{pp}}$	$\boldsymbol{P_{w_{rated}}}$ (MW)
0.0048	0.0059	3.953	0.092	0.099	2.5	2	2

$\boldsymbol{H_t}$ (s)	$\boldsymbol{k}$ ($\frac{\text{pu}}{\text{el.rad}}$)	$\boldsymbol{c}$ ($\frac{\text{pu.s}}{\text{el.rad}}$)	$\boldsymbol{v_{w_{rated}}}$ ($\frac{\text{m}}{\text{s}}$)	$\boldsymbol{R_{blade}}$ (m)	$\boldsymbol{n_{gb}}$	$\boldsymbol{C_{p_{max}}}$	$\boldsymbol{\lambda_{tip_{opt}}}$
0.5	0.3	0.01	17	45	100.5	0.45	7.84

teristic equation is a seventh-order equation; thus, it will yield seven eigenvalues for a specific steady-state value of the rotor speed. Therefore, in general, one of the eigenvalues must be real and the other six eigenvalues form three sets of complex conjugate pairs.

4.2.1 Effect of operating point

Synchronous operation: Firstly, the grid-connected DFIG wind turbine system at zero slip is studied. The active power injection to the grid is 0.5806 pu.

Table 4.2 shows the eigenvalues, eigenvalue properties and participation factors of the dominant states of the WT-DFIG at this operating point. It can be seen that the system is dynamically stable, since all the real parts of the eigenvalues have negative values.

There are three oscillating modes associated with stator and rotor dynamics and one non-oscillating mode associated with rotor dynamics. The mode with the highest oscillation frequency is an electrical mode associated with the DFIG stator state variables (i_{Sd}, i_{Sq}) which oscillates around 50 Hz. The medium frequency, at about 6 Hz, is an electro-mechanical mode associated with rotor electrical and rotor mechanical dynamics. It is contributed by the internal voltage e_{Sd}, and generator speed ω_R.

The lowest frequency mode is a mechanical mode associated with shaft and turbine dynamics, by torsion angle $\theta_{\omega t}$ and turbine speed ω_t, of frequency about 0.6 Hz. It is the dominant mode.

Table 4.2: Eigenvalues, properties and participation factors of the DFIG-WT at zero-slip

λ_i	$\sigma_i \pm j\omega_i$	f_{osc} (Hz)	ζ_i (pu)	p_{ni}
$\lambda_{1,2}$ (E)	-8.024 $\pm j$313.92	49.962	0.0255	i_{Sd} 50% i_{Sq} 50%
$\lambda_{3,4}$ (EM)	-6.159 $\pm j$41.699	6.6360	0.1461	e_{Sd} 48% ω_R 50%
$\lambda_{5,6}$ (M)	-0.600 $\pm j$4.1579	0.6610	0.1429	ω_t 50% θ_{ω_t} 47%
λ_7 (E)	-9.757	-	-	e_{Sq} 100%

The non-oscillating mode is a real eigenvalue associated with rotor electrical dynamics, by the internal voltage e_{Sq}. As it can be seen from Table 4.2, the $\lambda_{1,2}$ is a poorly damped mode ($\sim 2.5\%$). All other modes are well damped ($\zeta > 10$ %).

Sub/super-synchronous operating: In these cases, the total active power injected at the point of common coupling is 0.26146 pu at the sub-synchronous regime and 0.99583 pu at the super-synchronous regime.

Table 4.3 shows the eigenvalues, eigenvalue properties and participation factors of the dominant states of the WT-DFIG at sub-synchronous speed and Table 4.4 shows similar information but for the super-synchronous speed. It can be observed that the system is dynamically stable at both operating modes.

There are three oscillating modes associated with stator and rotor dynamics and one non-oscillating mode associated with mechanical dynamics. The mode with the highest oscillation frequency is an electrical mode associated with the DFIG stator state variables (i_{Sd}, i_{Sq}) which oscillates around 50 Hz. The medium frequency electrical mode, about 12-13 Hz, is associated with the rotor through the dynamics of the internal voltages e_{Sd} and e_{Sq} and a small contribution of rotor speed ($\sim 12\%$).

Table 4.3: Eigenvalues, properties and participation factors of the WT-DFIG at sub-synchronous operation

λ_i	$\sigma_i \pm j\omega_i$	f_{osc} (Hz)	ζ_i (pu)	p_{ni}
$\lambda_{1,2}$ (E)	-8.044 $\pm j$313.85	49.951	0.0256	i_{Sd} 50% i_{Sq} 50%
$\lambda_{3,4}$ (EM)	-8.086 $\pm j$84.031	13.374	0.0957	e_{Sd} 50% e_{Sq} 40% ω_R 12%
$\lambda_{5,6}$ (EM)	-3.078 $\pm j$8.910	1.418	0.3265	θ_{ω_t} 54% ω_R 33% ω_t 10% e_{Sq} 8%
λ_7 (M)	-0.881	-	-	ω_t 80% ω_R 17%

Table 4.4: Eigenvalues, properties and participation factors of the WT-DFIG at super-synchronous operation

λ_i	$\sigma_i \pm j\omega_i$	f_{osc} (Hz)	ζ_i (pu)	p_{ni}
$\lambda_{1,2}$ (E)	-8.014 $\pm j$313.96	49.969	0.02551	i_{Sd} 50% i_{Sq} 50%
$\lambda_{3,4}$ (EM)	-10.380 $\pm j$74.47	11.853	0.13805	e_{Sd} 50% e_{Sq} 30% ω_R 15%
$\lambda_{5,6}$ (EM)	-1.278 $\pm j$9.098	1.4481	0.13918	θ_{ω_t} 50% ω_R 27% ω_t 10% e_{Sq} 10%
λ_7 (M)	-0.00157	-	-	ω_t 77% ω_R 15%

The lowest frequency mode is contributed by shaft and rotor dynamics, by $\theta_{\omega t}$, ω_R and to a lesser extent by e_{Sq} ($\sim$ 10%), with an oscillation frequency of about 1.4 Hz. The non-oscillating mode is the dominant mode and consists in a mechanical mode contributed by the generator speed ω_R, and turbine speed ω_t. The stability margin of the low frequency and non-oscillating mode is smaller at super-synchronous operation.

The operating point has a significant effect on all the eigenvalues, except for the high frequency mode. Oscillation frequency of the $\lambda_{3,4}$ and the$\lambda_{5,6}$ modes is lower in the synchronous mode. At sub-synchronous operation, the damping ratio of the $\lambda_{3,4}$ mode is lower and the damping ratio of the $\lambda_{5,6}$ increases almost twice. At super-synchronous operating, the values of the damping ratio of all the modes are the same as those found in the case of synchronous operation.

Participation factors are also affected; in synchronous mode, dynamics tend to be more coupled.

As expected, the mechanical mode is the slowest mode at all speeds.

4.2.2 Effect of machine parameters

Electrical and mechanical parameters vary with the machine size, design and working conditions, so it is useful to consider the order of

magnitude of the various parameters and the extent to which each parameter influences particular modes.

In this subsection, a modal analysis of DFIG is carried out to investigate the effect of changing DFIG parameters on eigenvalues and the degree of participation of state variables in the system modes. Changes from 0.01% to around 300% in machine parameters were introduced to assess their impact at different operating modes, i.e., for the whole of rotor speed range.

Electrical parameters: Stator and rotor machine resistances and magnetization inductance.

The machine resistances R_S and R_R exert a significant effect on the open-loop eigenvalue placement and on the participation factor. The relationship between stator and rotor resistance is $R_R = 1.2292R_S$. Smaller resistance values alter the system stability at non- synchronous speed. Displacement of real part magnitude of all eigenvalues σ_i, is directly proportional to resistances variation, i.e., it tends to increase negatively with resistance value increases.

The real part magnitudes of the high-frequency and medium-frequency oscillating modes have an almost linear variation with resistance variation for the whole operating range. The frequency is affected more with resistance value increases. The most significant changes are for the oscillation frequency of the $\lambda_{3,4}$ and $\lambda_{5,6}$ modes. The oscillation frequency of $\lambda_{3,4}$ decreases up to -4.5% at synchronous speed and the oscillation frequency of $\lambda_{5,6}$ decreases up to -13% (from R_S to $3R_S$) below synchronous speed. The frequency of the $\lambda_{1,2}$ is affected to a lesser extent ($\sim -0.5\%$ from R_S to $3R_S$) for the whole operating range. The damping ratio improves with increasing resistance values.

The main outcomes at both, synchronous and non-synchronous operation are:

At synchronous speed, the system is dynamically stable for the

tested range of resistance variation as it can be seen in Fig. 4.1. The low-frequency mode is the dominant mode. Its real part magnitude and damping ratio decrease by up to -65% for resistances values of 0.01% and increase almost twice as much for resistance values of 300%.

The damping ratio of the high and medium-frequency modes improve linearly with increasing resistance values and oscillations are damped out faster. As shown in Fig. 4.1 participation factors are not significantly affected; they do not increase beyond 2% for larger resistive machines. At sub/super-synchronous operating, the variation of the stator and rotor resistance changes the placement of eigenvalues and affects the participation factor.

Fig. 4.2 and Fig. 4.3 show the eigenvalues, eigenvalue properties and participation factors of the WT-DFIG at both, sub-synchronous and super-synchronous regimes.

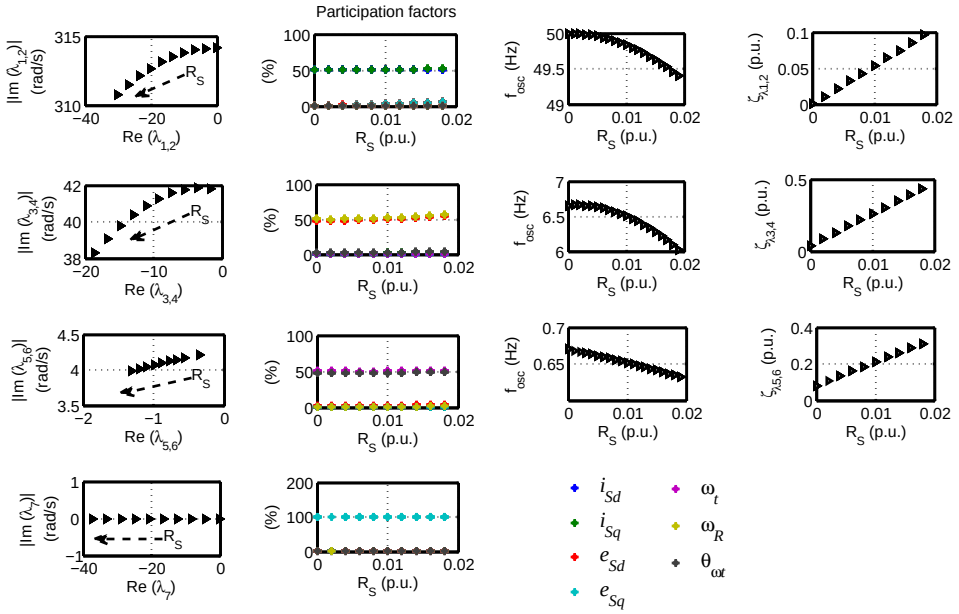

Figure 4.1: Effect of the machine resistances variation at synchronous regime.

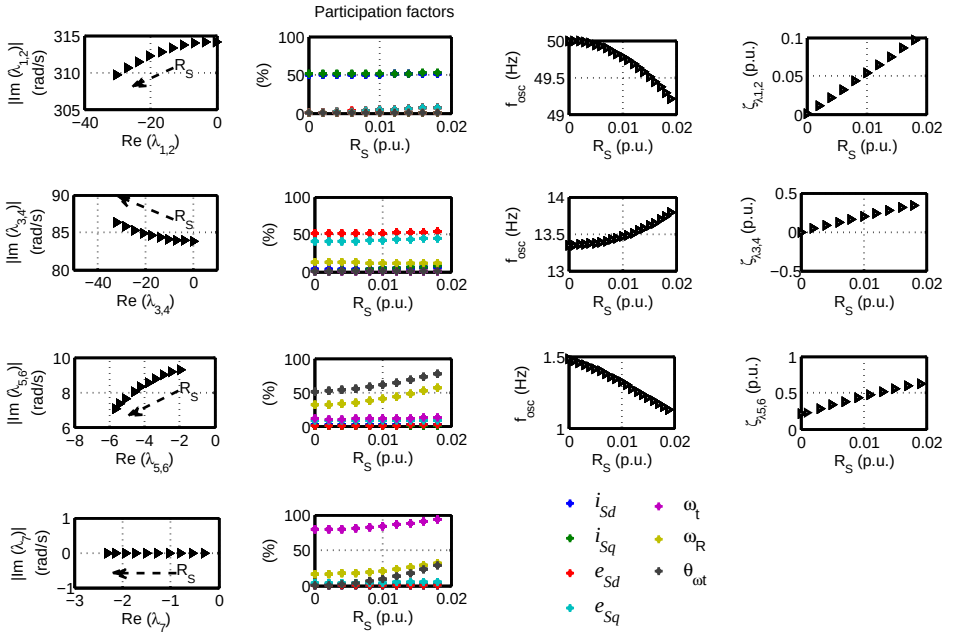

Figure 4.2: Effect of machine resistances variation at sub-synchronous operation.

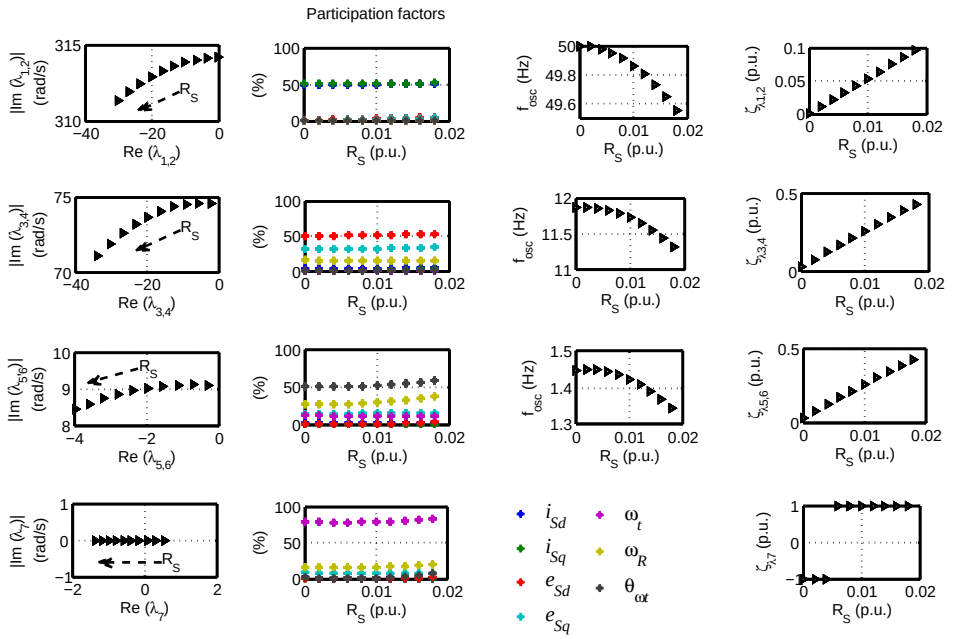

Figure 4.3: Effect of machine resistances variation at super-synchronous operation.

The medium-frequency mode becomes unstable at sub-synchronous operation if the resistance is neglected. The real part magnitude of the lowest frequency mode varies ±60% at sub-synchronous operation within the range of resistance value considered. As the real mode at non-synchronous operation is the closest to the imaginary axis, it is the dominant mode. At super-synchronous operation, it has the smallest stability margin and it becomes unstable for $R_S < 0.004$ pu (below $0.83R_S$).

As shown in Fig. 4.2, increasing resistance affects the participation factors of the mechanical and non-oscillating modes. Contribution of the state variables associated with $\lambda_{5,6}$ increases around 10%. The shaft dynamics, by $\theta_{\omega t}$, increases its participation in the real mode at sub-synchronous speed. Oscillations are damped out faster for more resistive machines (above R_S).

Variation on magnetization inductance L_o seems to alter only the stability of the real mode at super-synchronous operation when it increases above 5% ($L_o > 4.15$ pu), as shown in Figs. 4.4, 4.5 and 4.6.

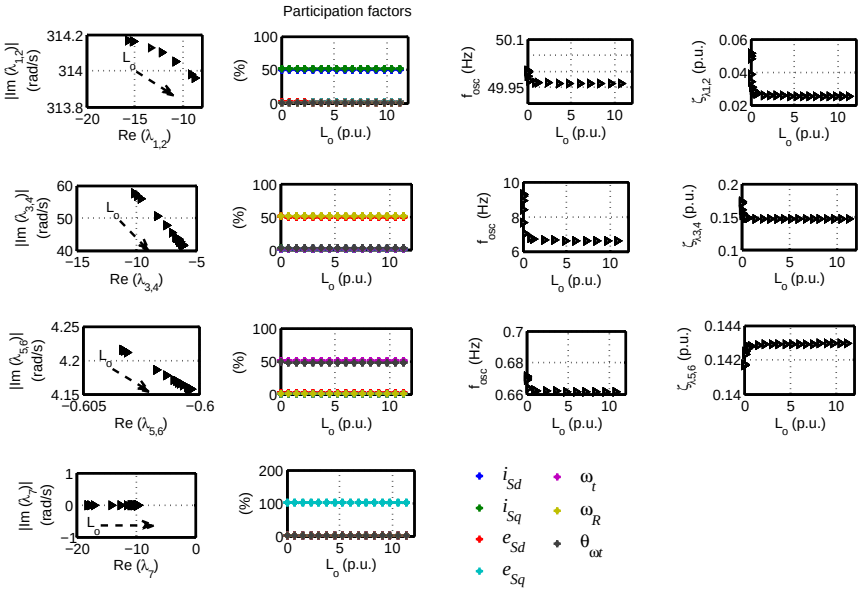

Figure 4.4: Effect of the leakage inductance variation at synchronous regime.

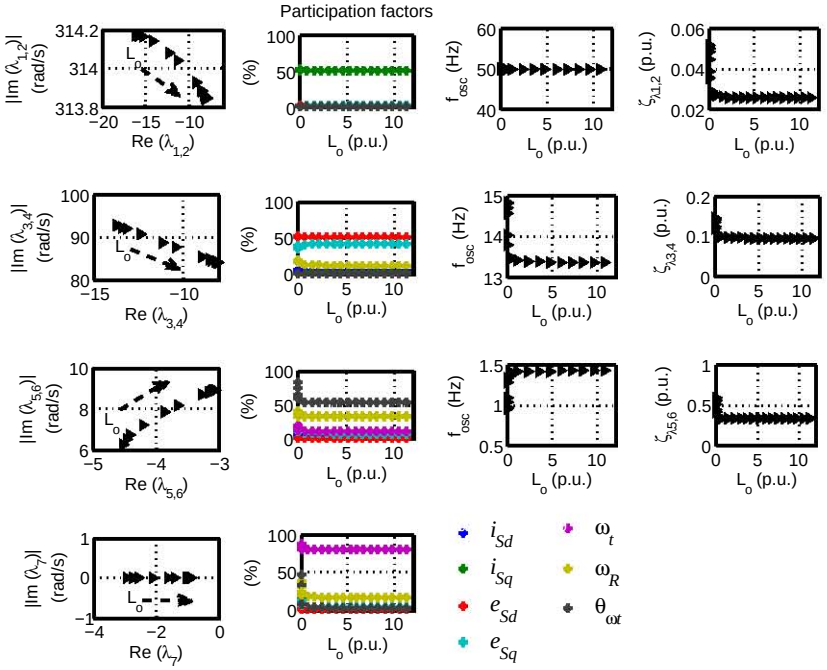

Figure 4.5: Effect of leakage inductance variation at sub-synchronous operation.

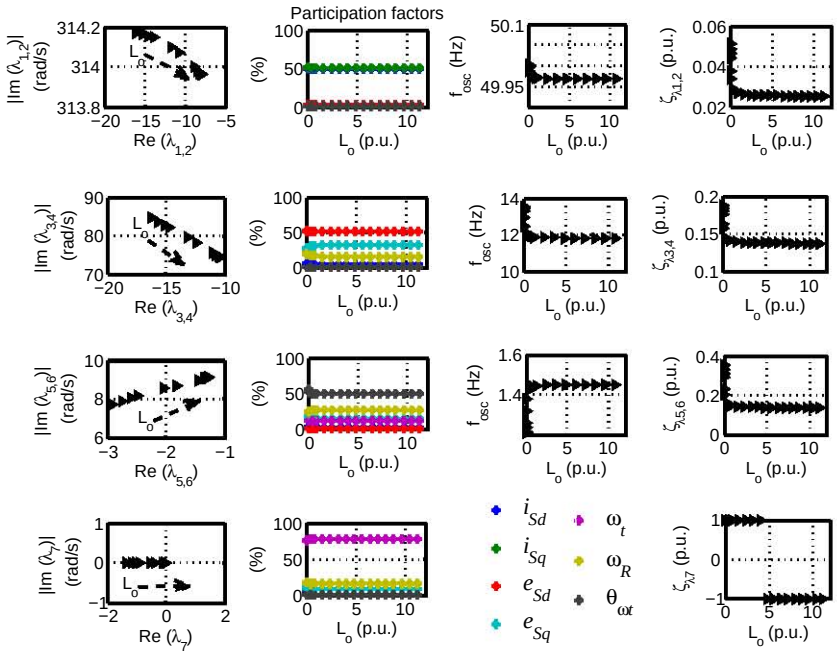

Figure 4.6: Effect of leakage inductance variation at super-synchronous operation.

The real part of the rest of the modes does not decrease beyond 1% with magnetization inductance increases. The effects are significant for smaller values of L_o below 15 % ($L_o < 0.5$). The stability margin of all modes increases 50 %. Hence, the damping ratio increases up to 50 %, as shown in Fig. 4.4. The oscillation frequency of the lowest frequency mode increases up to 30 %.

Effects of Lo on eigenvalue properties at both, sub-synchronous and super-synchronous operation are shown in Figs. 4.5 and 4.6, respectively. The $\lambda_{1,2}$ (E) mode is the fastest mode at sub/super-synchronous regime. Participation factors are influenced only to some extent at non-synchronous speed. The contribution of generator ω_R, to the electromechanical mode tends to increase; i.e., it tends to an EM mode for $L_o < 0.2$ (5%). Concerning the $\lambda_{5,6}$ and λ_7 modes, the participation of the associated variables varies by about ±5%. The contribution of rotor mechanical and shaft dynamics to the λ_7 mode increases at sub-synchronous speed.

Mechanical parameters.

As expected, varying inertia constants and stiffness do not affect the electrical modes significantly. The relationship between generator and turbine inertia constants is $H_g = 0.2H_t$. For heavier machines, the stability margin tends to decrease, except for the medium-frequency mode at sub-synchronous speed, which tends to increase (up to ±12% for $3H_t$), and also for the real mode at synchronous operation which does not change. For the electrical high-frequency mode, changes do take place in the real part but to a lesser extent, decreasing by about -0.5% with increases of H_t to $3H_t$ and increases up to 5% with the smaller inertia value considered, for whole range speed.

The main effects at synchronous speed, are shown in Fig. 4.7. The dominant mode is the lowest frequency mode, $\lambda_{5,6}$. The imaginary part tends to decrease with inertia constants increases.

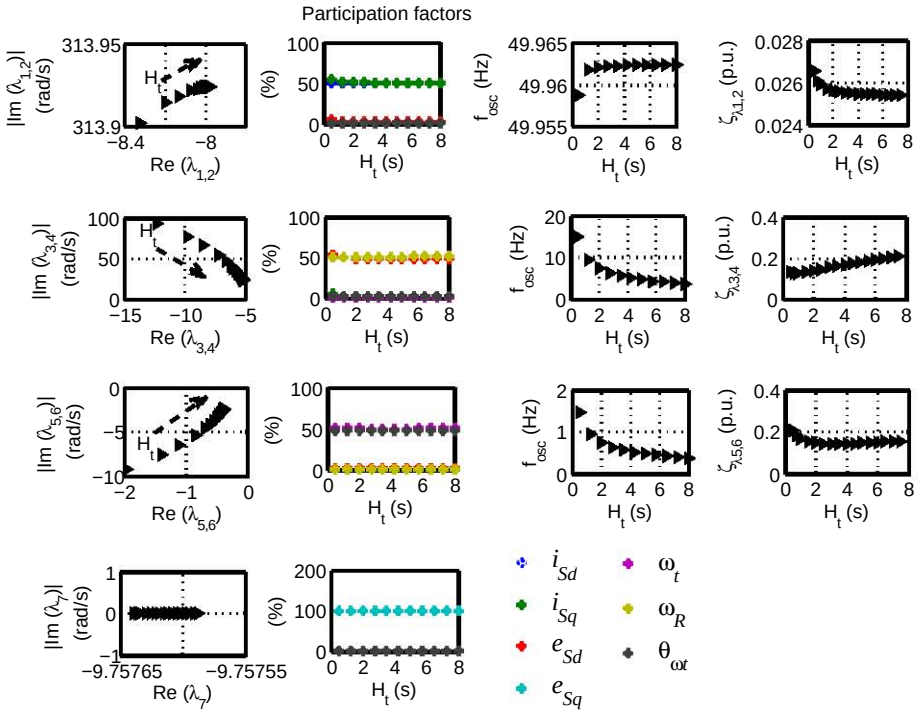

Figure 4.7: Effect of inertia constants variation at synchronous regime.

Therefore, as expected, heavier machines present lower oscillation frequencies. The oscillation frequency of $\lambda_{3,4}$ and $\lambda_{5,6}$ modes varies between 2.2 times and -40% in the range of variation considered for the inertia constants which go from $0.2H_t$ to $3H_t$.

Fig. 4.7 shows the effects of inertia constants on eigenvalue properties. It can be observed that the damping ratio of the medium-frequency mode increases/decreases by about ± 5 percent for $H_t = 7.5/H_t = 0.5$. As expected, the mechanical mode is the slowest mode and its τ increases with increasing H_t. Its damping ratio goes up to 5% with decreasing H_t. The participation factors do not seem to be affected at this operating point.

In case of non-synchronous operation, the λ_7 mode is the dominant mode. The stability margin of $\lambda_{5,6}$ and λ_7 modes reduces by about 60 percent with increases of H_t to $3H_t$, as shown in Figs. 4.8 and 4.9.

The oscillation frequency of the $\lambda_{3,4}$ grows (up to 40% and 60%) by decreasing the inertia constant to $0.5H_t$ at sub/super-synchronous operation. For heavier machines, it reduces by about 8%, at sub-synchronous speed and by about 2% at super-synchronous speed (for $3H_t$).

The oscillation frequency of the conjugate $\lambda_{5,6}$ mode increases 1.54 times for $0.5H_t$ and decreases by about 35% for $3H_t$ at sub-synchronous operation. On the other hand, it increases 1.63 times for $0.5H_t$ and decreases by about 40% for $3H_t$ at super-synchronous operation. Hence, the $\lambda_{5,6}$ mode is poorly damped out, having a large constant time, in case of heavier machines operating at higher speeds.

Participation factors are strongly affected by inertia constants. Electrical and mechanical dynamics tend to be more tightly coupled for lighter machines ($H < 2$), as shown in Figs. 4.8 and 4.9.

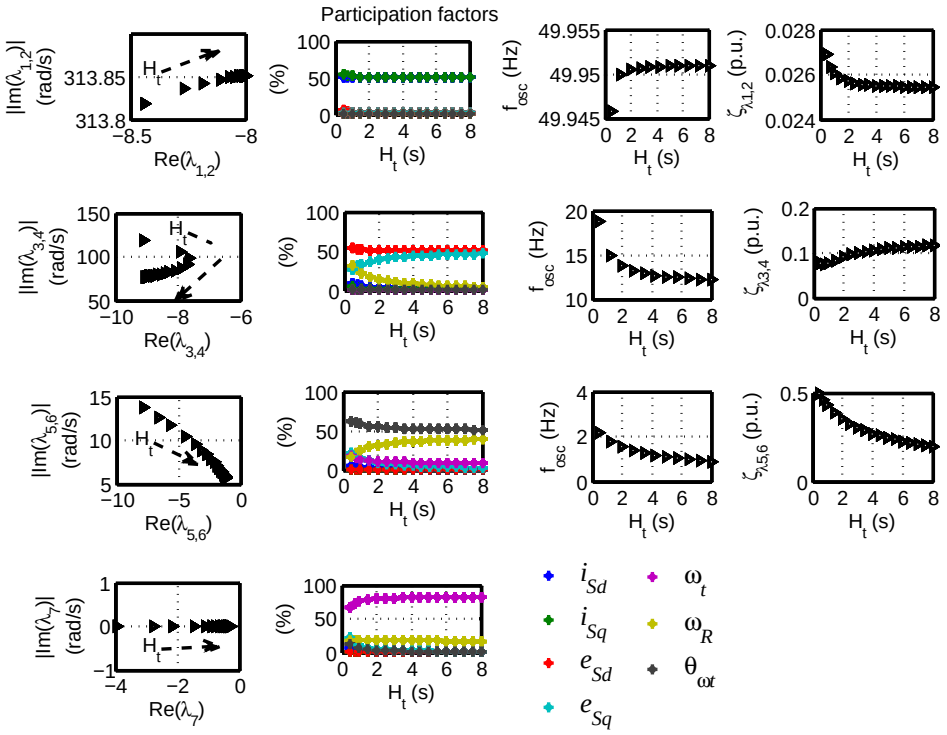

Figure 4.8: Effect of inertia constants variation at sub-synchronous regime.

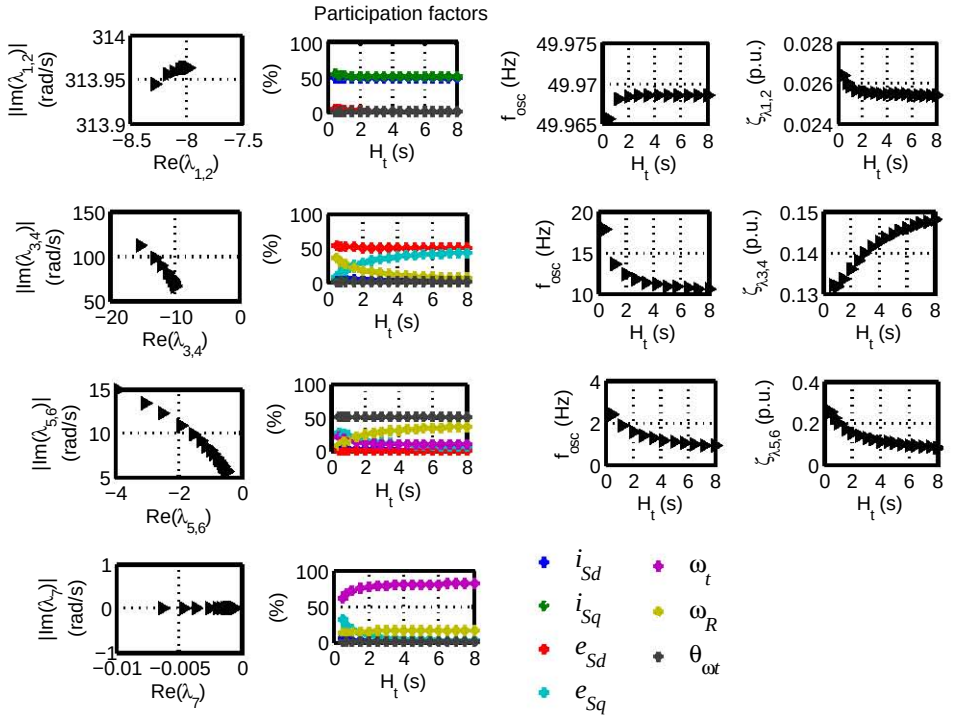

Figure 4.9: Effect of inertia constants variation at super-synchronous regime.

Concerning the shaft stiffness variations, changes are significant only in the medium-frequency and in the low-frequency modes. For stiffer drive trains, the stability margin of medium-frequency system modes decreases whereas the low-frequency mode tend to increase. Oscillation frequencies increase with k value increases and the damping ratios deteriorate for the whole range speed. The participation factors are also affected negatively.

At synchronous speed, the system dynamics change with increasing shaft stiffness above $6.6k$ ($k > 2$), as shown in Fig. 4.10. The dominant mode changes for stiffer drive trains at this regime, as observed from the results presented in Fig. 4.10.

With k less than 7.5, the $\lambda_{5,6}$ is the dominant mode; otherwise, the dominance passes onto $\lambda_{3,4}$. The $\lambda_{3,4}$ mode is the slowest mode for $k > 13$. There is an electro-mechanical mode of low oscillation

frequency (between 6-7 Hz) for $k < 2$, which is a mechanical mode, associated with rotor mechanical and shaft dynamics, by $k > 12$. The oscillation frequency increases to 17.9 Hz for $k = 30$. Th eigenvalue properties are shown in Fig. 4.10.

The oscillation frequency of the mechanical mode, $\lambda_{5,6}$, varies between 0.6 and 1.33 Hz for $0.003 < k < 1.5$ and remains constant up to about 2 Hz above $k = 7$. The $\lambda_{5,6}$ mode tends to become an electromechanical mode from $k > 3$ mainly contributed by turbine speed ω_t and internal voltage e_{Sd}. It can be seen in Fig. 4.10 that for stiffer drive trains, the $\lambda_{3,4}$ mode is a poorly damped mode having the longest time constant. The $\lambda_{3,4}$ diminishes below 10 percent for $k > 3$.

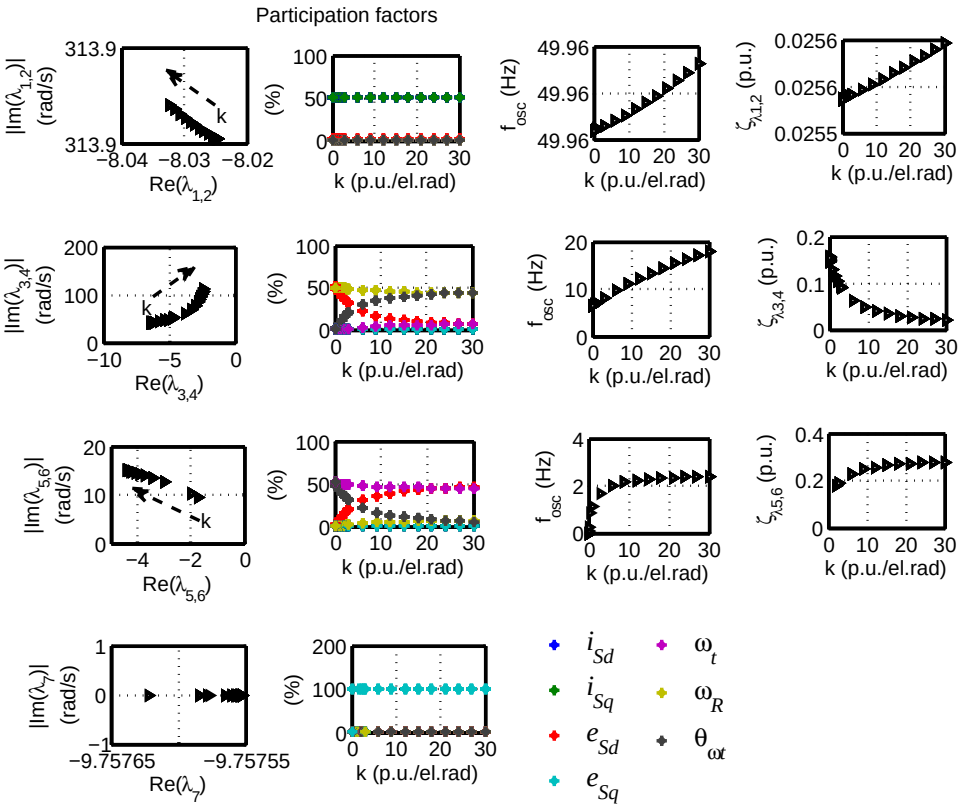

Figure 4.10: Effect of shaft stiffness variation on modes at synchronous regime.

At sub/super-synchronous speed, the system dynamics change in the case of very stiff mechanical systems ($k > 23$) and are strongly coupled for $6 < k < 23$. The λ_7 mode is the dominant mode at both, sub-synchronous and super-synchronous speed, as shown in Figs. 4.11 and 4.12.

For larger stiffness, the stability margin of $\lambda_{3,4}$ is significantly reduced (by about 65 percent for $k = 30$). The $\lambda_{3,4}$ mode is an electrical mode which oscillates with a frequency around 12-13 Hz for $k < 2$, but it becomes a mechanical mode with an oscillation frequency between 16-18 Hz, associated with rotor mechanical and shaft dynamics (ω_R, $\theta_{\omega t}$), by $k > 23$.

For stiffer drive trains, $\lambda_{3,4}$ mode is a poorly damped mode having the longest time constant. Its damping ratio diminishes below 10 percent for $k > 9$ at super-synchronous speed. The oscillation frequency of the $\lambda_{5,6}$ increases up to around 7-9 Hz for $k > 20$.

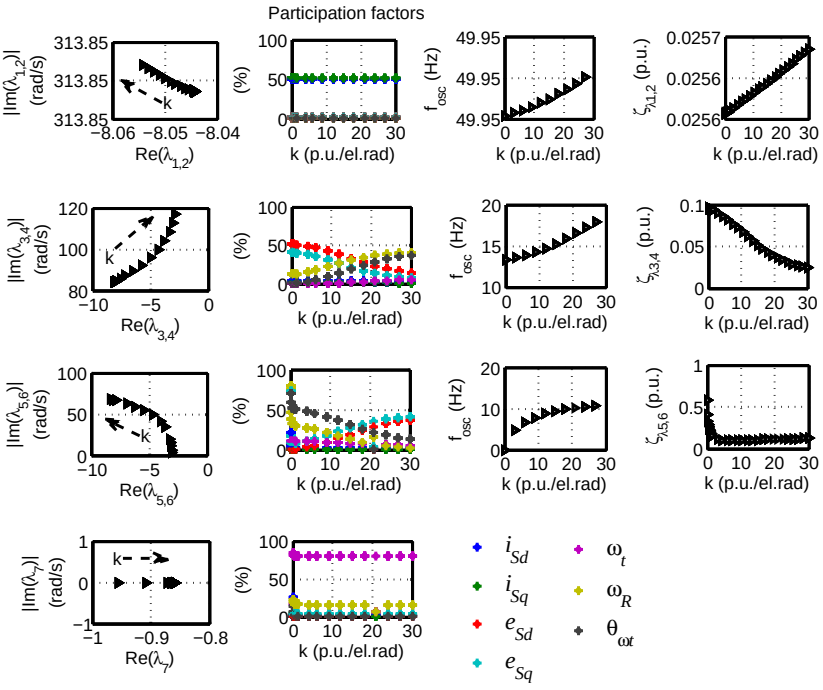

Figure 4.11: Effect of shaft stiffness variation on modes at sub-synchronous regime.

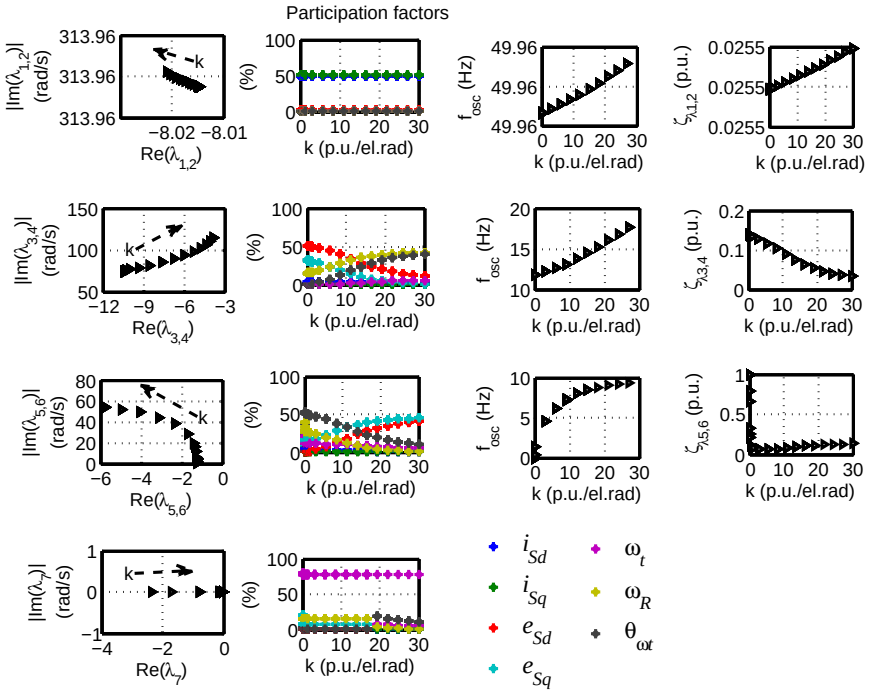

Figure 4.12: Effect of shaft stiffness variation on modes at super-synchronous regime.

4.2.3 Effect of DFIG-order model

A 5^{th} reduced order model (ROM) which does not include the stator transients has been used by several researches [55, 110, 111].

Table 4.5 shows the modal parameters of the DFIG machine when a 5^{th} reduced order model is employed. It is noticed that the stability margin reduces compared to the case when an exact 7^{th} order model is used (Table 4.2 - 4.4). The electrical high-frequency modes are eliminated.

An important aspect that could be highlighted is the fact that at super-synchronous regime one of the modes is unstable; however, this mode does not exist when an exact 7^{th} full-order model is employed.

Furthermore, the effects of the grid should be taken into account for more accurate results; the dynamics of the machine may be changed and push some of the modes into the right half plane.

Table 4.5: EIGENVALUES OF THE DFIG-WT MODELLED BY A 5TH ROM

λ_i	$\sigma_i \pm j\omega_i$ ($\omega_R = 0.7672$ p.u)	$\sigma_i \pm j\omega_i$ ($\omega_R = 1$ p.u)	$\sigma_i \pm j\omega_i$ ($\omega_R = 1.1981$ p.u)
$\lambda_{3,4}$ (EM)	-4.741 $\pm j80.26$	-5.31 $\pm j37.072$	-10.689 $\pm j73.323$
$\lambda_{5,6}$ (EM)	-3.1343 $\pm j9.27$	-0.617 $\pm j4.125$	-0.588 $\pm j9.206$
λ_7 (M)	-0.817	-7.8287	**+0.35455**

4.2.4 Effect of grid stiffness

The effect of the grid stiffness is assessed by varying the short circuit ratio of the grid. The results are shown in Fig. 4.13. It can be seen that grid impacts mainly the electrical high-frequency mode.

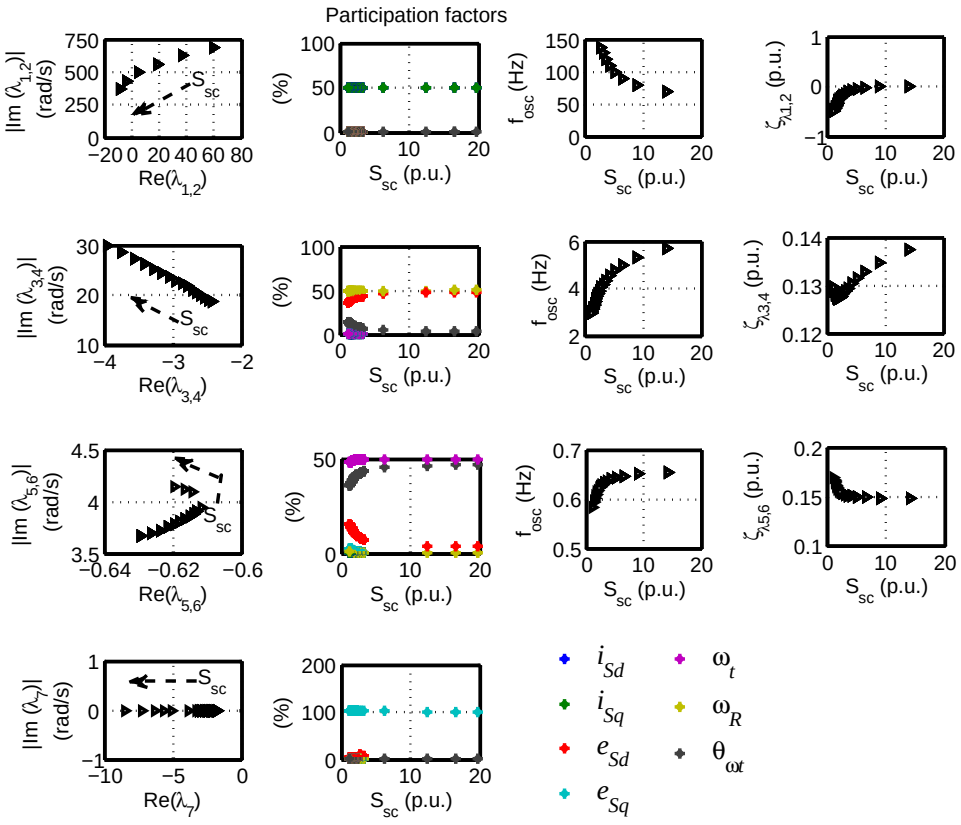

Figure 4.13: Effect of short circuit ratio variation at zero-slip.

Larger values of short circuit ratio S_{sc} slide the highest frequency mode (stator electrical mode) into the right half plane. Hence, the more inductive the external grid the more the need arises for series compensation or other controls measures in order to diminish the effective value of the equivalent inductance.

In case of a strong external networks, the high-frequency electrical dynamics decay quite fast. For the medium-frequency mode (rotor electro-mechanical mode), the damping ratio decreases with decreasing S_{sc}.

The low-frequency mode (turbine mechanical mode) is, relatively speaking, less sensitive to external line parameters. This is to be expected since the grid impedance is an electrical parameter. The non-oscillating mode (rotor electrical mode) is a real eigenvalue closer to the imaginary axis for large values of S_{sc}.

Participation factors are not significantly affected by grid strength. Although frequency and damping ratio change, the stator mode remains decoupled from the other modes, a situation that applies to both, strong and weak grids cases.

4.2.5 Influence of the control strategy

To assess the effect of the machine-side controller on local modes, two different control algorithms are applied to the 7^{th} full-order model DFIG wind turbine model. The control algorithms are the so-called FOC and SMC. The study is carried out for the whole range of rotor speed.

The WT-DFIG system under FOC is in fact an eleventh-order model. The state vector is defined by

$$x = \begin{bmatrix} i_{Sd} & i_{Sq} & e_{Sd} & e_{Sq} & \omega_t & \omega_R & \theta_{\omega t} & x_c \end{bmatrix}^T \tag{4.3}$$

with

$$x_c = \begin{bmatrix} \Phi_{id} & \Phi_{iq} & \Phi_{Te} & \Phi_{Qs} \end{bmatrix}^T$$

where x_c is the state vector of the machine-side converter controller.

The state vector of the WT-DFIG system under SMC is defined by (4.2).

Tables 4.6 and 4.7 show the eigenvalues, properties and the participation factors of dominant states of the WT-DFIG system under FOC. There are two oscillating modes. The highest frequency mode, unlike the mode in open-loop, is associated with a coupling between the q-axis stator current component (i_{Sq}) and rotor electrical dynamics (e_{Sd}), but it should be notice that the damping ratio is lower.

The lowest frequency mode is a mechanical mode contributed by $\theta_{\omega t}$ and ω_R, oscillating with a frequency of around 1.6 Hz with an acceptable damping ($> 10\%$).

Table 4.6: Eigenvalues and properties of the WT-DFIG with field-oriented control (FOC)

mode #	$\omega_R = 0.91535$ p.u. λ_i (f_{osc} (Hz), ζ_i (pu))	$\omega_R = 1$ p.u. λ_i (f_{osc} (Hz), ζ_i (pu))	$\omega_R = 1.1981$ p.u. λ_i (f_{osc} (Hz), ζ_i (pu))
λ_1	-14780	-15139	-14554
λ_2	-3391.2	-3636.7	-3634.5
$\lambda_{3,4}$	-25.815 $\pm j292$ (46.47, 0.08806)	-17.668 $\pm j289.75$ (46.11, 0.06086)	-10.403 $\pm j292.12$ (46.49, 0.03559)
λ_5	-438.71	-435.88	-440.29
λ_6	-180.57	-188.73	-195.12
λ_7	-22.69	-23.715	-23.734
$\lambda_{8,9}$	-1.8849 $\pm j10.466$ (1.66 ,0.1772)	-1.8903 $\pm j10.465$ (1.66, 0.1777)	-1.895 $\pm j10.464$ (1.66, 0.1781)
λ_{10}	-0.0884	-0.1004	-0.1128
λ_{11}	-6.234	-6.667	-6.641

Table 4.7: Participation factors of the modes of the WT-DFIG with field-oriented control (FOC)

mode #	Dom. States p_{ni}
λ_1	i_{Sd} 100%
λ_2	i_{Sq} 100%
$\lambda_{3,4}$	e_{Sq} 48%, e_{Sd} 47%
λ_5	Φ_{iq} 100%
λ_6	Φ_{id} 95%
λ_7	Φ_{Te} 99%
$\lambda_{8,9}$	ω_R 42%, $\theta_{\omega t}$ 50%
λ_{10}	ω_t 83%, ω_R 16%
λ_{11}	Φ_{Qs} 99%

Below synchronous speed, the mechanical mode, associated with rotor and turbine dynamics, moves close to zero, i.e., the stability margin decreases with decreasing rotor speed.

The modes associated with the controller depend on the tuning of the proportional-integral (PI) controllers. For example, it can be coupled with the state variables of the machine.

Eigenvalues, eigenvalue properties and participation factors of the dominant modes in a WT-DFIG system under SMC are shown in Tables 4.8 and 4.9. It can be observed that there are two conjugated modes and that there are no electro-mechanical modes as it was the case with FOC.

The highest frequency mode, which is associated with electrical dynamics by i_{Sq} and e_{Sq}, oscillates with a frequency of around 50 Hz. Its damping is much improved compared to the one obtained with FOC. The oscillating mechanical mode is a well damped out mode associated with shaft and rotor mechanical dynamics, $\theta_{\omega t}$ and ω_R. It oscillates with a frequency of around 1.6 Hz.

There are no modes associated with the controller.

Table 4.8: Eigenvalues and properties of the WT-DFIG with sliding-mode control (SMC)

mode #	$\omega_R = 0.91535$ p.u. λ_i (f_{osc} (Hz), ζ_i (pu))	$\omega_R = 1$ p.u. λ_i (f_{osc} (Hz), ζ_i (pu))	$\omega_R = 1.1981$ p.u. λ_i (f_{osc} (Hz), ζ_i (pu))
λ_1	-7086.1	-7107.1	-7107.2
λ_2	-7003.1	-7009.1	-7022.6
$\lambda_{3,4}$	-118.11 $\pm j$287.27	-74.272 $\pm j$302.31	-56.291 $\pm j$306.12
	(45.72, 0.38025)	(48.11, 0.23859)	(48.72, 0.18085)
$\lambda_{5,6}$	-1.886 $\pm j$10.466	-1.892 $\pm j$10.465	-1.897 $\pm j$10.464
	(1.66, 0.17818)	(1.66, 0.1779)	(1.66, 0.1783)
λ_7	-0.0816	-0.1004	-0.1128

Table 4.9: Participation factors of the modes of the WT-DFIG with sliding-mode control (SMC)

mode #	Dom. States p_{ni}
λ_1	i_{Sd} 94%
λ_2	i_{Sq} 94%
$\lambda_{3,4}$	e_{Sq} 49%, e_{Sd} 47%
$\lambda_{5,6}$	$\theta_{\omega t}$ 50%, ω_R 42%
λ_7	ω_t 83%, ω_R 16%

By control application, the electrical and mechanical dynamics are de-coupled at both synchronous and non-synchronous operation. The same degree of participation of state variables in the system modes remains throughout the whole range speed.

Effect of terminal voltage (Advantages of using SMC)

To demonstrate the effectiveness and robustness of the SMC, the dynamic behavior of the system regarding terminal voltage variation was examined. Fig. 4.14 shows the effect on the high-frequency mode. It can be noticed that SMC shows a superior performance.

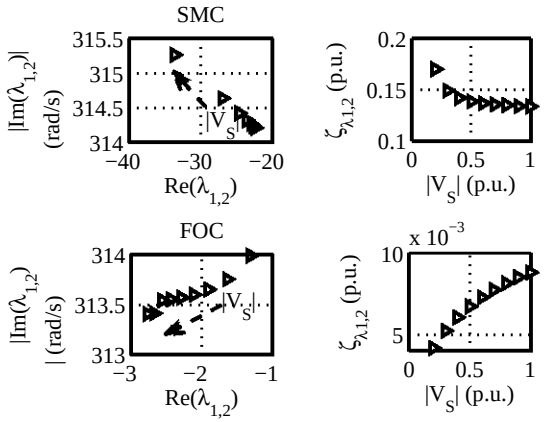

Figure 4.14: Eigenvalues and damping ratio of a DFIG with FOC and SCM under stator voltage variation.

In contrast to the FOC response, SMC improves the damping with decreasing terminal voltage, making it a good candidate for dealing with grid perturbations. Furthermore, the electrical dynamics of the WT-DFIG is faster with SMC.

4.3 Conclusions

DFIG models and control strategies have been presented for the study of small-signal stability. Modal analysis has been applied to assess the influence of different parameters such as order model, machine parameters, grid strength or control strategy. Stability of the DFIG wind turbine under FOC depends on the tuning of the proportional-integral controllers and on an appropriate knowledge of the impact of machine parameters. It has been proved that SMC is a very convenient way to improve the DFIG stability and that it is very robust under a wide range of machine parameters and networks variations.

The controller of the DFIG wind turbine under SMC ensures cancellation of electro-mechanical coupling without introducing additional modes. Moreover, this control scheme introduces additional damping which is amenable to reduce local oscillations and an overall better performance than the classical controller FOC.

Chapter 5

Stability Analysis of Multi-machine Systems with Wind Power Generation

All the studies presented in this chapter focus on assessing the impact of double-fed induction generators on oscillatory stability. The key factors influencing the system inherent oscillations are brought to the fore. Then, the main contributing factors of the double-fed induction generator to system stability are drawn by using modal analysis.

Throughout the chapter, a wide range of simulations are used to show by numerical example the prowess of the concepts and methods put forward in this research. Two different power systems are used: a three-machine system and a four-machine, two-area system. These enable a good understanding of the electromechanical oscillations phenomenon and illustrate rather well the improvements that can be achieved by using DFIG-based wind turbine controllers.

A small signal stability analysis is carried out for two scenarios. Firstly, all generators are considered to be conventional synchronous generators and, secondly, one of the synchronous generator is replaced by one DFIG-based wind farm which, in turn, is controlled by two different control schemes. One of them is the well-known and widely implemented Field Oriented Control FOC algorithm; the other is based

on a robust design technique termed Sliding Mode Control SMC. The latter represents a relatively new control application in the area of wind energy which is rapidly gaining adepts.

The first scenario is used to provide a base line case against which the impact of wind generation on the network dynamics, can be quantified with a degree of realism.

5.1 Background

The subject of power system stability has received a great deal of attention for decades. In the open literature, the phenomenon of stability in multi-machine power systems has been addressed from great many angles by hundreds of researchers. Over the years the research has addressed issues such as model development, power system equipment and topologies, control methods, system operating conditions, solution methods and many other issues.

Operation and dynamics characteristics of systems comprising synchronous generation are already well established and understood. Moreover, due to the tendency to operate systems near their stability limits, additional schemes have been added to maintain the system dynamics at acceptable levels. All this has increased further the awareness of power system oscillation and has provided the motivation to develop new technology to keep them at bay. A good example of this is the use of power electronic devices, referred to as FACTS (flexible AC transmission systems) devices [116, 117, 118].

Dynamic studies of mixed synchronous and induction generators is an issue that is receiving increasing attention, particularly over the last decade, as the growing penetration levels of DFIGs has increased.
Key contributions have been made toward the understanding of the interaction of conventional generation with wind power generation by resorting of transient and modal analysis studies.

In one of the early works [90], the dynamic and transient stability properties of wind turbine generators integrated into a power system were explored. The study addressed both, single and grouped wind turbines subjected to the influence of electrical and wind speed disturbances. Further studies on the dynamic characteristics of electrical networks with wind energy generation can be found in [52],[111].

The dynamic properties of electrical networks with wind generation seem to acquire a degree of improvement compared to those systems with no wind generation. One plausible explanations is that the demands on synchronous generators becomes less onerous with increases in wind energy, particularly under heavy wind regimes. In addition, from the DFIG-based wind turbines point of view, the decoupling capability of the power electronic converter control does not introduce new oscillatory modes and, consequently, this prevents the wind turbine from being involved in power system oscillations.

A topic that is becoming increasingly important in the field of power system stability is related to small signal stability of grid-connected wind power generation [4, 52, 119, 120]. In particular, the damping of oscillations which characterizes the phenomena of stability has seen increased research activity in recent years [74, 115, 119, 120, 121, 122, 123]. A point of great relevance has been the influence of increased DFIG penetration on the stability of inter-area oscillations.

It is shown in [120] that the effect of increased DFIG penetration is generally favorable since the damping of the inter-area oscillation increases. However, there are certain cases where the wind turbine is in voltage control mode and the system becomes stiffer, resulting in a less well damped inter-area mode which may even become unstable. Therefore an appropriate controller tuning of the voltage/VAR control loop is necessary to avoid instability.

An assessment of the impact of eigenvalues location of inter-area modes has been addressed by conducting a study of wind power level variations, [4, 52, 54, 74, 119]. Careful observation of the movement of

the eigenvalues through the complex plane, lead to the conclusion that for high levels of wind power penetration the dynamic performance is superior since the eigenvalue damping increases and the dynamic response of the frequency improves [74]. Further evidence of this was presented in [54], in connection with the impact that a large wind farm exerts on the oscillation modes of a two-area, four-generator power system. The study indicates that the inter-area mode tends to become more stable as the wind generator approaches its rated power, whereas the opposite is true for systems with synchronous generator.

It has been further verified in [4] that a small increase of both damping and frequency occurs for the inter-area modes by increasing gradually the wind power and by reducing, by the same amount, conventional power production, within the same area. However, it was also observed from several patterns of increasing wind power and load, that damping reduces whit wind power increases and contributes to congestion in weak interconnection lines, i.e. when increasing wind power generation pushes the power system stress level up [124].

In [121], the affected modes by inertia changes (due to the premise that the increased penetration of DFIG-based wind farms reduces the system inertia) are identified and then excited by introducing appropriate disturbances. The method suitably identifies the benefits and drawbacks of increasing DFIG penetration from the vantage of small signal stability and related studies.

Other interesting proposals have been put forward to enhance the system dynamic performance. By way of example,the use of power system stabilizers (PSSs) in DFIGs has been proposed recently [55, 122, 125, 126, 127]. The authors in [55] quite insightfully identified the control capabilities of the DFIG and put forward the idea of a power system stabilizer for a wind turbine employing the DFIG; they showed that the PSS can significantly influence the contribution that

a DFIG-based wind farm can make to network damping. The power system stabilizer was designed to operate with a flux magnitude and angle controller (FMAC) scheme, where the terminal voltage and stator power output can be controlled through the magnitude of the rotor flux vector and its angular position.

In [128] and [129] other types of PSS configurations and controllers for DFIGs were also introduced. In [128] a conventional PSS was compared with two other PSSs in which their output signals were added to the power and to the voltage side of the DFIG control system, respectively. It was concluded that a DFIG fitted with the capability to improve PSS to improve the damping of inter-area power system oscillations and that the wind farm may have the potential to positively contribute to power system damping. The impact of the voltage control loop on system dynamic performance is examined in [129]. It was found that besides the penetration level, this control loop has the greatest impact on inter-area oscillations in comparison with other control loops such as phase-locked loop (PLL) and pitch angle control, which exerts a negligible impact.

Since the active and reactive power of variable-speed wind turbines can be modulated to damp power system oscillations [123], auxiliary controllers with power modulation (active, reactive or a combination thereof) have been employed. Power damping control is achieved by adding auxiliary corrective signals to the control of the machine side converter of a DFIG-based wind turbine.

In [125], it is pointed out that by active power modulation, additional damping to inter-area oscillations can be introduced. The proposed active power modulation is accomplished by introducing a supplemental signal at the control loops which contains the inter-area oscillation information. Results demonstrated that with proper control, DFIGs have the capability to damp inter-area oscillations. However,

one potential disadvantage of active power modulation of wind generation is its interaction with torsional dynamics of the wind turbines, since the active power is directly related to the electromagnetic torque. If P modulation yields oscillations of low-frequency in wind generators, these may interact with torsional oscillation because of theirs low-frequency oscillations. This concern, already addressed in [126], led to the outcome that the damping of the shaft mode decreases due to active power modulation in wind farms while reactive power modulation is immune to such risk.

Likewise, a combined PSS and active damping controller by eigenstructure assignment to improve both, the DFIG shaft oscillation and the power system electromechanical damping was a worthwhile contribution put forward in [127]. The authors demonstrated the use and capability of the method via its application to the design of a DFIG controller required to improve both, the damping of DFIG shaft oscillatory modes and the network electromechanical damping.

In [122], a coordinated tuning of the damping controller to enhance the damping of the oscillatory modes by using a bacteria foraging technique was developed. However, the study was limited to a single DFIG WT system connected to an infinite bus. Hence, extensions to a multimachine DFIG system should be made to quantify the actual impact of DFIGs on power system stability.

It is stated in [130] that the PSS function in variable-speed wind generators does not actually require the use of compensators to produce damping torque due to the fast action of power electronic converter controllers. However, it is possible to increase the selectivity of the modal damping capabilities and to reduce the sensitivity to disturbances through the use of tuned filters. PSS functions based on the energy function approach (EFA-PSS) and frequency deviation (WPSS), are normally used in VSC-HVDC and FACTS devices, and may also be

used in this application. The energy function method consists of defining a function to represent the energy in the system, which is composed of kinetic and potential energy. The gradient of this energy is minimized by active and reactive power control laws. Both PSS controllers use active and reactive power modulation.

Similar damping capabilities of wind farms with both PSS functions are given but both require high proportional gains. On the other hand, with the tubed Band-Pass Filter in the WPSS, the reactive power control loop of the EFA-PSS showed vulnerability to voltage disturbances, which can limit the proportional gain. Active power modulation is more effective if the PCC of the DFIG-based wind farm is located electrically close to a synchronous generator plant. The opposite holds for reactive modulation but it requires a large reactive power modulation. By careful examination of results pertaining to the various scenarios, it was observed that the amount of PQ modulation impacts directly the damping potential. Moreover, it was noticed that with a broader distribution of wind resources, the damping capabilities of the PSS controller increase while the real and reactive power modulation level decrease.

Nevertheless, in spite of the fact that the design methodologies for active and reactive power modulation-based PSSs have great potential, published work on PSSs remains scant [123].

5.2 The Three-Machine, Nine-Bus System

The nine-bus power system of the Western Systems Coordinating Council (WSCC) [24] shown in Fig 5.1 is used as the first test case. It comprises three generators, three loads, three transformer and six transmission lines.

Generator 1 is a hydro-generator. Generator 3 is a steam-generator and Generator 2 is a double fed induction generator (DFIG) although Generator 2 is considered first to be a steam turbine-driven synchronous

generator in order to provide a baseline case against which to compare the impact on the network dynamic performance, by the wind generator. The loads are modelled as constant power load type.

The synchronous generators are represented by their two-axis model and fitted with an IEEE Type I exciter (slow acting with low gain), shown in Fig. 5.2. The fourth-order two-axis model in the *dq* frame is described by equations (5.1)-(5.4). Equations (5.5)-(5.7) are the differential equations for the IEEE Type I exciter (Fig. 5.2).

$$\frac{d\delta_i}{dt} = \omega_{SG_i} - \omega_e \tag{5.1}$$

$$\frac{2H_i}{\omega_e}\frac{d\omega_{SG_i}}{dt} = T_{Mi} - E'_{di}I_{di} - E'_{qi}I_{qi} - \left(X'_{qi} - X'_{di}\right) I_{di}I_{qi} - \ldots$$

$$\ldots - D_i\left(\omega_{SG_i} - \omega_e\right) \tag{5.2}$$

$$T'_{qo_i}\frac{E'_{di}}{dt} = -E'_{di} + \left(X_{qi} - X'_{qi}\right) I_{qi} \tag{5.3}$$

$$T'_{do_i}\frac{E'_{qi}}{dt} = -E'_{qi} + \left(X_{di} - X'_{di}\right) I_{di} + E_{fd_i} \tag{5.4}$$

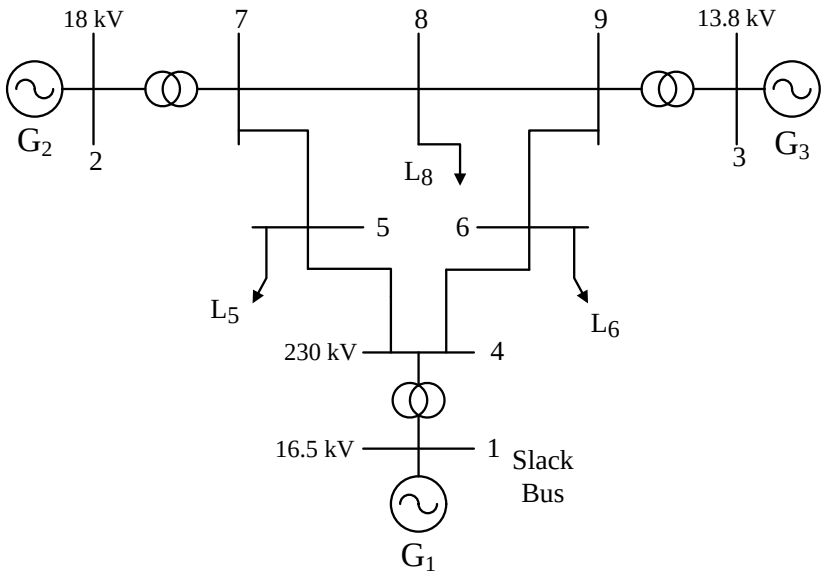

Figure 5.1: 3-Machine, 9-Bus System

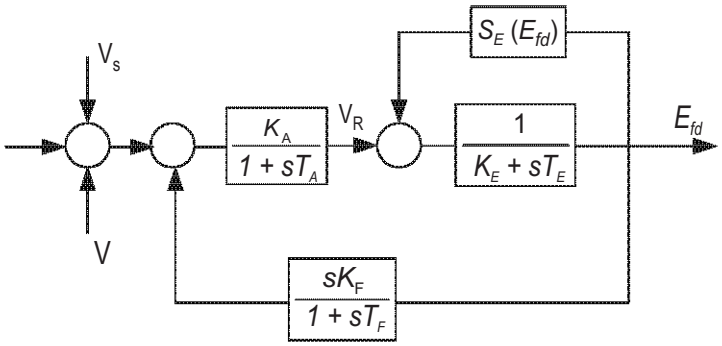

Figure 5.2: IEEE Type I exciter

$$T_{E_i}\frac{E_{fd_i}}{dt} = -\left(K_{E_i}+S_{E_i}\right)E_{fd_i}+V_{R_i} \tag{5.5}$$

$$T_{F_i}\frac{R_{f_i}}{dt} = -R_{f_i}+\frac{K_{F_i}}{T_{F_i}}E_{fd_i} \tag{5.6}$$

$$T_{A_i}\frac{V_{R_i}}{dt} = -V_{R_i}+K_{A_i}R_{f_i}-\frac{K_{A_i}K_{F_i}}{T_{F_i}}E_{fd_i}+\ldots$$
$$\ldots+K_{A_i}\left(V_{ref_i}-V_{SG_i}+V_{si}\right) \tag{5.7}$$

The exciter is assumed to be identical for all three machines. Power System Stabilizers (PSS) were not employed in this model so as to enable a more straightforward assessment of the impact of Generator 2. The machine data and the exciter data are given in Table 5.1.

The double fed induction generator is modelled by a 7^{th} order model as described in Chapter 3. The electrical and mechanical data for the DFIG-WT are given in Table 5.1.

The system MVA base is 100, and the system frequency is 50 Hz. The rated power of generators is: Generator 1 = 247.5 MVA, Generator 2 = 192 MVA, and Generator 3 = 128 MVA.

The impedances are in per unit on the system 100 MVA base and are given in Table 5.2. The power flow solution for the nominal case, is shown in Table 5.3.

V_{ref}

Table 5.1: Machines Data

Generator Data

Bus #	X_d (pu)	X_q (pu)	X'_d (pu)	X'_q (pu)	T'_{do} (s)	T'_{qo} (s)	H (s)	D
1	0.146	0.0969	0.0608	0.0969	8.96	0.31	23.64	0.0254
2	0.8958	0.8645	0.1198	0.1969	6.0	0.535	6.4	0.0066
3	1.3125	1.2578	0.1813	0.25	5.89	0.6	33.01	0.0026

Exciter Data

K_A	T_A (s)	K_E	T_E (s)	K_F	T_F (s)	A_{exc}	B_{exc}
20	0.2	1	0.314	0.063	10.35	0.0039	1.555

DFIG parameters

R_S (pu)	R_R (pu)	L_o (pu)	L_{sl} (pu)	L_{rl} (pu)	H_g (s)	n_{pp}	$P_{w_{rated}}$ (MW)
0.0048	0.0059	3.953	0.092	0.099	2.5	2	2
H_t (s)	k ($\frac{\text{pu}}{\text{el.rad}}$)	c ($\frac{\text{pu.s}}{\text{el.rad}}$)	$v_{w_{rated}}$ ($\frac{\text{m}}{\text{s}}$)	R_{blade} (m)	n_{gb}	$C_{p_{max}}$	$\lambda_{tip_{opt}}$
0.5	0.3	0.01	17	45	100.5	0.45	7.84

Table 5.2: System data for the 3-machine System (Fig. 5.1)

System line data				
From bus	To bus	R	X	B_c (total)
1	4	0.00	0.0576	0.00
7	2	0.00	0.0625	0.00
3	9	0.00	0.0586	0.00
4	6	0.0170	0.0920	0.158
9	6	0.0390	0.1700	0.358
9	8	0.0119	0.1008	0.209
7	8	0.0085	0.0720	0.149
7	5	0.0320	0.1610	0.306
5	4	0.0100	0.0850	0.176

Table 5.3: Load Flow Results of the 3-machine, 9 bus system

Bus	**Bus Type**	**Voltage** (pu)	$\mathbf{P_G}$ (pu)	$\mathbf{Q_G}$ (pu)	$\mathbf{P_L}$ (pu)	$\mathbf{Q_L}$ (pu)
1	Swing	$1.0400\angle 0.000°$	0.7163	0.2671	-	-
2	P-V	$1.0250\angle 9.242°$	1.6300	0.0668	-	-
3	P-V	$1.0250\angle 4.642°$	0.8500	-0.1085	-	-
4	P-Q	$1.026\angle -2.216°$	-	-	-	-
5	P-Q	$0.996\angle -3.982°$	-	-	1.25	0.50
6	P-Q	$1.013\angle -3.693°$	-	-	0.90	0.30
7	P-Q	$1.0260\angle 3.685°$	-	-	-	-
8	P-Q	$1.0160\angle 0.700°$	-	-	1.00	0.35
9	P-Q	$1.0330\angle 1.945°$	-	-	-	-

Modal analysis is carried out for different operating conditions. Four active power output values by the generator connected at bus 2 are chosen in order to consider the effects of increasing wind power penetration levels on the grid: 15%, 30%, 50% and 85%. The dispatch of the generator at bus 3 is kept constant.

The system performance for all four operating conditions is assessed by comparing the results when Generator 2 is modelled as a conventional synchronous generator (base case) with those obtained when the DFIG wind turbine generator replaces the conventional synchronous generator. This establishes the dynamic stability characteristics of the system and quantifies the contribution of wind generation to system stability.

The DFIG was simulated with two control schemes, one is the classical Field Oriented Control (FOC) and the other is a control approach based on the Sliding Mode Control (SMC).

The system state vector is $x_n = [x_1 \quad x_2 \quad x_3]^T$, where x_n is the state variables vector of the generator connected at bus i.

The state vector of the synchronous generator is made up of the states of the two-axis model as well as the state variables of the exciter model

$$x_{SG} = \begin{bmatrix} \delta & \omega & E'_d & E'_q & E_{fd} & R_f & V_R \end{bmatrix}^T \tag{5.8}$$

where three last three states correspond to the exciter model.

The state variables vector of the DFIG WT takes of the form

$$x_{WT} = \begin{bmatrix} i_{Sd} & i_{Sq} & e_{Sd} & e_{Sq} & \omega_t & \omega_R & \theta_{\omega_t} & x_c \end{bmatrix}^T \tag{5.9}$$

with x_c being the state vector of the DFIG controller.

The order of the state variables vector for the DFIG depends on the order of the type of applied control strategy. This is detailed in Chapter 3.

For each operating condition two cases are analyzed:

a. *Power network with no wind generation*

   In this case the eigenvalue analysis is performed assuming that all three generation units are conventional synchronous generators. The system is a 21^{th} order one,

$$x_{SG_n} = \begin{bmatrix} \delta_i & \omega_i & E'_{d_i} & E'_{q_i} & E_{fd_i} & R_{f_i} & V_{R_i} \end{bmatrix}^T \tag{5.10}$$

   for $i = 1, 2, 3$.

b. *Power network with wind generation*

   In these studies the generator at bus 2 is assumed to be a DFIG-based wind farm and two different controllers are utilized, namely FOC and SMC. When the FOC-based controller is used, the system is a 24^{th} order system with the following state variables

$$x_n = \begin{bmatrix} x_{SG_i} & x_{WT} \end{bmatrix}^T \tag{5.11}$$

with x_{SG_i} being the state vector of the synchronous generators for $i = 1, 2$ and, $x_{WT} =$ being the state vector of the DFIG-based wind turbine given by (5.9), where $x_c = \begin{bmatrix} X_{i_d} & X_{i_q} & X_{T_e} & X_{Q_S} \end{bmatrix}^T$ are the state variables of the FOC-based controller.

When the SMC-based controller is used, the system is a 21^{th} order system with the state vector given by equation (5.11) where x_{WT} is a 7^{th} order system.

5.2.1 Power Network with no Wind Generation

An electrical power system in which the exported power is supplied by a conventional synchronous generator is considered first to provide a base line against which wind penetration studies can be assessed.

Table 5.4 summarizes all the relevant information concerning the small-signal study for this case. It can be noticed that the system is stable.

This test system shows two rotor angle oscillations ($\lambda_{1,2}$ and $\lambda_{3,4}$) and one real rotor speed mode (λ_{19}). The 1.74 Hz mode $\lambda_{3,4}$ corresponds to rotor speed of the machines 3 and 2, where the machine 3 is dominant, and the 1.17 Hz mode $\lambda_{1,2}$ is related to machines 1 and 2, with the latter providing most of the contribution. This is the least damped mode with a damping ratio of 4.395%.

The real rotor speed mode, λ_{19}, contributed by machines 1 and 2, depends mainly on the rotor speed of machine 1.

The rest of the modes are the local and inter-machine modes associated with excitation control. The exciter's modes are all very well damped. The zero eigenvalue is not shown.

Table 5.4: System Modes of the 3-machine system: Two-axis Synchronous Generator with IEEE I exciter

Mode #	Eigenvalue $\sigma_i \pm j\omega_i$	Frequency f (Hz)	Damping ratio ζ(pu)	Dominant states	Machine at bus	Participation factor (%)
$\lambda_{1,2}$	-0.3261 $\pm j$7.4138	1.1799	0.04395	δ, ω	2 1	31.6, 31.7 13.4, 13.4
$\lambda_{3,4}$	-0.9092 $\pm j$10.982	1.7479	0.08250	δ, ω	3 2	41.5, 41.5 9.5, 9.5
$\lambda_{5,6}$	-5.6101 $\pm j$7.9667	1.2679	0.57576	V_R, E_{fd}, R_f	2	45.6, 45.1, 13.0
$\lambda_{7,8}$	-5.2139 $\pm j$7.8330	1.2467	0.55410	V_R, E_{fd}, R_f	1	45.7, 44.4, 13.8
$\lambda_{9,10}$	-5.4107 $\pm j$7.9291	1.2619	0.56366	V_R, E_{fd}, R_f	3	45.1, 44.2, 13.5
λ_{11}	-5.3428	-	-	E'_d	2 3	53.58 49.0
λ_{12}	-4.0872	-	-	E'_d	3 2	53.4 47.8
$\lambda_{13,14}$	-0.3891 $\pm j$1.1145	0.17738	0.32967	$E'q$, R_f	1 2	29.9, 21.7 16.8, 12.4
$\lambda_{15,16}$	-0.3830 $\pm j$0.7370	0.11731	0.46110	$E'q$, R_f	1 2	25.5, 19.0 23.3, 18.2
$\lambda_{17,18}$	-0.3136 $\pm j$0.5031	0.08007	0.52899	$E'q$, R_f	3 2	37.7, 32.3 18.5, 13.2
λ_{19}	-0.1645	-	-	ω	1 2	72.4 18.6
λ_{20}	-3.2258	-	-	E'_d	1	100

Fig. 5.3, describes the eigenvalues movement of the two rotor angle oscillatory modes $\lambda_{1,2}$ and $\lambda_{3,4}$ for the 9 bus system when the active power output of the generator 2 changes from 15% to 85%; four levels are considered: 15%, 30%, 50%, 85%.

The top two figures of Fig. 5.3 show the eigenvalues movement and their respective participation factors are shown in the lower row. The arrow indicates the direction of increasing power output.

From the participation factors results, it can be observed that the x_n state variable contribution changes little at all the various operating conditions considered, namely (15%, 30%, 50% and 85% of Generator 2's power output.

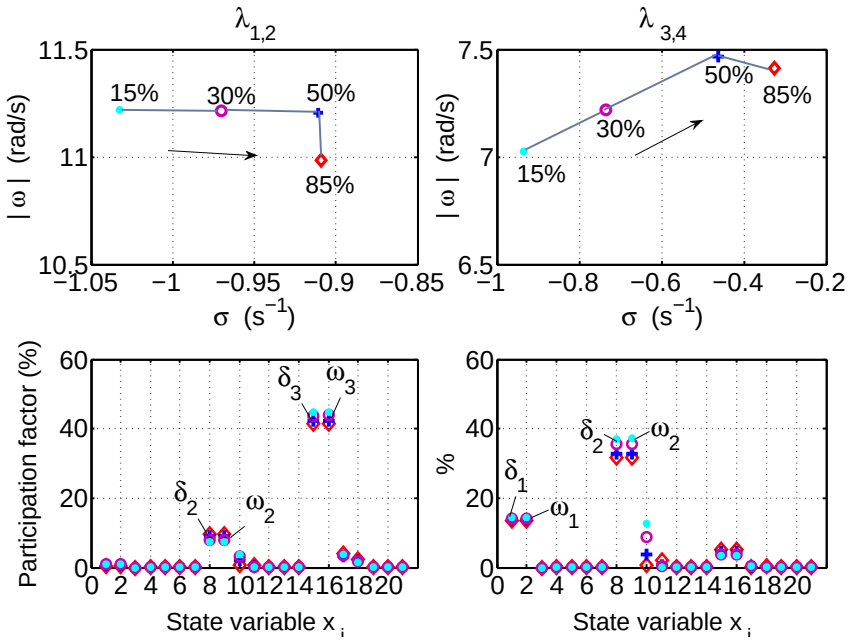

Figure 5.3: Impact of power output of G_2 on the swing-rotor modes of the WSCC system. The upper figures depict the eigenvalues movement and; the lower figures the participation factors.

The small-signal stability margin of the rotor-speed oscillations, which is understood to be the distance of the real-part of the eigenvalues (stable eigenvalues with negative real-part) measured from the imaginary axis of the complex plane; decreases with progressive increases of active power (Fig. 5.3).

The real part magnitude of the inter-machine mode, $\lambda_{1,2}$, decreases up to 65% from lower to higher power whilst the real part magnitude of the mode $\lambda_{3,4}$, decreases up to 15%. Hence, the damping is reduced from 13.2% to 4.4% and, from 9.17% to 8.25%, respectively (Fig. 5.4).

The oscillation frequencies of the modes, as shown in Fig. 5.4 (left), are affected little by power generation changes, with the variation being less than 5% between the two extreme operating conditions (15% and 85% of P of G_2).

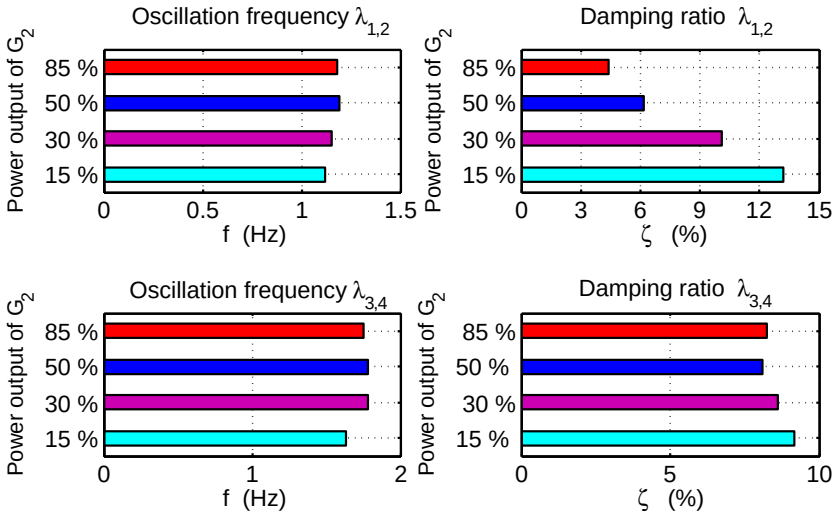

Figure 5.4: Properties of the swing-rotor modes of the WSCC system with active power output of G_2 increases . The upper figures depict the eigenvalue properties of the $\lambda_{1,2}$ mode and; the lower figures depict the eigenvalue properties of the $\lambda_{3,4}$ mode.

5.2.2 Power Network with Wind Generation

In these studies the generator connected at bus 2 is now assumed to be a DFIG-based wind farm. The DFIG is fitted with the two distinct control strategies, which have been introduced in previous chapters. The first one is based on the conventional Field Oriented Control (FOC) and the second is based on the robust design technique Sliding Mode Control (SMC).

The benefits of using mixed power generation, involving conventional synchronous generators and DFIG WT, is assessed below, with two different kinds of DFIG controls being implemented.

Three cases are singled out for analyses:

Case 1: All three generators G_1, G_2, G_3 are of the conventional synchronous generation type

Case 2: G_2 represents wind generation with a DFIG-WT with FOC

Case 3: G_2 represents wind generation with a DFIG-WT with SMC

The damping ratio is the key parameter with which to assess the impact that the DFIG has on the dynamics of the system.

Under this scenario, depicted in Fig. 5.5, the system shows two rotor angle oscillations ($\lambda_{1,2}$, $\lambda_{3,4}$): $\lambda_{1,2}$ relating to the machine connected at bus 1 and, $\lambda_{3,4}$ relating to the machine connected at bus 3. The upper figures (first row) depict the eigenvalues movement and the lower figures the participation factors corresponding to Case 2: Generator 2 is a DFIG-WT with FOC, (middle row figures) and for Case 3: Generator 2 is a DFIG-WT with SMC, (bottom row figures).

Firstly, it can be seen that the system stability is strongly affected by the operating point. The oscillatory modes tend to become more stable as the wind power penetration increases; this is in contrast to

the base case (power network with no wind generation), where the system stability margin decreases with output power generation increases (Fig. 5.3, top).

As expected, oscillations associated to the machine 2 only exist in the base case (with no wind generation).

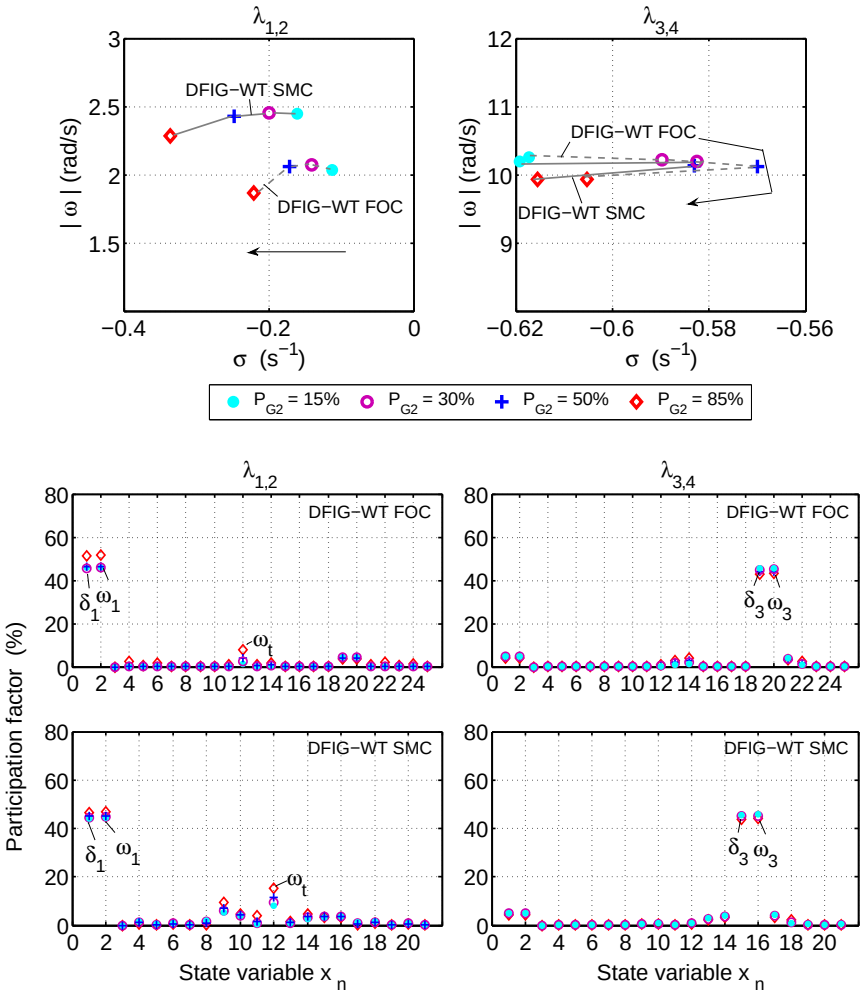

Figure 5.5: Impact of increasing wind power penetration on the swing-rotor oscillatory modes of the 9 bus system. The upper figures (first row) depict the eigenvalues movement and the lower figures the participation factors corresponding to the case 2, (middle row figures) and the case 3, (bottom row figures).

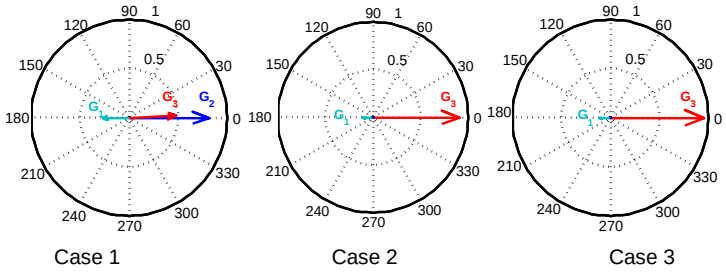

(a)

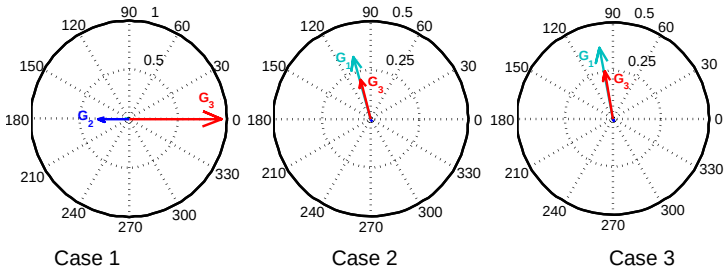

(b)

Figure 5.6: Mode shape of the oscillatory modes. Case 1: Base case; Case 2: G_2 as a DFIG-WT with FOC; and Case 3: G_2 as a DFIG-WT with SMC.

This can also be checked by examining the mode shape given by the elements of the right eigenvectors. Fig. 5.6 shows the mode shape corresponding to the rotor-speed state, where the presence of the generators' rotor-angle modes can be appreciated as well as the absence of the Generator 2's contribution. This applies to both cases, 2 and 3:

- Case 1: All synchronous generators. G_1, G_2 and, G_3 participate in the rotor-speed mode $\lambda_{1,2}$ where G_1 oscillates against the other two. From the rotor-speed mode $\lambda_{3,4}$ it is possible to observe the participation of the G_2 and G_3, which oscillate against each other.

- Case 2: DFIG WT with FOC. G_2 does not contribute to the oscillatory modes.

- Case 3: DFIG WT with SMC. Activity of G_2 to the oscillatory modes is not noticeable.

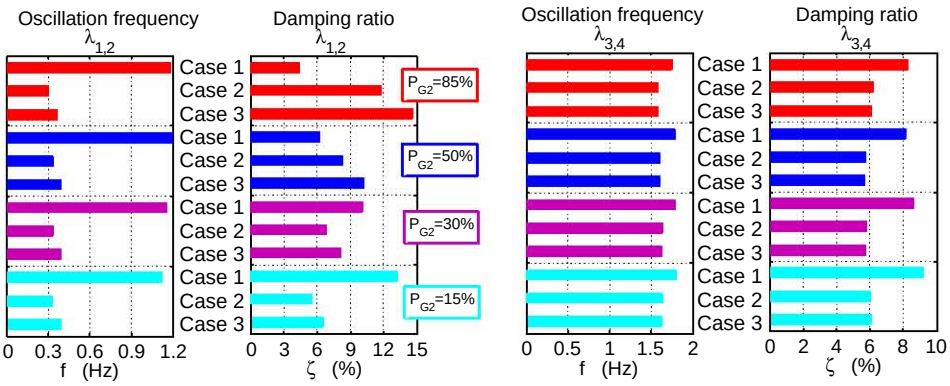

Figure 5.7: Eigenvalues properties of the a) mode $\lambda_{1,2}$; b) mode $\lambda_{3,4}$; of the 9 bus system with wind power penetration increases. Case 1: Base case; Case 2: G_2 as a DFIG-WT with FOC controller; and Case 3: G_2 as a DFIG-WT with SMC controller.

The relevant property modes of the wind power penetration and the DFIG controller type are shown in Fig. 5.7. This figure shows the oscillation frequencies of the swing-rotor modes (left plot) and the damping ratios (right plot).

The mode $\lambda_{1,2}$,corresponds to the machine at bus 1 which oscillates with a frequency close to one-third the frequency in the base case (case 1). It can be seen that for Case 3, when the DFIG-WT is controlled by SMC, there is an enhancement of the mode damping of up to 5% compared to the one obtained by FOC in Case 2.

The oscillation frequency of mode $\lambda_{3,4}$, associated to Generator 3, in Fig. 5.7(b), is about 10% higher than when Generator 2 is a synchronous generator. The reason is that the hydro-turbine unit is quite heavy and the contribution of Generator 2 to this mode in the base case is quite marginal, as it can be observed from Fig. 5.3. Likewise, the damping ratio is around 2% better than the base case.

This case has furnished preliminary results that show that a DFIG WT with SMC yields excellent results in small-signal stability assess-

ment of small systems and that it has a great deal of potential in this area of electrical power systems; hence, a larger system is investigated next.

5.3 The Two-area System

The small signal studies presented in this section were performed using a similar system to that of [21]. The one-line diagram is given in Fig. 5.8. It consists of two areas, each one containing two generators. The loads are modelled as constant MVA.

Generators G_1, G_3 and G_4 represent conventional synchronous generation; G_2 represents either conventional synchronous generation or wind power generation. In the latter case, a DFIG-based wind turbine represents a wind farm.

The synchronous generators are all identical machines which are represented using the detailed two-axis model with IEEE type I exciter model. The differential equations for the synchronous unit are given by equations (5.1)-(5.4). The synchronous machine data is given in Table. 5.5. The exciter model in block diagram form and its associated data are given in Fig. 5.2 and Table. 5.1.

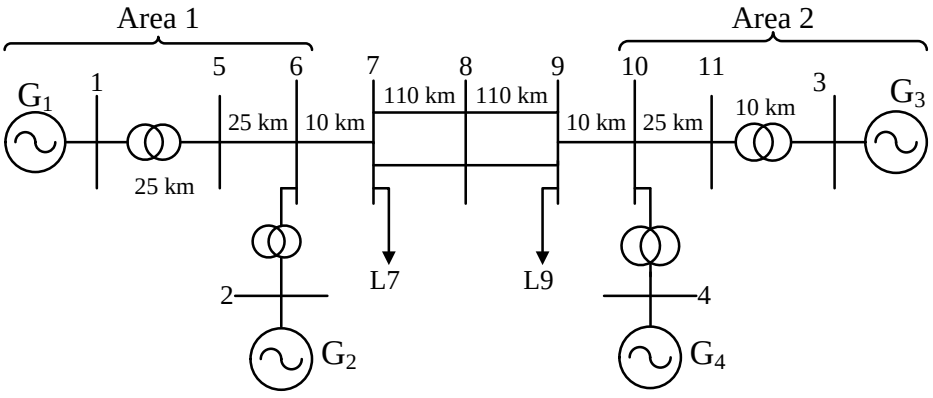

Figure 5.8: Two-area system

Table 5.5: Machine Data in per unit on the rated MVA base

R_s	X_d	X_q	X'_d	X'_q	T'_{do}	T'_{qo}	H	D
0.00028	1.8	1.7	0.3	0.55	8.0	0.4	54	0.0

Both, the synchronous generators models and the DFIG WT models are assumed to operate under the same conditions as in the previous section. Data for the DFIG-WT is given in Table 4.1.

The system base power is 100 MVA and the system frequency is 50 Hz. The generator rated powers are: Generator 1 = 1000 MW, Generator 2 = 500 MW, Generator 3 = 1000 MW, and Generator 4 = 500 MW.

The parameters of the lines in per unit on the system 100 MVA base and 230 kV base are:

$$r = 0.0001\text{pu/km} \quad x_L = 0.001\text{pu/km} \quad b_C = 0.00175 \text{ pu/km}$$

Table 5.6 summarizes the power flow results for the case of 42% of generation from Generator 2.

Table 5.6: Load Flow Results of the two-area system

Bus #	**Bus type**	**Voltage** (pu)	P_G (pu)	Q_G (pu)	P_L (pu)	Q_L (pu)
1	P-V	$1.0100 \angle 0.6290°$	4.9000	0.3218	—	—
2	P-V	$1.0100 \angle -8.164°$	2.1000	-0.0492	—	—
3	Swing	$1.0100 \angle 0.0000°$	4.9205	0.3326	—	—
4	P-Q	$1.0100 \angle -7.242°$	2.3000	-0.0254	—	—
5	P-Q	$1.0080 \angle -4.770°$	—	—	—	—
6	P-Q	$1.003 \angle -11.730°$	—	—	—	—
7	P-Q	$1.002 \angle -15.712°$	—	—	7.00	0.35
8	P-Q	$1.023 \angle -15.610°$	—	—	—	—
9	P-Q	$1.001 \angle -15.260°$	—	—	7.00	0.35
10	P-Q	$1.002 \angle -11.150°$	—	—	—	—
11	P-Q	$1.0080 \angle -4.159°$	—	—	—	—

Modal analyses for four different operating conditions were carried out. The conditions correspond to a variation of the output power from Generator 2 by considering wind power penetration levels of 0.28%, 0.42%, 0.6%, and 0.76%. The dispatch from generators G_1, and G_4 is kept constant.

For each one of the four operating conditions considered, the results when Generator 2 in Area 1 is modelled as a conventional synchronous generator are compared against those obtained when the generator is replaced by a single DFIG wind turbine generator. The aim is to establish the dynamic stability characteristics that enable an assessment of the contribution of wind generation to stability at various levels of wind penetration.

The state variables vector of the system is composed of

$$x_n = \begin{bmatrix} x_1 & x_2 & x_3 & x_4 \end{bmatrix}^T$$

where x_n indicates the state variables vector of generator connected at bus i.

The state vector of a synchronous generator is made up of the states of the two-axis model as well as of the state variables of the exciter model described in previous section (equation (5.8)).

For each operating condition two cases are analyzed:

a. *Power network with no wind generation.*

   In this case the eigenvalue analysis is carried out assuming that all generation, in both areas, are of the conventional synchronous generator type.

   From power dispatch variations, the response of electro-mechanical oscillatory modes is analyzed. This is accomplished by increasing the power output of Generator 2.

In this case the system is a 28^{th} order model with equation (5.10) providing the basic building block, with $i = 1, 2, 3, 4$.

b. *Power network with wind generation.*

Generator 2 of Area 1 is assumed to be a DFIG-based wind farm and two different controllers are employed, namely the FOC-based and SMC-base controllers.

The influence of the wind power penetration on the behaviour of the swing modes of the system is examined. The assessment of this impact is compared to the one obtained from the case with no wind power generation.

When the FOC-based controller is used, the system is a 32^{nd} order one with the following state variables

$$x_n = \begin{bmatrix} x_{SG_i} & x_{WT} \end{bmatrix}^T \tag{5.12}$$

with x_{SG_i} being the state vector of the synchronous generators for $i = 1, 2, 3$ and, x_{WT} = state vector of the DFIG-based wind turbine where $x_c = \begin{bmatrix} X_{i_d} & X_{i_q} & X_{T_e} & X_{Q_S} \end{bmatrix}^T$ being the state variables of the FOC-based controller.

When a SMC-based controller is used, the system is a 28^{th} order one with the state vector given by equation (5.12) where x_{WT} is a 7^{th} order system.

5.3.1 Power Network With No Wind Generation. The Base Line Case

In this case the exported power is supplied by a steam turbine driven synchronous generator. It provides the base line case against which the results obtained with the system containing wind power generation, will be contrasted to.

Table 5.7 reports on the eigenvalues and modal properties for the operating point given in Table 5.6. The zero eigenvalues are not shown.

It can be observed that the system is stable, since the real part magnitudes of all eigenvalues are on the left side of the complex plane. The oscillatory modes correspond to local and inter-area modes associated with generator angles and speeds, and exciter state variables.

The swing-rotor modes ($\lambda_{1,2}$, $\lambda_{3,4}$, $\lambda_{5,6}$) are the dominant modes; they are poorly damped ($< 5\%$) and exhibit the largest time constants. They have a frequency within the range from 1.7 to 2.5 Hz.

The test system shows an intra-area oscillation between buses 1 and 2, $\lambda_{1,2}$, and inter-area oscillations between buses 1 and 3 and 4, $\lambda_{3,4}$, and, between buses 2 and 4, $\lambda_{5,6}$. Notice that the generators in the test system do not represent one single generator, but a group of strongly coupled, coherent generators.

The influence of the active power dispatch variations on the behaviour of the swing modes is depicted in Figs. 5.9, 5.10 and 5.11. The figures at the top show the eigenvalues movement; their respective participation factors are shown below the figure of eigenvalues movement.

The behaviour of the mode $\lambda_{1,2}$ is shown in Fig. 5.9, Fig. 5.10 shows the mode $\lambda_{3,4}$ and, Fig. 5.11 shows the behaviour of the mode $\lambda_{5,6}$. The arrow in the figures indicates the direction of increasing dispatch from Generator 2.

Mode $\lambda_{1,2}$ is an intra-area oscillation associated to generators in Area 1 (G_1, G_2) (Fig. 5.9(a) - bottom figure). From the top plot in Fig. 5.9(a), the reduction in stability margin is quite striking (up to about -40% reduction) for this intra-area oscillation, when the active power output of Generator 2 increases progressively for the whole range of power output considered.

Table 5.7: System modes of the two-area system without wind generation

Mode #	Eigenvalue $\sigma_i \pm j\omega_i$	Frequency f (Hz)	Damping ratio ζ(pu)	Dominant states	Machine at bus	Participation factor (%)
$\lambda_{1,2}$	-0.9123 $\pm$ j15.426	2.4551	0.05903	δ, ω	1	18.5, 18.5
					2	15.6, 15.6
$\lambda_{3,4}$	-0.7759 $\pm$ j15.741	2.5053	0.04923	δ, ω	3	22.2, 22.2
					1	12.1, 12.1
					4	12.0, 12.0
$\lambda_{5,6}$	-0.4370 $\pm$ j11.09	1.7650	0.03937	δ, ω	2	17.8, 17.8
					4	17.1, 17.1
$\lambda_{7,8}$	-5.2165 $\pm$ j7.813	1.2435	0.55527	V_R, E_{fd}	1	14.2, 13.9
					3	13.4, 13.1
					2	10.5, 10.2
					4	9.2, 8.9
$\lambda_{9,10}$	-5.2674 $\pm$ j7.895	1.2565	0.55499	V_R, E_{fd}	3	17.4, 17.0
					1	15.5, 15.2
$\lambda_{11,12}$	-5.3042 $\pm$ j7.947	1.2648	0.55514	V_R, E_{fd}	2	29.9, 29.0
					1	17.9, 17.4
$\lambda_{13,14}$	-5.3112 $\pm$ j7.949	1.2653	0.55551	V_R, E_{fd}	4	30.6, 29.8

					3	17.0, 16.5
λ_{15}	-4.6106	-	-	E'_d	2	64.6
					1	36.8
λ_{16}	-4.7404	-	-	E'_d	4	71.0
					3	30.1
λ_{17}	-3.8543	-	-	E'_d	3	40.7
					1	34.0
					2	14.7
					4	13.5
λ_{18}	-2.9843	-	-	E'_d	1, 3	29.9, 28.1
					2, 4	22.0, 18.3
$\lambda_{19,20}$	-0.4132 $\pm$ j1.1113	0.1768	0.3485	E'_q, R_f	3	17.8, 13.2
					1	17.2, 12.8
$\lambda_{21,22}$	-0.4341 $\pm$ j0.77713	0.1236	0.4876	E'_q, R_f	1	20.9, 16.4
					3	20.8, 16.3
$\lambda_{23,24}$	-0.4179 $\pm$ j0.47285	0.0752	0.6622	E'_q, R_f	2	22.5, 18.3
					4	11.8, 9.6
$\lambda_{25,26}$	-0.4149 $\pm$ j0.45413	0.0722	0.6745	E'_q, R_f	4	26.4, 21.5
					2	15.1, 12.3

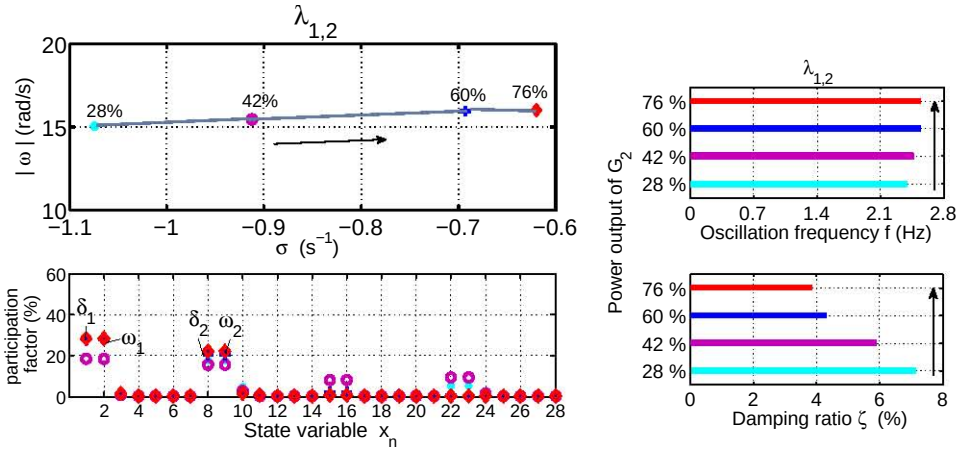

(a) Mode $\lambda_{1,2}$ (b) Eigenvalue properties

Figure 5.9: Impact of power output increases of G_2 on the intra-area mode $\lambda_{1,2}$ of the two-area system. a) Eigenvalue movement (top) and participation factors (bottom). b) Oscillation frequency (top) and damping ratio (bottom). The arrow indicates the direction of increasing wind power penetration. Base case.

The frequency of oscillation is only lightly affected by power variation, (Fig. 5.9(b) - top), but it nevertheless increases at the higher power output rate of Generator 2, e.g., from 2.39 Hz at 28% of P to 2.47 Hz at 76% of P; representing a change of about 6%. Conversely, the damping is much affected; it reduces by about 45% (Fig. 5.9(b) - bottom.

Mode $\lambda_{3,4}$ is an intra-area oscillation associated to generators in Area 2 (G_3, G_4) (Fig. 5.10(a) - bottom). However, the angle and rotor speed of G_1 contribute, to a smaller extent, depending on the specific operating conditions. It is observed from Fig. 5.10 (a) - bottom that this mode tends to be an inter-area mode when generation of G_2 is about 42% but, the rotor speed and angle of generator 3 in Area 2 are the dominant states.

From Fig. 5.10(a) - top, it can be seen that real part magnitude of the eigenvalue moves to the left half plane, from the origin; it changes by about 20%.

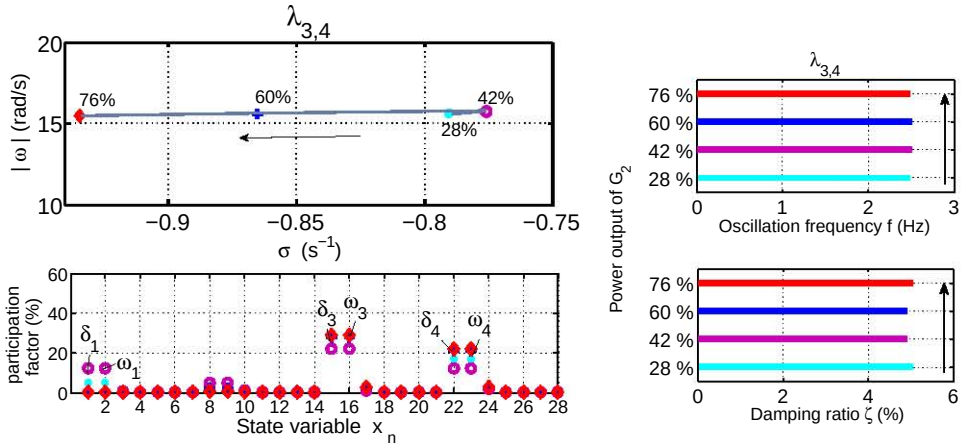

(a) Mode $\lambda_{3,4}$ (b) Eigenvalue properties

Figure 5.10: Impact of power output increases of G_2 on the intra-area mode $\lambda_{3,4}$ of the two-area system. a) Eigenvalue movement (top) and participation factors (bottom). b) Oscillation frequency (top) and damping ratio (bottom). The arrow indicates the direction of increasing wind power penetration . Base case.

The frequency of oscillation is to a lesser degree influenced by the power dispatch change, (Fig. 5.10(b) - top). It only increases by about 1.6%. Hence, the damping ratio decreases up to 18%, Fig. 5.10(b) - bottom.

Mode $\lambda_{5,6}$ is an inter-area oscillation as it can be confirmed by looking at the participation factors in Fig. 5.11(a) - bottom. From Fig. 5.11(a) - top, it can be observed that the stability margin of this oscillatory mode reduces with increases of the active power output of Generator 2. It decreases up to 60% between extreme operating conditions (from 28% to 76% of P_{G_2}).

The frequency of oscillation in Fig. 5.11(b) - top varies only up to 2%, and hence the damping is reduced from 5.4% for $P_{G_2} = 28\%$ to 3.4% for $P_{G_2} = 76\%$, Fig. 5.11(b) - bottom. This is the dominant mode.

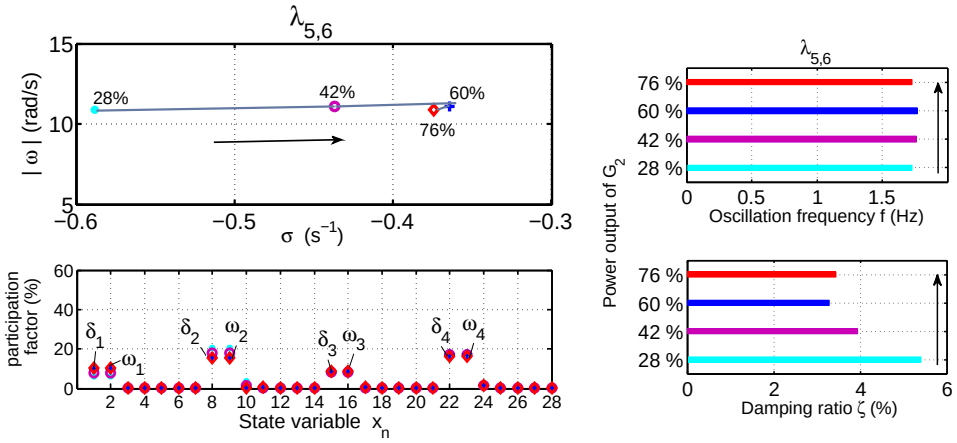

(a) Mode $\lambda_{5,6}$ (b) Eigenvalue properties

Figure 5.11: Impact of increasing power output of G_2 on the intra-area mode $\lambda_{5,6}$ of the two-area system. a) Eigenvalue movement (top) and participation factors (bottom). b) Oscillation frequency (top) and damping ratio (bottom). The arrow indicates the direction of increasing wind power penetration. Base case.

5.3.2 Power Network with Wind Generation

To assess the potential benefits that wind power may bring into the operation of the power system, the conventional synchronous Generator 2 of Area 1 is replaced by a DFIG wind farm. The power contributed by wind farm was taken to represent a variable wind penetration into Area 1.

The study carried out in this section with the DFIG WT uses both the FOC and the SMC strategies, one at the time. The oscillatory modes of the test system with the two DFIG-WT controllers are shown below.

Table 5.8, indicates the exciter-field oscillatory modes corresponding to the three cases under study: 1) Generator 2 as a steam turbine synchronous generator, 2) Generator 2 as a DFIG WT controlled by FOC and 3) Generator 2 as a DFIG WT controlled by SMC. These low frequency and well-damped modes remain practically with no change. The same is true for all other operating conditions.

Table 5.8: Properties and dominant states of the exciter-field modes

Case	f_{osc} (Hz)	ζ (pu)	**Dominant states**	**Machine at bus**	**Case**	f_{osc} (Hz)	ζ (pu)	**Dominant states**	**Machine at bus**
1	1.2432	0.5539	V_R, E_{fd}	1, 2	2	1.2408	0.5555	V_R, E_{fd}	1, 3, 4
					3	1.2405	0.5560	V_R, E_{fd}	1, 3, 4
1	1.2633	0.5534	V_R, E_{fd}	2, 1	2	-	-	-	-
					3	-	-	-	-
1	1.2564	0.5542	V_R, E_{fd}	4, 3, 1	2	1.2574	0.5542	V_R, E_{fd}	1, 3, 4
					3	1.2574	0.5542	V_R, E_{fd}	1, 3, 4
1	1.2646	0.5557	V_R, E_{fd}	4, 3	2	1.2647	0.5557	V_R, E_{fd}	3, 4
					3	1.2647	0.5557	V_R, E_{fd}	3, 4
1	0.1805	0.3426	E'_q, R_f	3, 1	2	0.1941	0.2986	E'_q, R_f	1, 3
					3	0.1854	0.3057	E'_q, R_f	1, 3
1	0.1233	0.4942	E'_q, R_f	1, 3	2	0.1196	0.5020	E'_q, R_f	1, 3
					3	0.1188	0.5050	E'_q, R_f	1, 3
1	0.0782	0.6671	E'_q, R_f	2, 1, 4	2	-	-	-	-
					3	-	-	-	-
1	0.0718	0.6798	E'_q, R_f	4, 3	2	0.0721	0.6778	E'_q, R_f	4, 3
					3	0.0721	0.6779	E'_q, R_f	4, 3

Figs. 5.12-5.17 present the results of the two cases, variation of wind power penetration and DFIG WT controlled by both control options. The impact on the eigenvalues of the oscillatory modes of the system is illustrated in Figs. 5.12, 5.13, 5.14. The eigenvalue movement is depicted in Figs. 5.12(a), 5.13(a), and 5.14(a) with their respective participation factors in Figs. 5.12(b), 5.13(b), and 5.14(b). The participation factors of the DFIG WT controlled by FOC are shown on top and those of the DFIG WT controlled by SMC are shown at the bottom. The eigenvalue properties are shown in part (c) of Figs. 5.12, 5.13 and, 5.14; the frequency of oscillation on the LHS and the damping ratio on the RHS.

In this case, the system shows an intra-area oscillation between buses 3 and 4 ($\lambda_{1,2}$) and inter-area oscillations between bus 1 and bus 4 ($\lambda_{3,4}$) and between bus 1 and buses 3 and 4 ($\lambda_{5,6}$), as observed from the participation factors in Figs. 5.12(b), 5.13(b), and, 5.14(b), respectively.

As expected, the intra-area mode, associated with the area in which the type of generation is modified, does not exist. Likewise, inter-are oscillations involving Generator 2 in the baseline case do not existent when Generator 2 is a DFIG WT, they are distributed the remaining synchronous generators.

The system stability is strongly affected by the point of operation in which the controller algorithm of the DFIG WT plays an important role, as seen below.

The behaviour of the intra-area mode of Area 2 ($\lambda_{1,2}$) at different wind power penetration levels is depicted in Fig. 5.12. The intra-area mode loci drawn with solid and dashed lines correspond to the DFIG-FOC and to the DFIG-SMC, respectively. It can be seen that the effect of the DFIG controller scheme is practically the same for both algorithms; the response of $\lambda_{1,2}$ by SMC is only 1% better than the one offered by FOC.

The stability margin of $\lambda_{1,2}$, increases by about 15% when wind generation increases from 28% to 76% while the frequency of oscillation changes by only 1%, as shown in Fig. 5.12(a).

The contribution of state variables on the modes remains with no change in both circumstances, with wind power penetration variations and with changes in DFIG controllers. This can be corroborated from Figs. 5.12(b) where the participation factors with FOC are shown on top and the participation factors with SMC are shown at the bottom.

The $\lambda_{1,2}$ is a low frequency oscillatory mode at around 2.49 Hz (Fig. 5.12(c), left) which is poorly damped, it reaches around 5% for 28% of P and 6% at high levels of wind penetration, i.e., 76% of P (Fig. 5.12(c), right).

The behaviour of the inter-area modes $\lambda_{3,4}$ and $\lambda_{5,6}$ at different wind power penetration levels is depicted in Figs. 5.13 and 5.14, respectively.

The effect of the DFIG controller schemes on the inter-area mode $\lambda_{3,4}$ is very much the same for both, FOC and SMC. The magnitudes $|\sigma_{3,4}|$ of the FOC controller for the four operating points considered (from 28% to 76%) are: $0.4425\,\mathrm{s}^{-1}$, $0.4507\,\mathrm{s}^{-1}$, $0.4858\,\mathrm{s}^{-1}$ and, $0.5463\,\mathrm{s}^{-1}$ whereas for the SMC controller are: $0.4653\,\mathrm{s}^{-1}$, $0.4708\,\mathrm{s}^{-1}$, $0.5128\,\mathrm{s}^{-1}$ and, $0.5724\,\mathrm{s}^{-1}$. The phase angles decrease in value from $12.71\,{}^{rad}/_{\mathrm{s}}$ to $12.58\,{}^{rad}/_{\mathrm{s}}$ for the FOC-based controller and from $12.67\,{}^{rad}/_{\mathrm{s}}$ to $12.36\,{}^{rad}/_{\mathrm{s}}$ for the SMC controller. The oscillation frequency is about 2 Hz and it is a poorly damped mode ($\zeta_{3,4} < 5$)% (Fig.5.13(c), LHS for FOC and RHS for SMC).

It can be noticed that the effect of the DFIG controller scheme is practically the same for both algorithms; the response of $\lambda_{3,4}$ by the SMC-based controller is only a 1 % better than the one furnished by the FOC-based controller.

In the case of the inter-area mode $\lambda_{5,6}$ the impact of the controller is markedly different. The system with the SMC-based controller shows a much improved performance than the FOC-based controller.

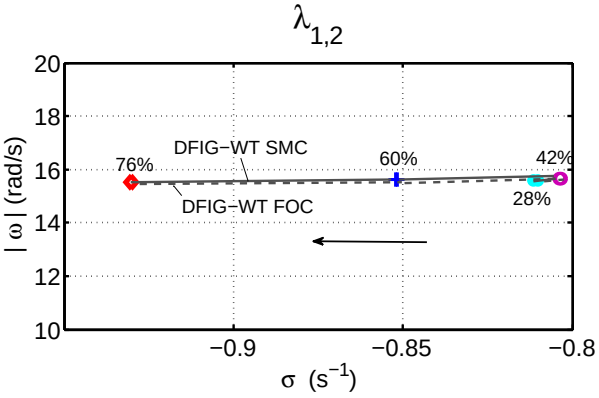

(a)Mode $\lambda_{1,2}$

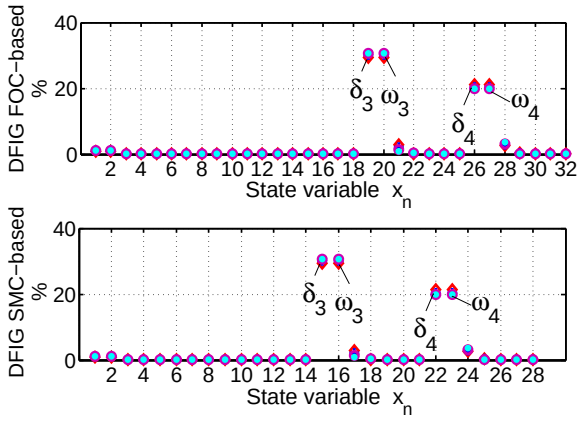

(b)Participation factors

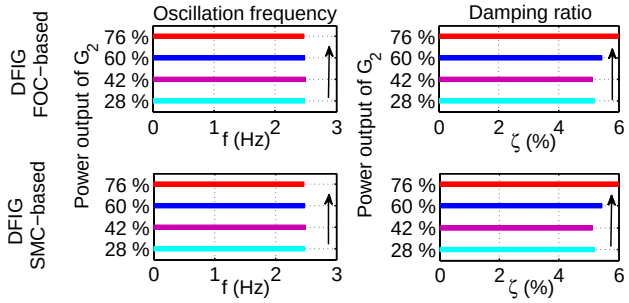

(c)Eigenvalue properties

Figure 5.12: Impact of increasing wind power penetration at bus 2 on the intra-area mode $\lambda_{1,2}$ of the two-area system. a) Eigenvalue movement; b) Participation factors with FOC-based controller (top) and with SMC-based controller (bottom); c) Oscillation frequency (left) and damping ratio (right). The arrow indicates the direction of increasing wind power penetration. Case 2 and Case 3.

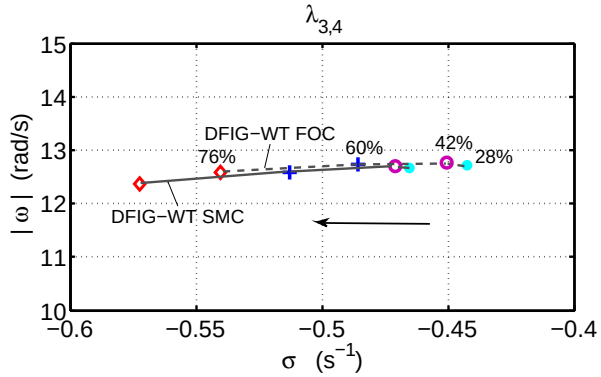

(a)Mode $\lambda_{3,4}$

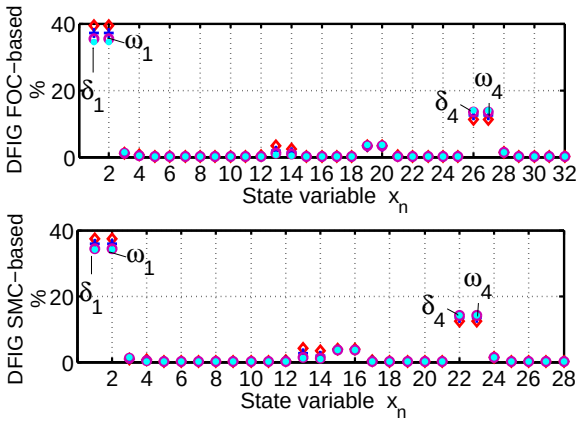

(b)Participation factors

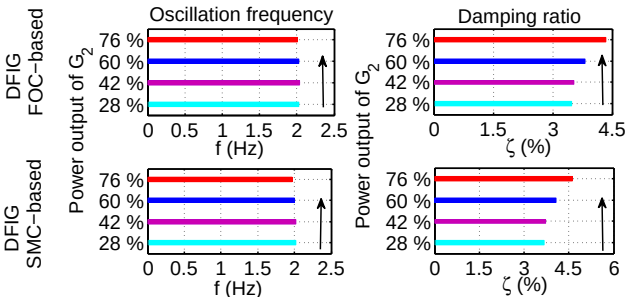

(c)Eigenvalue properties

Figure 5.13: Impact of increasing wind power penetration at bus 2 on the intra-area mode $\lambda_{3,4}$ of the two-area system. a) Eigenvalue movement; b) Participation factors with FOC-based controller (top) and with SMC-based controller (bottom); c) Oscillation frequency (left) and damping ratio (right). The arrow indicates the direction of increasing wind power penetration. Case 2 and Case 3.

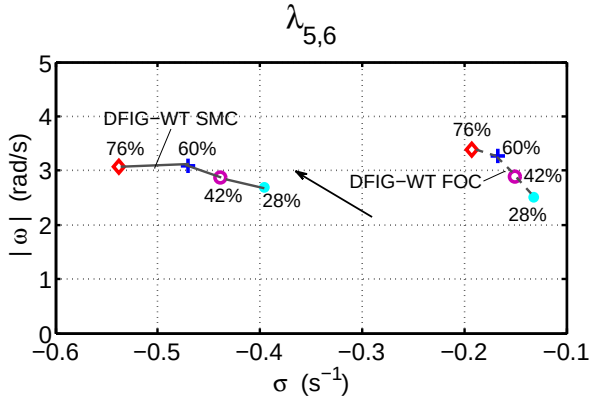

(a)Mode $\lambda_{5,6}$

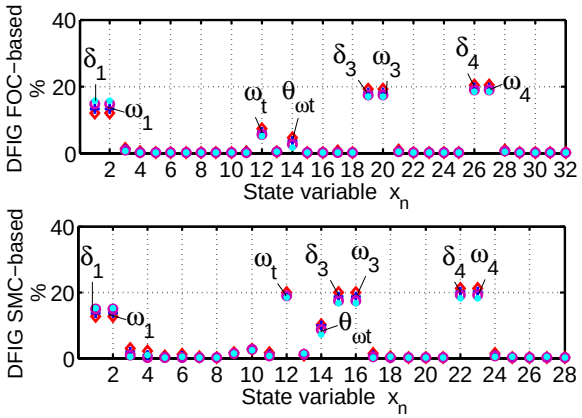

(b)Participation factors

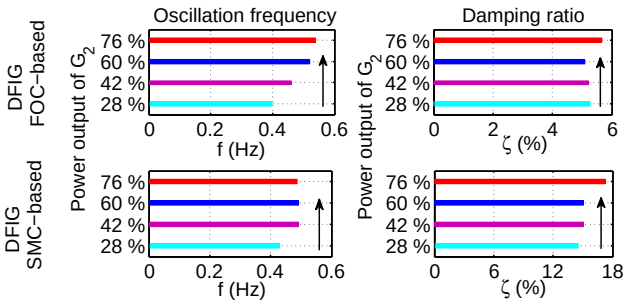

(c)Eigenvalue properties

Figure 5.14: Impact of increasing wind power penetration at bus 2 on the intra-area mode $\lambda_{5,6}$ of the two-area system. a) Eigenvalue movement; b) Participation factors with FOC-based controller (top) and with SMC-based controller (bottom); c) Oscillation frequency (left) and damping ratio (right). The arrow indicates the direction of increasing wind power penetration. Case 2 and Case 3.

The stability margin of this mode ($\lambda_{5,6}$), by the DFIG WT controlled with SMC is almost three times as high as that of the DFIG WT with FOC. Moreover, the magnitude $|\sigma_{3,4}|$, shown in Fig. 5.14(a) for increasing wind power penetrations, shows increases with FOC from $0.1321\,\mathrm{s}^{-1}$ to $0.1925\,\mathrm{s}^{-1}$ whereas with SMC shows values between $0.3955\,\mathrm{s}^{-1}$ and $0.5377\,\mathrm{s}^{-1}$. The difference in the oscillation frequency is of up to 9%. Hence, the damping ratios for the SMC controller for 28% and 76% of wind power are 14.54% and 17.28% (Fig. 5.14(c), bottom) and the damping ratios for the FOC controller are 5.27% and 5.67% (Fig. 5.14(c), top), respectively.

From these results, it may be concluded that just as in the WSCC system the oscillatory modes tend to be more stable as the DFIG WT's active power output approaches its nominal value. This is in stark contrast to the system with a steam turbine driven synchronous generator.

As illustrated in Fig. 5.15, the intra-area mode of Area 2 of the two-area system with wind power generation $\lambda_{1,2}$, is compared to the intra-area mode of Area 2 of the two-area system with no wind power generation, $\lambda_{3,4}$ in Fig 5.15(a).

The comparison between the effects of the wind power penetration and the DFIG controller type on the inter-area mode with wind power generation $\lambda_{3,4}$, and the inter-area mode of the system with no wind power generation $\lambda_{5,6}$ is shown in Fig. 5.15(b). The latter are the dominant modes in each case, with and with no wind generation

The oscillation frequency of the swing-rotor mode is slightly higher when generator at bus 2 is a DFIG, since the equivalent generator in Area 1 becomes lighter by the change of synchronous inertia. This means effectively that this effect is related to the removal of the synchronous generator.

It can be seen that the greater change (around 13%) is in the inter-area mode (Fig. 5.15(b)) while the intra-area mode is practically not affected by the presence of the wind turbine.

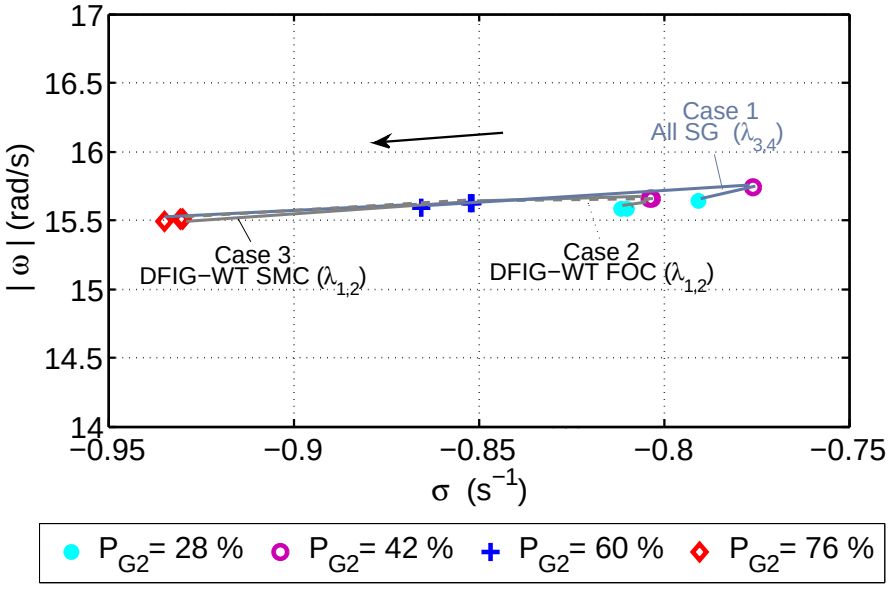

(a)Intra-area mode of Area 2

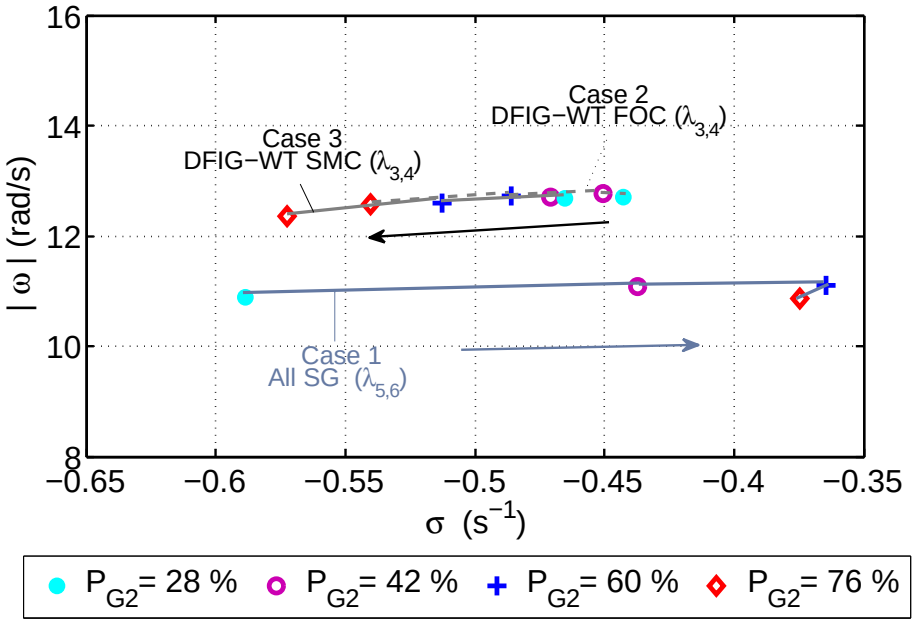

(b)Inter-area mode

Figure 5.15: Impact of wind power penetration on (a) the intra-area mode of Area 2, and (b) the inter-area mode, compared with the base case. The arrow indicates the direction of increasing wind power dispatch.

It should be noticed that the inter-are mode of the test power system with wind power penetration is not linked to the same buses as in the base case (with no wind generation).

The damping ratio is a critical parameter in the system stability. Thus, the obtained damping ratio for the three cases (G_2 as a SG, G_2 as a DFIG WT FOC and G_2 as a DFIG WT SMC) can then be used to judge the effect of DFIG control algorithms on the stability phenomena. Moreover, it can directly be assessed by means of graphical information about the eigenvalue movement.

The SMC controller case exhibits more desirable characteristics than the FOC controller. Although the damping ratio of the SMC controller for the inter-area mode between buses 1 and 4 ($\lambda_{3,4}$), is only 5% better than the FOC controller, its impact on the damping of the inter-area mode between bus 1 and the buses in the Area 2 is far mode significant, it is about three times higher.

Moreover, the increase of wind power level contributes to enhance the performance of the system with DFIG WT SMC, whereas the operating condition does not affect the performance with FOC controller.

It is noticed that DFIG oscillations are also present in this case, similarly to the case of a DFIG directly connected to a strong grid. The DFIG with SMC presents a better dynamic behaviour than the DFIG with FOC.

The behaviour of the electrical mode of the DFIG, $\lambda_{7,8}$, is shown in Fig. 5.16. In Fig. 5.16(a), the magnitude of the DFIG with SMC exhibits values twice as larger as the DFIG with FOC. The magnitudes $|\sigma_{9,10}|$ in Case 2 are $10.17\,\mathrm{s}^{-1}$, $14.19\,\mathrm{s}^{-1}$, $19.59\,\mathrm{s}^{-1}$ and, $23.77\,\mathrm{s}^{-1}$ while in Case 3 are: $24.39\,\mathrm{s}^{-1}$, $30.52\,\mathrm{s}^{-1}$, $38.34\,\mathrm{s}^{-1}$ and $44.17\,\mathrm{s}^{-1}$. These values correspond to increases in wind power generation of 28%, 42%, 60% and, 76%, respectively.

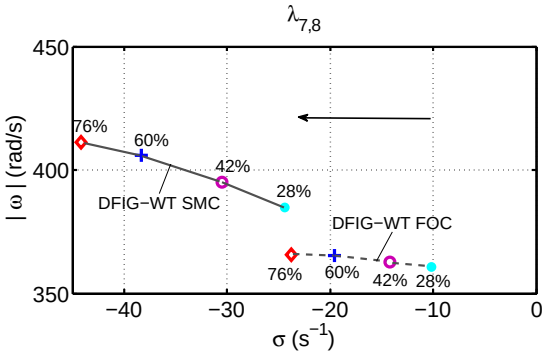

(a)Mode $\lambda_{7,8}$

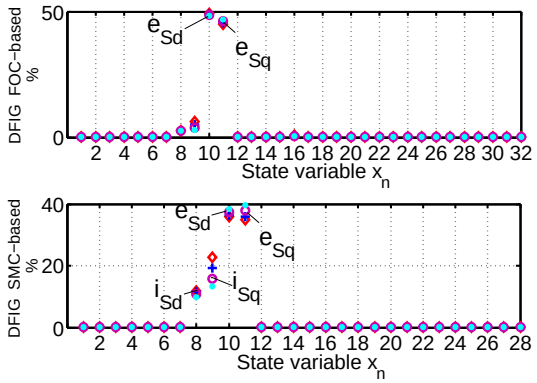

(b)Participation factors

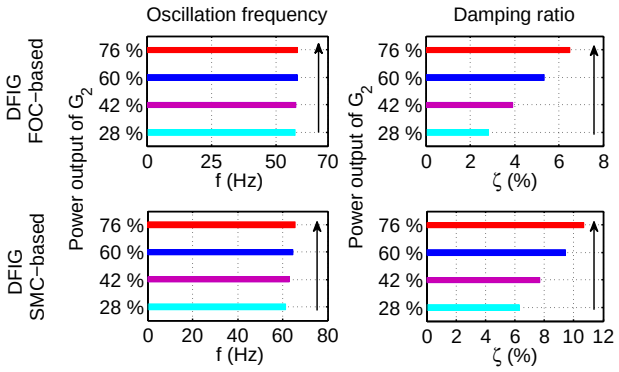

(c)Eigenvalue properties

Figure 5.16: Impact of increasing wind power penetration at bus 2 on the intra-area mode $\lambda_{7,8}$ of the two-area system. a) Eigenvalue movement; b) Participation factors with FOC-based controller (top) and with SMC-based controller (bottom); c) Oscillation frequency (left) and damping ratio (right). The arrow indicates the direction of increasing wind power penetration. Case 2 and Case 3.

This is a high frequency oscillatory mode near the grid frequency, Fig. 5.16(c), left.

As shown in Fig. 5.16(c), right, the damping is higher using the SMC-based strategy (bottom plot).

When the DFIG supplies power operating above synchronous speed (for instance 76% of P), the damping of the electrical mode by SMC control is 10.7% in contrast to the 6.5% offered by the FOC control.

The behaviour of the mechanical mode of the DFIG, $\lambda_{9,10}$, is shown in Fig. 5.17. Similarly to the case of the electrical mode, the magnitude of the mechanical oscillation with the DFIG under SMC-based control scheme also exhibits values twice as large as than those under FOC, as shown in Fig. 5.17(a); while $|\sigma_{7,8}|$ has values of around $4\,\mathrm{s}^{-1}$, in Case 3 and it has values of around $1.8\,\mathrm{s}^{-1}$ in Case 2.

This mode oscillates with a frequency of around 1.6 Hz, Fig.5.17(c), LHS plot. As shown in Fig. 5.17(c), RHS plot, the damping is higher with SMC, bottom plot. Despite the fact that this is a well damped out mode ($> 15\%$), the damping of the electrical mode by SMC control is about 37% compared to the 17% offered by the FOC control.

The damping of the mechanical mode remains almost with no change in the face of DFIG WT power generation changes.

Therefore, the stability margins afforded by SMC to both electrical and mechanical modes, is about double the stability margins offered by FOC.

These results show quite amply that the SMC controller exhibits a superior performance over the FOC controller. Hence,power system stability may be improved through a wider deployment of the DFIG SMC wind technology.

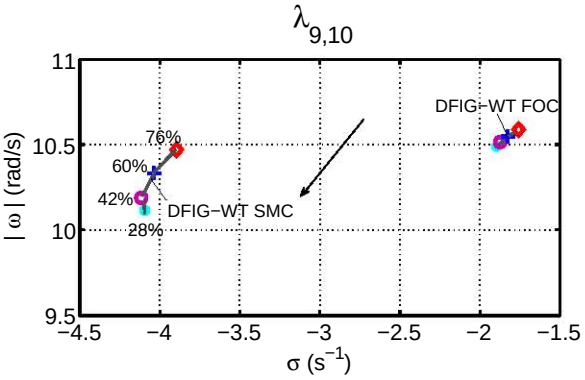

(a) Mode $\lambda_{9,10}$

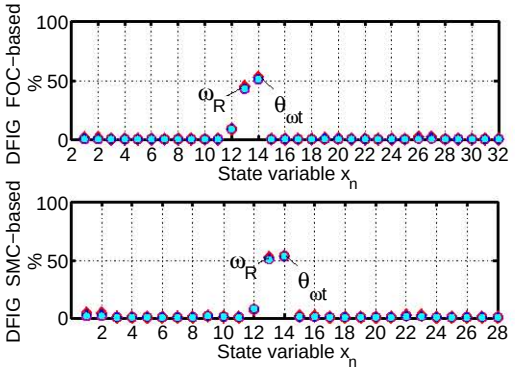

(b) Participation factors

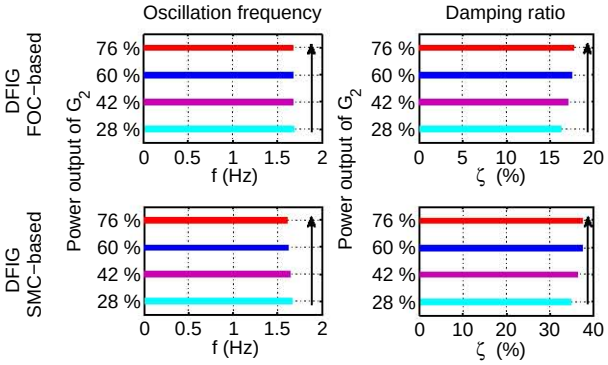

(c) Eigenvalue properties

Figure 5.17: Impact of increasing wind power penetration at bus 2 on the intra-area mode $\lambda_{9,10}$ of the two-area system. a) Eigenvalue movement; b) Participation factors with FOC-based controller (top) and with SMC-based controller (bottom); c) Oscillation frequency (left) and damping ratio (right). The arrow indicates the direction of increasing wind power penetration. Case 2 and Case 3.

5.4 Conclusions

The impact of the integration of wind power generation systems with double-fed induction generators has been assessed in this chapter. The advantage of using this variable-speed wind turbine concept in mixed generation to improve on the stability of power networks has been demonstrated under different test case scenarios, by computer simulation.

Field Oriented Control and Sliding Mode Control strategies have been used to elucidate on the contribution that wind generator controllers may exert on network damping. The analytical validation illustrates the effectiveness and potential capability of the proposed Sliding Mode Control approach to provide a dynamic enhancement of the DFIG itself, and to achieve a much superior performance of grid connected wind turbines.

Chapter 6

Transient Stability

This chapter addresses the issue of transient stability assessment of wind power generators with particular reference to power system oscillations damping. A control system based on Sliding Mode Control principles is investigated in DFIG WT systems to contribute to network operational support. Simulation results are provided and discussed to show the potential of the nonlinear controller to enhance damping of inter-area oscillations.

6.1 Background

It should be remarked that many important contributions have been made toward the understanding of dynamic interactions between conventional generation and wind power generation, by resorting to transient stability models and methods and linearized models suitable for modal analyses.

In early works [90], the dynamic and transient stability properties of wind turbine generators integrated into power systems were explored. The study was addressed considering both, single and grouped wind turbines and the influence of electrical and wind speed disturbances. Further studies to understand the dynamic characteristics of electrical network comprising wind energy generation can also be found in [52],[111].

Determining the impact of DFIG generation on large-scale power system stability has been a major concern for quite some time, including among others things, the dynamic response to short-circuit faults and system perturbations due to synchronous generators and transmission line outages, damping of oscillations, etc.

It has been reported in the open literature that DFIG WT have the capacity to augment the transient stability margin of conventional synchronous generators when integrated in the same electrical network [100, 131, 132]. One of the reasons given is that the DFIG's two rotor current regulators also act upon the other generators in the vicinity, improving their dynamic behaviour. Moreover, DFIG deployment reduces the dynamic reactive compensation demands on both neighbouring generators and the power network, which would reduce instances of voltage collapses in the power network.

In [132], simulation studies carried out with and with no wind power integrated into the power grid, showed that in cases of severe grid faults the fast control schemes of the DFIG converters do help to ride through the fault and to maintain the integrity of the whole system. It was also pointed out that a DFIG WT does not suffer problems of angular stability, as it is the case with conventional synchronous generators and that DFIG WT integration makes up for an improved transient performance of the system.

A great deal of very useful conclusions have been drawn by comparing the transient stability margins of power networks with variable-speed wind system and those of power networks with fixed speed wind systems. Attention has been drawn to the inherent risk that fixed speed wind turbines have of undergoing voltage and rotor speed instability, initiated by a short-circuit fault or by the tripping of a synchronous generator and a key conclusion has been that that risk is much lower with variable speed wind turbines [133].

The impact of DFIG WT on weak transmission systems was investigated in [56], where the results showed that DFIGs yield an improved damping performance compared to conventional synchronous generators of equivalent ratings, a study carried out for various wind plant load factors and covering a range of dynamic response of the turbines to short-circuit faults. It is recommended in [134] that transient simulation studies be carried out to assess the post-disturbance behaviour of a power system for a range of credible operating scenarios and disturbances, even if the system eigenvalues have been determined and showed the system to be stable.

The impact of short-circuit faults, load disturbances and voltage dips on the dynamic performance of DFIG WTs has also been addressed in [135, 136, 119]. It was found in [135] that the dynamic behaviour of a DFIG subjected to a voltage dip is dominated by the stator dynamics with poorly damped modes. These, in turn, are greatly affected by the rotor current control bandwidth and active damping, rotor back-emf voltages and DFIG power factor. In [136] a new control scheme was put forward in order to provide the DFIG WT with a much improved voltage control and voltage recovery following a fault. Furthermore, the authors claim that the new control scheme give the DFIG WT the capacity to withstand fault clearances over synchronous generator with conventional excitation control, for an ample margin.

At the modelling and simulation level, a major disadvantage of the DFIG WT has been the relative complexity and computing demands of its mathematical model, which hinders the transient analysis of the system and limits the simulations studies of whole wind generation system. Great many research efforts have been made to overcome this outstanding issue. In order to reduce simulation times and the power system model complexity, DFIG-based wind turbine models compatible with transient analysis programs have been developed and published in the open literature [110, 137, 138]. By way of example, in [110] a sim-

plified DFIG WT model was developed where the power converter is represented by an equivalent voltage source, which regulates the rotor current to meet the scheduled active and reactive power production. The model performance was tested by simulating the interaction between the Arklow Bank Wind Farm and the Irish National Grid. The proposed model is computationally efficient and suitable for large scale power system analysis but owing to the intrinsic assumption made in the model, it cannot be used to study the internal dynamic performance of the power converter.

The authors in [137] published a simplified model of the DFIG, alternative to the third-order model, which renders a more intuitive estimation of the DFIG performance under transient conditions. The model yields explicit information of the active and reactive power injections through the stator, as well as balance and unbalanced voltage drops due to grid faults. The model reproduces the behaviour of the DFIG by resorting to two second-order transfer functions. The work at [138], puts forward yet another alternative, it uses selective modal analysis to reduce the wind turbine model for time domain simulations by focusing on the most relevant modes and variables. The model was applied in two test systems and it showed to match closely the behaviour of the original power system, in cases of transmission lines and synchronous generators outages.

The impact of reduced inertia (due to increased wind power penetration) on transient stability performance has been also examined. It has been found that the transient performance is negatively affected by certain disturbances, which nevertheless may be ameliorated by control to overcome the decoupling of the inertia in DFIGs.

It has been discussed in Chapter 2, that various mechanisms are available to provide the DFIG with frequency response capability; for instance, primary frequency control based on grid frequency deviation

[19], frequency response by unloading the wind turbine [20, 72], supplementary control similar to the natural inertial response [67], etc.

The authors in [121], assessed the impact of increased DFIG penetration on transient stability through the excitation of the dominant modes, by applying specific faults at buses close to the generators with the largest participation factors. Both detrimental and beneficial effects of increased DFIG penetration on the system were identified by applying this technique covering a range of fault scenarios.

6.2 DFIG dynamic model

In a double-fed induction generator the wound rotor is fed through a variable frequency converter via the slip rings which are attached to the rotor circuit. The rotor converter is commonly referred to as the machine side converter (MSC). The stator windings are directly connected to the grid. This arrangement is schematically depicted in Fig. 6.1.

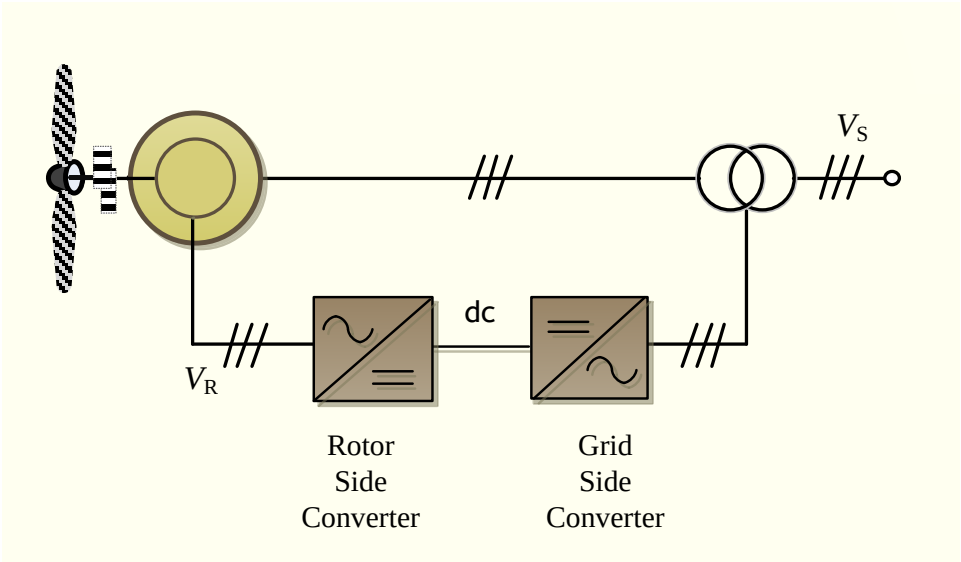

Figure 6.1: Converter configuration for the DFIG-based wind turbine

6.2.1 Dynamic equations of the machine

In this study the DFIG is represented by a balanced continuous-time model by replacing the flux-currents relations in equations (3.70)-(3.73).

This yields the following dq axis equations expressed in per unit,

$$\underline{v}_{S_{dq}} = -R_S\underline{i}_{S_{dq}} - \frac{L_S}{\omega_{elB}}\frac{d\underline{i}_{S_{dq}}}{dt} - \frac{L_o}{\omega_{elB}}\frac{d\underline{i}_{R_{dq}}}{dt} + j\omega_S L_S\underline{i}_{S_{dq}} + j\omega_S L_o\underline{i}_{R_{dq}} \tag{6.1}$$

$$\underline{v}_{R_{dq}} = -R_R\underline{i}_{R_{dq}} - \frac{L_o}{\omega_{elB}}\frac{d\underline{i}_{S_{dq}}}{dt} - \frac{L_R}{\omega_{elB}}\frac{d\underline{i}_{R_{dq}}}{dt} + js\omega_S L_o\underline{i}_{S_{dq}} + js\omega_S L_R\underline{i}_{R_{dq}} \tag{6.2}$$

where ω_{elB}, is the electrical base speed, $s = 1 - \dfrac{\omega_R}{\omega_S}$, is the slip frequency, and ω_R, is the rotor speed.

6.3 DFIG Control Design

6.3.1 Sliding Control Design in the Machine Side Converter

From equations (6.1)-(6.2), the rotor voltage at the machine side converter terminals can be obtained as follows:

$$\begin{pmatrix}\underline{v}_{S_{dq}}\\ \underline{v}_{R_{dq}}\end{pmatrix} = -\frac{1}{\omega_{elB}}\begin{pmatrix}L_S & L_o\\ L_o & L_R\end{pmatrix}\frac{d}{dt}\begin{pmatrix}\underline{i}_{S_{dq}}\\ \underline{i}_{R_{dq}}\end{pmatrix} + \begin{pmatrix}-R_S + jL_S & j\omega_S L_o\\ js\omega_S L_o & -R_R + js\omega_S L_R\end{pmatrix}\begin{pmatrix}\underline{i}_{S_{dq}}\\ \underline{i}_{R_{dq}}\end{pmatrix}$$

Solving for the current derivatives,

$$\frac{d}{dt}\begin{pmatrix}\underline{i}_{S_{dq}}\\ \underline{i}_{R_{dq}}\end{pmatrix} = \frac{\omega_{elB}}{\sigma L_R L_S}\begin{pmatrix}L_R & -L_o\\ -L_o & L_S\end{pmatrix}\begin{pmatrix}-R_S + jL_S & j\omega_S L_o\\ js\omega_S L_o & -R_R + js\omega_S L_R\end{pmatrix}\begin{pmatrix}\underline{i}_{S_{dq}}\\ \underline{i}_{R_{dq}}\end{pmatrix} - \dots$$

$$\dots - \frac{\omega_{elB}}{\sigma L_R L_S}\begin{pmatrix}L_R & -L_o\\ -L_o & L_S\end{pmatrix}\begin{pmatrix}\underline{v}_{S_{dq}}\\ \underline{v}_{R_{dq}}\end{pmatrix}$$

with $\sigma = 1 - \dfrac{L_o^2}{L_S L_R}$

$$\frac{d}{dt}\begin{pmatrix}\underline{i}_{S_{dq}}\\ \underline{i}_{R_{dq}}\end{pmatrix} = \frac{\omega_{elB}}{\sigma L_S L_R}\begin{pmatrix} L_R\left(-R_S + jL_S\right) - L_o j s\omega_S L_o & -j\omega_S L_R L_o - L_o\left(-R_R + js\omega_S L_R\right)\\ -L_o\left(-R_S + jL_S\right) + L_S s\omega_S j L_o & -j\omega_S L_o L_o + L_S\left(-R_R + js\omega_S L_R\right)\end{pmatrix}\cdots$$

$$\cdots\begin{pmatrix}\underline{i}_{S_{dq}}\\ \underline{i}_{R_{dq}}\end{pmatrix} + \frac{\omega_{elB}}{\sigma L_S L_R}\begin{pmatrix} L_R & -L_o\\ -L_o & L_S\end{pmatrix}\begin{pmatrix}\underline{v}_{S_{dq}}\\ \underline{v}_{R_{dq}}\end{pmatrix}$$

Developing further this equations and separating imaginary and real terms, yields,

$$\frac{d}{dt}\begin{pmatrix} i_{S_d} + j i_{S_q}\\ i_{R_d} + j i_{R_q}\end{pmatrix} = \frac{\omega_{elB}}{\sigma L_S L_R}\begin{pmatrix} -R_S L_R + j\left(L_S L_R - L_o^2 s\omega_S\right) & L_o R_R + j L_R L_o \omega_S\left(1-s\right)\\ L_o R_S - j L_o L_S\left(1 - s\omega_S\right) & -R_R L_S + j\omega_S\left(L_S L_R s - L_o^2\right)\end{pmatrix}\cdots$$

$$\cdots\begin{pmatrix} i_{S_d} + j i_{S_q}\\ i_{R_d} + j i_{R_q}\end{pmatrix} + \frac{\omega_{elB}}{\sigma L_S L_R}\begin{pmatrix} L_R & -L_o\\ -L_o & L_S\end{pmatrix}\begin{pmatrix} v_{S_d} + j v_{S_q}\\ v_{R_d} + j v_{R_q}\end{pmatrix}$$

$$\frac{d}{dt}\begin{pmatrix} i_{S_d}\\ i_{S_q}\\ i_{R_d}\\ i_{R_q}\end{pmatrix} = \frac{\omega_{elB}}{\sigma L_S L_R}\left[K_{sr,1}\begin{pmatrix} i_{S_d}\\ i_{S_q}\\ i_{R_d}\\ i_{R_q}\end{pmatrix} + \begin{pmatrix} L_R & 0 & -L_o & 0\\ 0 & L_R & 0 & -L_o\\ -L_o & 0 & L_S & 0\\ 0 & -L_o & 0 & L_S\end{pmatrix}\begin{pmatrix} v_{S_d}\\ v_{S_q}\\ v_{R_d}\\ v_{R_q}\end{pmatrix}\right]$$

with

$$K_{sr,1} = \begin{pmatrix} -R_S L_R & -L_S L_R + L_o^2 s\omega_S & L_o R_R & L_R L_o \omega_S\left(1-s\right)\\ L_S L_R - L_o^2 s\omega_S & -R_S L_R & L_R L_o \omega_S\left(1-s\right) & L_o R_R\\ L_o R_S & -L_o L_S\left(1 - s\omega_S\right) & -R_R L_S & -\omega_S\left(L_S L_R s - L_o^2\right)\\ L_o L_S\left(1 - s\omega_S\right) & L_o R_S & \omega_S\left(L_S L_R s - L_o^2\right) & -R_R L_S\end{pmatrix}$$

This expression may be expressed in a more general form;

$$\frac{d}{dt}\mathbf{x} \;=\; \mathbf{A}\mathbf{x} + \mathbf{B}\mathbf{u} = \mathbf{A}\mathbf{x} + \mathbf{B_S}\mathbf{u_S} + \mathbf{B_R}\mathbf{u_R} \tag{6.3}$$

with

$$\mathbf{A} = \frac{\omega_{elB}}{\sigma L_S L_R}\,K_{sr,1}, \quad \mathbf{B_S} = \frac{\omega_{elB}}{\sigma L_S L_R}\begin{pmatrix} L_R & 0\\ 0 & L_R\\ -L_o & 0\\ 0 & -L_o\end{pmatrix}, \quad \mathbf{B_R} = \frac{\omega_{elB}}{\sigma L_S L_R}\begin{pmatrix} -L_o & 0\\ 0 & -L_o\\ L_S & 0\\ 0 & L_S\end{pmatrix}$$

Furthermore equation (6.3) may be transformed into an expression given in terms of state variables and control inputs applying the transformation matrix,

$$T = \begin{pmatrix} L_S & 0 & L_o & 0 \\ 0 & L_S & 0 & L_o \\ 0 & 0 & 1 & 0 \\ 0 & 0 & 0 & 1 \end{pmatrix} \tag{6.4}$$

which coincides with the stator flux expression, $\Psi_S = L_S i_S + L_o i_R$

Then, the product $T\,B_R$ is,

$$\begin{pmatrix} L_S & 0 & L_o & 0 \\ 0 & L_S & 0 & L_o \\ 0 & 0 & 1 & 0 \\ 0 & 0 & 0 & 1 \end{pmatrix} \frac{\omega_{elB}}{\sigma L_S L_R} \begin{pmatrix} -L_o & 0 \\ 0 & -L_o \\ L_S & 0 \\ 0 & L_S \end{pmatrix} = \frac{\omega_{elB}}{\sigma L_S L_R} \left(\begin{array}{cc} 0 & 0 \\ 0 & 0 \\ \hline L_S & 0 \\ 0 & L_S \end{array}\right)$$

These equations may be expressed as a non-linear equation

$$\dot{\mathbf{x}} = \mathbf{f}(\mathbf{x}) + \mathbf{B}\mathbf{u} \tag{6.5}$$

where

- $\mathbf{x} = \begin{bmatrix} i_{S_d}, & i_{S_q}, & i_{R_d}, & i_{R_q}, & \omega_R \end{bmatrix}^T \in \Re^n$ is state vector with $n = 5$
- $\mathbf{u} = \begin{bmatrix} v_{R_d}, & v_{R_q} \end{bmatrix}^T \in \Re^m$ the control input vector with $m = 2$, i.e., the rotor voltages as seen from the Machine Side Converter (MSC).

To implement the sliding mode control, the dynamic system (6.5) ought to be expressed as a discrete difference equation. In this case, the first derivative is approximated with the backward Euler rule, yielding a model of the form:

$$\dot{x}(t) \approx \frac{x[k+1] - x[k]}{\tau} \tag{6.6}$$

where τ is the sampling time.

Then the discrete version of the continuous equation (6.5) is

$$\mathbf{x}[k+1] = \mathbf{f}(\mathbf{x}) + \mathbf{B}\mathbf{u} \tag{6.7}$$

The extended linearization method, also termed apparent linearization, enables to identify the existence of a family of equilibrium operating points with inputs and outputs identical to the non-linear system. Thus, the extended linear system of (6.7) takes the form

$$\mathbf{x}[k+1] = \mathbf{A}[k]\mathbf{x}[k] + \mathbf{B}[k]\mathbf{u}[k] + \mathbf{D}[k] \tag{6.8}$$

where $\mathbf{A}[k]$, $\mathbf{B}[k]$ and $\mathbf{D}[k]$ are matrices that depend on the k^{th} sample and are taken to be constant during each sampling time τ.

Equilibrium point. To find the equilibrium point of the machine voltage equations (6.1)-(6.2) all the time derivatives are set to zero

$$\underline{v}_{S_{dq}} = -R_S\,\underline{i}_{S_{dq}} + j\omega_S L_S\,\underline{i}_{S_{dq}} + j\omega_S L_o\,\underline{i}_{R_{dq}} \tag{6.9}$$

$$\underline{v}_{R_{dq}} = -R_R\,\underline{i}_{R_{dq}} + js\,\omega_S L_o\,\underline{i}_{S_{dq}} + js\,\omega_S L_R\underline{i}_{R_{dq}} \tag{6.10}$$

Neglecting the stator and rotor resistances [139, 140, 141] yields,

$$\begin{aligned}\underline{v}_{S_{dq}} &= j\omega_S L_S\,\underline{i}_{S_{dq}} + j\omega_S L_o\,\underline{i}_{R_{dq}}\\ \underline{v}_{R_{dq}} &= js\,\omega_S L_o\,\underline{i}_{S_{dq}} + js\,\omega_S L_R\underline{i}_{R_{dq}}\end{aligned}$$

expressed in matrix form

$$\begin{pmatrix}\underline{v}_{S_{dq}}\\ \underline{v}_{R_{dq}}\end{pmatrix} = \begin{pmatrix}j\omega_S L_S & j\omega_S L_o\\ js\,\omega_S L_o & js\,\omega_S L_R\end{pmatrix}\begin{pmatrix}\underline{i}_{S_{dq}}\\ \underline{i}_{R_{dq}}\end{pmatrix}$$

and by equating to zero

$$0 = -\begin{pmatrix}j\omega_S L_S & j\omega_S L_o\\ js\,\omega_S L_o & js\,\omega_S L_R\end{pmatrix}\begin{pmatrix}\underline{i}_{S_{dq}}\\ \underline{i}_{R_{dq}}\end{pmatrix} + \begin{pmatrix}\underline{v}_{S_{dq}}\\ \underline{v}_{R_{dq}}\end{pmatrix}$$

and pre-multiplying by $\begin{pmatrix} L_R & -L_o \\ -L_o & L_S \end{pmatrix}$

$$0 = \begin{pmatrix} L_R & -L_o \\ -L_o & L_S \end{pmatrix} \left[\begin{pmatrix} -j\omega_S L_S & -j\omega_S L_o \\ -js\,\omega_S L_o & -js\,\omega_S L_R \end{pmatrix} \begin{pmatrix} \underline{i}_{S_{dq}} \\ \underline{i}_{R_{dq}} \end{pmatrix} + \begin{pmatrix} \underline{v}_{S_{dq}} \\ \underline{v}_{R_{dq}} \end{pmatrix} \right]$$

yields

$$\begin{aligned} 0 \;=\; & \begin{pmatrix} -j\omega_S L_S L_R + js\,\omega_S L_o L_o & -j\omega_S L_R L_o + js\,\omega_S L_R L_o \\ j\omega_S L_S L_o - js\,\omega_S L_o L_S & j\omega_S L_o^2 - js\,\omega_S L_R L_S \end{pmatrix} \begin{pmatrix} \underline{i}_{S_{dq}} \\ \underline{i}_{R_{dq}} \end{pmatrix} + \dots \\ & \dots + \begin{pmatrix} L_R & -L_o \\ -L_o & L_S \end{pmatrix} \begin{pmatrix} \underline{v}_{S_{dq}} \\ \underline{v}_{R_{dq}} \end{pmatrix} \end{aligned}$$

$$\begin{aligned} 0 \;=\; & \begin{pmatrix} -j\omega_S \left(L_R L_S - sL_o^2\right) & -j\omega_S L_o L_R \left(1-s\right) \\ jL_o L_S \omega_S \left(1-s\right) & -j\omega_S \left(sL_R L_S - L_o^2\right) \end{pmatrix} \begin{pmatrix} i_{S_d} + ji_{S_q} \\ i_{R_d} + ji_{R_q} \end{pmatrix} + \dots \\ & \dots + \begin{pmatrix} L_R & -L_o \\ -L_o & L_S \end{pmatrix} \begin{pmatrix} v_{S_d} + jv_{S_q} \\ v_{R_d} + jv_{R_q} \end{pmatrix} \end{aligned}$$

yields,

$$0 = K_{sr,2} \begin{pmatrix} i_{S_d} \\ i_{S_q} \\ i_{R_d} \\ i_{R_q} \end{pmatrix} + \begin{pmatrix} L_R & 0 & -L_o & 0 \\ 0 & L_R & 0 & -L_o \\ -L_o & 0 & L_S & 0 \\ 0 & -L_o & 0 & L_S \end{pmatrix} \begin{pmatrix} v_{S_d} \\ v_{S_q} \\ v_{R_d} \\ v_{R_q} \end{pmatrix}$$

where

$$K_{sr,2} = \begin{pmatrix} 0 & \omega_S \left(L_R L_S - sL_o^2\right) & 0 & \omega_S L_o L_R \left(1-s\right) \\ -\omega_S \left(L_R L_S - sL_o^2\right) & 0 & -\omega_S L_o L_R \left(1-s\right) & 0 \\ 0 & -\omega_S L_o L_S \left(1-s\right) & 0 & \omega_S \left(sL_R L_S - L_o^2\right) \\ \omega_S L_o L_S \left(1-s\right) & 0 & -\omega_S \left(sL_R L_S - L_o^2\right) & 0 \end{pmatrix}$$

pre-multiplying this expression by a transformation matrix

$$T = \begin{pmatrix} L_S & 0 & L_o & 0 \\ 0 & L_S & 0 & L_o \\ 0 & 0 & 1 & 0 \\ 0 & 0 & 0 & 1 \end{pmatrix}$$

yields an expression which coincides with the stator flux $\Psi_S = L_S i_S + L_o i_R$, gives the system around the equilibrium point 0

$$0 = \mathbf{A}_0 \mathbf{x}_0 + \mathbf{B_{S0}} \mathbf{u_{S0}} + \mathbf{B_{R0}} \mathbf{u_{R0}} \tag{6.11}$$

with

$\mathbf{x}_0 = \begin{bmatrix} i_{S_d} & i_{S_q} & i_{R_d} & i_{R_q} \end{bmatrix}^T$, being the state vector

$\mathbf{u_{R0}} = \begin{bmatrix} v_{R_{d0}} & v_{R_{q0}} \end{bmatrix}^T$, being the control input vector

$\mathbf{u_{S0}} = \begin{bmatrix} v_{S_{d0}} & v_{S_{q0}} \end{bmatrix}^T$, being the stator input vector

$\mathbf{A}_0$, $\mathbf{B_{S0}}$, $\mathbf{B_{R0}}$, being constant matrices given by

$$\mathbf{A}_0 = \begin{pmatrix} 0 & \omega_S L_S \sigma L_S L_R & 0 & \omega_S L_o \sigma L_S L_R \\ -\omega_S L_S \sigma L_S L_R & 0 & -\omega_S L_o \sigma L_S L_R & 0 \\ 0 & -\omega_S L_o L_S (1-s) & 0 & \omega_S (s L_R L_S - L_o^2) \\ \omega_S L_o L_S (1-s) & 0 & -\omega_S (s L_R L_S - L_o^2) & 0 \end{pmatrix}$$

$$\mathbf{B_{S0}} = \begin{pmatrix} \sigma L_R L_S & 0 \\ 0 & \sigma L_R L_S \\ -L_o & 0 \\ 0 & -L_o \end{pmatrix}, \quad \mathbf{B_{R0}} = \begin{pmatrix} 0 & 0 \\ 0 & 0 \\ L_S & 0 \\ 0 & L_S \end{pmatrix}$$

Sliding Control

A controller is designed to be constrained to the sampling frequency with the control signal changing only at sampling instances. As described in Chapter 3 the design procedure of the controller comprises two steps, one related to computation of the sliding surface and the other to the establishment of the control law. The design procedure in discrete form is described below:

- **Step 1** Computation of a sliding surface $s[k] = Sx[k]$ with suitable internal dynamics. In order to find the sliding surface $s[k]$ a linear transformation is performed to bring the system (6.5) into the so called *regular form* [6],

$$\begin{aligned} \dot{x_1} &= f_1(x_1, x_2, t) \\ \dot{x_2} &= f_2(x_1, x_2, t) + B_2(x_1, x_2, t)u \end{aligned} \tag{6.12}$$

where $x_1 \in \Re^{n-m}$, $x_2 \in \Re^m$, and B_2 is an $m \,\mathrm{x}\, m$ non-singular matrix. The block $\dot{x_1}$ does not depend on control, whereas the dimension of $\dot{x_2}$ coincides with that of the control.

For the controllable system (6.5) there exists an invertible transformation $T_{rx} \in \Re^{n(x)n}$, defined as:

$$z = T_{rx}x \tag{6.13}$$

with $T_{rx} \in \Re^{n \times n}$ being the matrix of the linear transformation. In this new state coordinates the system becomes:

$$\mathbf{z}[k+1] = \bar{\mathbf{A}}[k]\mathbf{z}[k] + \bar{\mathbf{B}}[k]\mathbf{u} + \bar{\mathbf{D}}[k] \tag{6.14}$$

or in a more explicit form,

$$\begin{aligned} \begin{bmatrix} z_1[k+1] \\ z_2[k+1] \end{bmatrix} = \begin{bmatrix} A_{11}[k] & A_{12}[k] \\ A_{21}[k] & A_{22}[k] \end{bmatrix} \begin{bmatrix} z_1[k] \\ z_2[k] \end{bmatrix} + \dots \\ \dots + \begin{bmatrix} \mathbf{0}_{n-m \times m} \\ \bar{B}_2[k] \end{bmatrix} u[k] + \begin{bmatrix} \bar{D}_1[k] \\ \bar{D}_2[k] \end{bmatrix} \end{aligned} \tag{6.15}$$

where $z_1 \in \Re^{n-m}$ and $z_2 \in \Re^m$ are all matrices $\bar{A}_{ij} \forall i, j = 1..2$, $\bar{D}_i \forall i = 1..2$ of appropriate dimensions and $\bar{B}_2 \in \Re^{m \times m}$ has full rank.

Let $e[k] = z[k] - z^{ref}$ be the new state vector where z^{ref} is the requested reference value. The system may be expressed in these

new coordinates as

$$e[k+1] = \bar{A}[k]e[k] + \bar{B}[k]u + \tilde{D}[k] \tag{6.16}$$

where $\tilde{D}[k] = \bar{D} + (\bar{A}[k] - I)\, z^{ref}$

If the sliding mode manifold in these new coordinates is linear, then

$$s[k] = Ce[k] = \begin{bmatrix} F & I_{m\times m} \end{bmatrix} \begin{bmatrix} e_1[k] \\ e_2[k] \end{bmatrix} = Fe_1[k] + e_2[k] \tag{6.17}$$

with $F \in \Re^{m\times n}$. Assuming that a controller exits that forces the system into sliding mode (i.e. $s[k] = \mathbf{0}$), the following relationship applies

$$e_2[k] = -Fe_1[k] \tag{6.18}$$

Substituting the above equation into Eq. (6.15) yields

$$e_1[k+1] = (A_{11}[k] - A_{12}[k]F)e_1[k] = A_{sm}[k]e_1[k] \tag{6.19}$$

Matrix F is chosen such that $A_{sm}[k] = A_{11} - A_{12}F$ has stable eigenvalues and performs the desired dynamics of the closed-loop while the system is in sliding mode.

Notice that once the system is in sliding mode the order of the closed loop system dynamics is characterized by Eq. (6.19) whose order is $(n - m)$, an order that it is less than the order of the original uncontrolled system (n).

- **Step 2** Establishing a control law that steers the system towards the sliding surface at a finite time and keeps the closed loop dynamics confined to the manifold. To reach the sliding surface in one sampling period, i.e. $s[k+1] = 0$, the reaching law is

$$s[k+1] = C\bar{A}[k]e[k] + C\bar{B}[k]u[k] + C\tilde{D}[k] = 0$$

$$u_{eq}[k] = -\left(CB\right)^{-1}\left(CA[k]e[k] + C\tilde{D}[k]\right)$$

This can be decomposed as the sum of

$$\begin{aligned} u_{eq}[k] &= -\left(CB\right)^{-1}\left(CAe[k] + C\tilde{D}[k]\right) - \left(CB\right)^{-1}Ce + \left(CB\right)^{-1}Ce \\ &= -\left(CB\right)^{-1}s[k] - \left(CB\right)^{-1}\left((CA - C)e[k] + C\tilde{D}[k]\right) \end{aligned}$$

and

$$s[k+1] = s[k] + (CA[k] - C)e[k] + CB[k]u[k] + C\tilde{D}[k] \quad (6.20)$$

To circumvent the problem of excessively large control inputs a typical approach is to bound the control input [142]. Assuming that the control can vary within certain limits $\|u[k]\| \leq u_o$ such as

$$\left\|\left(CB\right)^{-1}\right\| \left\|(CA[k] - C)e[k] + C\tilde{D}[k]\right\| \leq u_o$$

the control

$$u[k] = \begin{cases} u_{eq}[k] & \text{for } \|u_{eq}[k]\| \leq u_o \\ u_o \dfrac{u_{eq}[k]}{\|u_{eq}[k]\|} & \text{for } \|u_{eq}[k]\| > u_o \end{cases} \quad (6.21)$$

satisfies the constraints on the control resources and yields motion in the sliding manifold. To prove convergence, consider the case $\|u_{eq}[k]\| > u_o$. From Eq.(6.20)

$$\begin{aligned} s[k+1] &= s[k] + (CA[k] - C)e[k] + CB[k]u[k] + C\tilde{D}[k] \\ &= s[k] + (CA[k] - C)e[k] + CBu_o\frac{u_{eq}[k]}{\|u_{eq}[k]\|} + C\tilde{D}[[k] \\ &= s[k] + (CA[k] - C)e[k] + C\tilde{D}[[k] \\ &\quad - u_o\frac{s[k] + \left((CA - C)e[k] + C\tilde{D}[k]\right)}{\|u_{eq}[k]\|} \\ &= (s[k] + (CA[k] - C)e[k] + C\tilde{D}[[k])\left(1 - \frac{u_o}{\|u_{eq}[k]\|}\right) \end{aligned}$$

Thus

$$\begin{aligned}\|s[k+1]\| &= \left\|s[k] + (CA[k] - C)e[k] + C\tilde{D}[[k]\right\| \left(1 - \frac{u_o}{\|u_{eq}[k]\|}\right) \\ &\leq \|s[k]\| + \left\|(CA[k] - C)e[k] + C\tilde{D}[[k]\right\| - \frac{u_o}{\left\|(CB)^{-1}\right\|} \\ &\leq \|s[k]\|\end{aligned}$$

Hence, $\|s[k]\|$ decreases monotonously and, after a finite number of steps $\|u_{eq}[k]\| < u_o$ is achieved and discrete-time sliding mode will take place from next sample.

Similarly to Eq.(6.21), the control law [143],

$$u[k] = \begin{cases} -(CB)^{-1}s[k] & \text{for } \|(CB)^{-1}s[k]\| \leq u_o \\ \\ -u_o\dfrac{(CB)^{-1}s[k]}{\|(CB)^{-1}s[k]\|} & \text{for } \|(CB)^{-1}s[k]\| > u_o \end{cases} \tag{6.22}$$

does not depend on the plant parameters A, D.

Example

The dynamic performance of the machine-side converter controller is assessed by transient analysis of a DFIG directly connected to an equivalent grid, for a number of different commanded values, i.e. the Sliding Mode Control designed for the machine side converter control is tested under mechanical torque and stator reactive power step changes.

The wind turbine system is modelled by its 5^{th} order model, where the stator and rotor currents and the rotor speed are the state variables, thus, the state vector is defined as:

$$x = \begin{bmatrix} i_{Sd} & i_{Sq} & i_{Rd} & i_{Rq} & \omega_R \end{bmatrix}^T \tag{6.23}$$

The terminal voltage is 1 pu and remains constant.

Table 6.1: DFIG-WT DATA

DFIG parameters

R_S (pu)	R_R (pu)	L_o (pu)	L_S (pu)	L_R (pu)	H (s)	$P_{w_{rated}}$ (MW)
0.0038	0.0044	3.00	3.2250	3.2100	3.5	2

The parameters of the DFIG wind turbine system are listed in Table 6.1.

Firstly, the mechanical torque is forced to its lower value and the wind turbine operates with zero reactive power output. Then, the mechanical torque is kept constant at -1 per unit whereas the reference of reactive power is step changed.

The proposed control method provides a torque-reactive power decoupled control through the regulating q-axis current and d-axis current, respectively.

- *Change in the input mechanical torque*:

A change in the input mechanical torque is caused by a change in the active power output reference; with the active power output obtained from the optimal power-speed curve.

Fig. 6.2 shows the simulated results where the input mechanical torque step changed at 0.2 sec from -1 pu to -0.5 pu. It can be observed that the active power is controlled by the q-axis stator and rotor current while d-axis stator and rotor current remains constant during the mechanical torque variation.

The output rotor voltage of the MSC, determined by SMC, is shown in Fig. 6.3 and Fig. 6.4 depicts the control law functions of the MSC regulator.

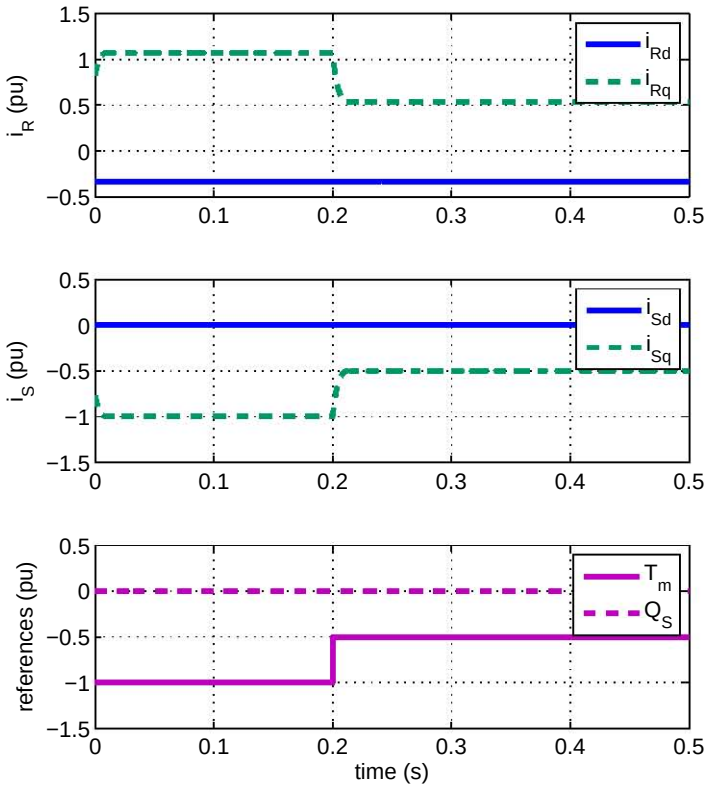

Figure 6.2: Stator and rotor currents with T_m reference variation

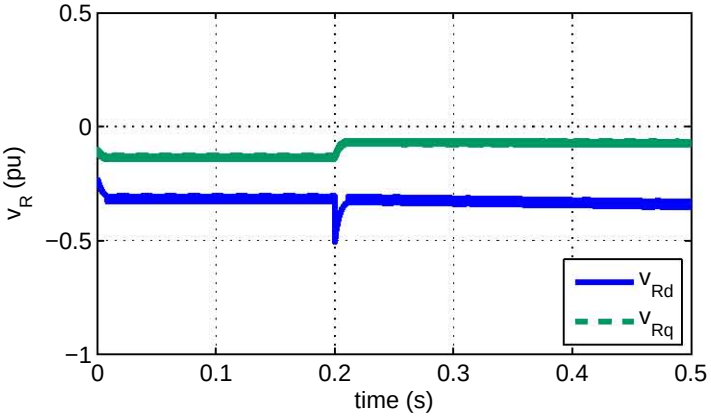

Figure 6.3: Rotor voltage with T_m reference variation

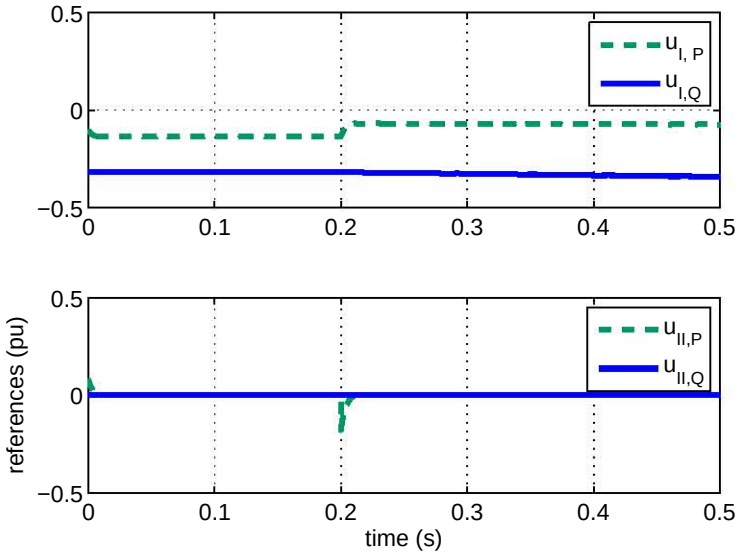

Figure 6.4: Control law functions with T_m reference variation

- *Change in the stator reactive power reference:*

A variation on the stator reactive power reference is a rather effective mean to demonstrate the influence of the d-axis current control in modulating the reactive power output in order to enable the control of the generator terminals.

Fig. 6.5 shows the stator and rotor currents and Fig. 6.6 shows the voltage control at the machine terminals.

The rotor voltage output of the MSC is shown in Fig. 6.7. It can be observed that the d-axis component of the rotor voltage varies according to the change of reactive power and the q-axis component of the rotor voltage remains practically constant following the reactive power command variation.

Fig. 6.8 depicts the SMC control law functions of the MSC regulator.

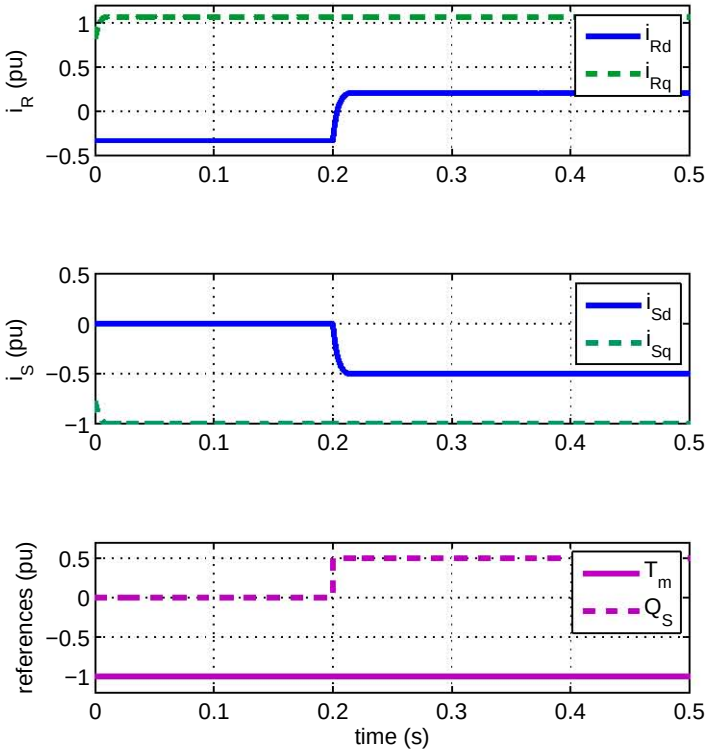

Figure 6.5: Stator and rotor currents with Q_S reference variation

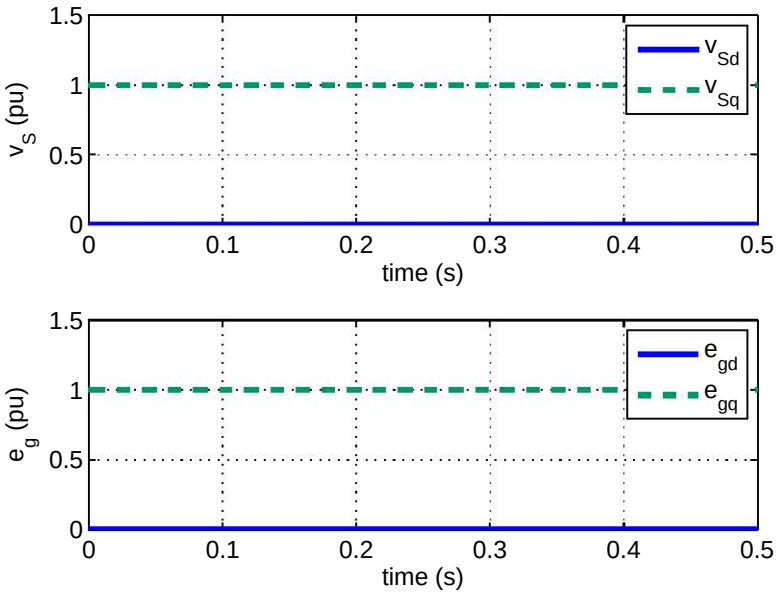

Figure 6.6: Voltage (d-q) at generator terminals with Q_S reference variation

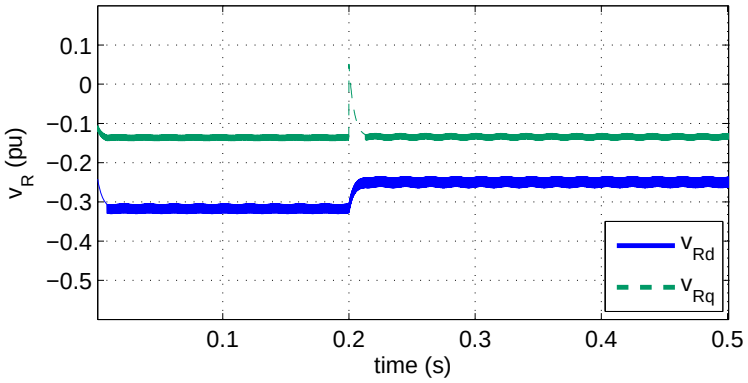

Figure 6.7: Rotor voltage with Q_S reference variation

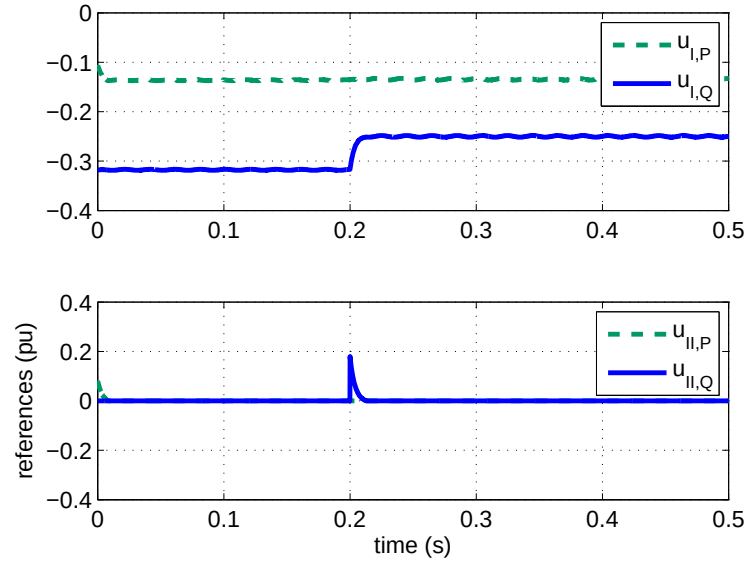

Figure 6.8: Control law functions with Q_S reference variation

6.3.2 Sliding Control Design in the Grid Side Converter

The GSC is connected to the grid through a grid-side filter and it is used to control dc-link voltage and reactive power exchange with the grid. Fig. 6.9 shows the diagram of the back-to-back converter, where Z_f is the grid-side filter impedance, v_f is the output voltage at the grid-side converter, E_g is the grid voltage and v_{dc} is the dc bus voltage.

Dynamic equations of the GSC

The per unit dq axis voltage equations can be written as

$$\begin{aligned} v_{fd} + jv_{fq} &= e_{gd} + je_{gq} + R_f\left(i_{fd} + ji_{fq}\right) + L_f\frac{1}{\omega_{elB}}\frac{d}{dt}\left(i_{fd} + ji_{fq}\right) + \ldots \\ &\quad \ldots + j\omega_S L_f\left(i_{fd} + ji_{fq}\right) \end{aligned} \tag{6.24}$$

$$v_{fd} = e_{gd} + R_f i_{fd} + L_f\frac{1}{\omega_{elB}}\frac{d}{dt}i_{fd} - \omega_S L_f i_{fq} \tag{6.25}$$

$$v_{fq} = e_{gq} + R_f i_{fq} + L_f\frac{1}{\omega_{elB}}\frac{d}{dt}i_{fq} + \omega_S L_f i_{fd} \tag{6.26}$$

The stator and the rotor converters are related through the active power balance in the dc link capacitor:

$$v_{dc}C_{dc}\frac{dv_{dc}}{dt} = \left(-P_g - P_R\right) \tag{6.27}$$

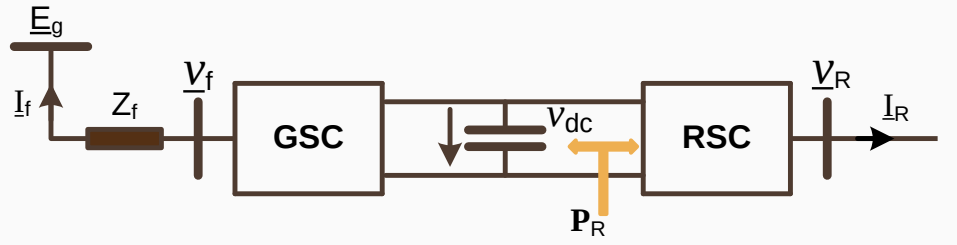

Figure 6.9: Diagram of the GSC for the DFIG-based wind turbine

with

$$\begin{aligned} P_R &= \Re\left\{\underline{v}_R \underline{i}_R^*\right\} \\ P_g &= \Re\left\{\underline{e}_g \underline{i}_f^*\right\} \end{aligned} \tag{6.28}$$

By aligning the d q-axis with the voltage $\underline{e}_g$ such that $\underline{e}_g = e_{gd}$, and $e_{gq} = 0$, the direct axis component of the grid side converter current controls the active power trough the stator converter,

$$P_g = \Re\left\{e_{gd}\left(i_{fd} - j i_{fq}\right)\right\} = e_{gd} i_{fd} \tag{6.29}$$

thereby equation (6.27) becomes,

$$v_{dc} C_{dc} \frac{dv_{dc}}{dt} = \left(-e_{gd} i_{fd} - P_R\right)$$

and reordering the voltage and dc link capacitor equations

$$\begin{aligned} v_{fd} &= e_{gd} + R_f i_{fd} + L_f \frac{1}{\omega_{elB}} \frac{d}{dt} i_{fd} - \omega_S L_f i_{fq} \\ v_{fq} &= e_{gq} + R_f i_{fq} + L_f \frac{1}{\omega_{elB}} \frac{d}{dt} i_{fq} + \omega_S L_f i_{fd} \\ v_{dc} C_{dc} \frac{dv_{dc}}{dt} &= \left(-e_{gd} i_{fd} - P_R\right) \end{aligned}$$

gives,

$$\frac{d}{dt} i_{fd} = \frac{\omega_{elB}}{L_f}\left(v_{fd} - e_{gd} - R_f i_{fd} + \omega_S L_f i_{fq}\right) \tag{6.30}$$

$$\frac{d}{dt} i_{fq} = \frac{\omega_{elB}}{L_f}\left(v_{fq} - e_{gq} - R_f i_{fq} - \omega_S L_f i_{fd}\right) \tag{6.31}$$

$$\frac{dv_{dc}}{dt} = \frac{1}{C_{dc} v_{dc}}\left(-e_{gd} i_{fd} - P_R\right) \tag{6.32}$$

and in matrix form,

$$\frac{d}{dt}\begin{pmatrix} i_{fd} \\ i_{fq} \\ v_{dc} \end{pmatrix} = \begin{pmatrix} \frac{\omega_{elB}}{L_f}\left(-e_{gd} - R_f i_{fd} + \omega_S L_f i_{fq}\right) \\ \frac{\omega_{elB}}{L_f}\left(-e_{gq} - R_f i_{fq} - \omega_S L_f i_{fd}\right) \\ \frac{1}{C_{dc} v_{dc}}\left(-e_{gd} i_{fd} - P_R\right) \end{pmatrix} + \begin{pmatrix} \frac{\omega_{elB}}{L_f} \\ 0 \\ 0 \end{pmatrix} v_{fd} + \begin{pmatrix} 0 \\ \frac{\omega_{elB}}{L_f} \\ 0 \end{pmatrix} v_{fq} \tag{6.33}$$

The system equations can be written in the form

$$\dot{\mathbf{x}} = \mathbf{f}(\mathbf{x}) + \mathbf{g_1}(\mathbf{x})\mathbf{u_1} + \cdots + \mathbf{g_m}(\mathbf{x})\mathbf{u_m} \tag{6.34}$$

$$y_1 = h_1(\mathbf{x})$$

$$\vdots$$

$$y_m = h_m(\mathbf{x}) \tag{6.35}$$

where

$$y_1 = h_1(\mathbf{x}) = i_{fq} \tag{6.36}$$

$$y_2 = h_2(\mathbf{x}) = v_{dc} \tag{6.37}$$

Feedback Linearization

The key idea of feedback linearization is to algebraically transform the non-linear system dynamics into fully or partly linear control problem; then linear control techniques can be applied [144]. The basic method for accomplishing input-output linearization is to differentiate the outputs y_i with respect to time until the control inputs appear and then new inputs are designed that cancel out the non-linearities.

Consider the MIMO system described by (6.34)- (6.35). It is assumed that each output y_i has a defined relative degree γ_i, which represents the times that the output is differentiated.

By using Lie's [144, 145] derivatives the process of repeated differentiation begins with

$$\dot{y_i} \;=\; L_{\mathbf{f}}h(x) + L_g h(x)u \tag{6.38}$$

with a Lie derivative given by $L_{\mathbf{f}}h = \dfrac{\partial h}{\partial \mathbf{x}}\mathbf{f}$.

Lie's derivative of order zero is denoted by $L_{\mathbf{f}}\,h$ and Lie's derivatives of higher order are given by $L^i_{\mathbf{f}}h = L_h\left(L^{i-1}_{\mathbf{f}}h\right)$.

In terms of Lie derivatives the output y_i has a relative degree γ_i if, $\exists$ an integer $L_{gi}L_{\mathbf{f}}^{\ell} \equiv 0\ \forall\, \ell < \gamma_i - 1$, $\forall\, 1 \leq i \leq m$, $\forall\, x \in U$, and $L_{gi}\, L_{\mathbf{f}}^{\gamma_i - 1} h(\mathbf{x}) \neq 0$. $U \subset \Re^n$ which is in a given neighbourhood of the equilibrium point of the system. The system's relative degree r, is defined to be the sum of the relative degrees of all the output variables. Lie's derivative for the i^{th} output is given by

$$y_i^{(r_i)} \;=\; L_{\mathbf{f}}^{r_i} h_i(\mathbf{x}) + \sum_{j=1}^{m} L_{g_j} L_{\mathbf{f}}^{r_i - 1} h_i(\mathbf{x}) u_j \tag{6.39}$$

assuming that r_i is the smallest integer such that at least one of the inputs appears in the i^{th} output and with $L_{g_j} L_{\mathbf{f}}^{r_i - 1} h_i(\mathbf{x}) \neq 0$ for at least one j. By taking the Lie's derivative for each i^{th} output, yields,

$$\begin{bmatrix} y_i^{(\gamma_1)} \\ \vdots \\ y_i^{(\gamma_{mi})} \end{bmatrix} = \begin{bmatrix} L_{\mathbf{f}}^{\gamma_1} h_1(\mathbf{x}) \\ \vdots \\ L_{\mathbf{f}}^{\gamma_m} h_m(\mathbf{x}) \end{bmatrix} + \mathbf{E}(\mathbf{x})\mathbf{u} \tag{6.40}$$

where

$$\mathbf{E}(\mathbf{x}) = \begin{bmatrix} L_{g_1} L_{\mathbf{f}}^{r_1 - 1} h_1(\mathbf{x}) & \cdots & L_{g_m} L_{\mathbf{f}}^{r_1 - 1} h_1(\mathbf{x}) \\ \vdots & \ddots & \vdots \\ L_{g_1} L_{\mathbf{f}}^{r_m - 1} h_m(\mathbf{x}) & \cdots & L_{g_m} L_{\mathbf{f}}^{r_m - 1} h_m(\mathbf{x}) \end{bmatrix}$$

If the decoupling matrix $\mathbf{E}(\mathbf{x})$ is invertible, then the input transformation

$$\mathbf{u} = \mathbf{E}(\mathbf{x})^{-1} \begin{bmatrix} v_1 - L_{\mathbf{f}}^{\gamma_1} h_1(\mathbf{x}) \\ \vdots \\ v_m - L_{\mathbf{f}}^{\gamma_m} h_m(\mathbf{x}) \end{bmatrix} \tag{6.41}$$

yields the decoupled dynamics

$$\mathbf{y}_i^{(\gamma_i)} = \mathbf{v}_i \tag{6.42}$$

The output variables of the GSC aimed at achieving a reactive power control in order to maintain the dc voltage constant are given by (6.36)-(6.37).

Differentiation of the output y_1 with respect to time reveals a relative degree of one

$$\dot{y}_1 = \frac{\omega_{elB}}{L_f}\left(-e_{gq} - R_f i_{fq} - \omega_S L_f i_{fd}\right) + \frac{\omega_{elB}}{L_f} v_{fq} \tag{6.43}$$

Now, differentiation of the output y_2 with respect to time twice ($r_i = 2$), yields,

$$\dot{y}_2 = \frac{\omega_{elB}}{C_{dc} v_{dc}}(-e_{gd} i_{fd} - P_R) \tag{6.44}$$

$$\begin{aligned}\ddot{y}_2 =& \frac{\omega_{elB}}{C_{dc} v_{dc}}\left(-e_{gd}\frac{\omega}{L_f}\left(-e_{gd} - R_f i_{fd} + \omega_S L_f i_{fq} + v_{fd}\right) - \dot{P}_R\right) - \dots \\ & \dots - \frac{\omega_{elB}}{C_{dc} v_{dc}^2}\frac{\omega_{elB}}{C_{dc} v_{dc}}(-e_{gd} i_{fd} - P_R)(-e_{gd} i_{fd} - P_R)\end{aligned} \tag{6.45}$$

Hence, the whole system has a relative degree of three.

These equations may be expressed in compact form as

$$\begin{pmatrix} \dot{y}_1 \\ \ddot{y}_2 \end{pmatrix} = \alpha + \beta \begin{pmatrix} v_{fd} \\ v_{fq} \end{pmatrix} \tag{6.46}$$

where

$$\alpha = \begin{pmatrix} -\frac{\omega_{elB}}{L_f} v_{fq_{ss}} \\ \frac{\omega_{elB}}{C_{dc} v_{dc}}\left(\frac{\omega_{elB}}{L_f} e_{gd} v_{fd_{ss}} - \dot{P}_R\right) - K_{dc}(-e_{gd} i_{fd} - P_R)^2 \end{pmatrix}$$

$$\beta = \begin{pmatrix} 0 & \frac{\omega_{elB}}{L_f} \\ -e_{gd}\frac{\omega_{elB}^2}{L_f C_{dc} v_{dc}} & 0 \end{pmatrix}$$

with

$$\begin{aligned} v_{fq_{ss}} &= e_{gq} + R_f i_{fq} + \omega_S L_f i_{fd}, \\ v_{fd_{ss}} &= e_{gd} + R_f i_{fd} - \omega_S L_f i_{fq}, \\ K_{dc} &= \frac{\omega_{elB}^2}{C_{dc}^2 v_{dc}^3} \end{aligned}$$

Thereafter, equation (6.46) can be rewritten as:

$$\begin{pmatrix} v_1 \\ v_2 \end{pmatrix} = \alpha + \beta \begin{pmatrix} v_{fd} \\ v_{fq} \end{pmatrix} \tag{6.47}$$

and the following linear form results:

$$\begin{pmatrix} \dot{y}_1 \\ \ddot{y}_2 \end{pmatrix} = \begin{pmatrix} v_1 \\ v_2 \end{pmatrix} \tag{6.48}$$

Since β is non-singular (except for $-e_{gd}\frac{\omega_{elB}^3}{L_f^2 C_{dc} v_{dc}} = 0$) in the operating range of v_{dc} and e_{gd}, the control law can be computed as follows

$$\begin{pmatrix} v_{fd} \\ v_{fq} \end{pmatrix} = \beta^{-1}\left(\begin{pmatrix} v_1 \\ v_2 \end{pmatrix} - \alpha\right) \tag{6.49}$$

Sliding Control

To design two sliding control for the equation (6.48), two decoupled controllers for each variable (y_1, y_2) are realized as follows:

- *Reactive current controller of the GSC:*

The output reactive current is defined as (6.36) by

$$\dot{y}_1 \;=\; v_1$$

Using the Euler's discretization, gives the first derivative

$$\dot{x}(t) \approx \frac{x[k+1] - x[k]}{\tau}$$

where τ is the sampling time, yields

$$y_{11,k+1} \;=\; y_{11,k} + \tau v_{1,k} \tag{6.50}$$

Defining the following sequence of maps

$$\begin{aligned} \omega_{0,k} &= y_{11,k} - y_k^{ref} \\ \omega_{1,k} &= \omega_{0,k+1} = y_{11,k+1} - y_{k+1}^{ref} \\ &= y_{11,k} + \tau v_{1,k} - y_{k+1}^{ref} \end{aligned} \tag{6.51}$$

which clearly expresses the dependence of the output variable y_1 at time $k+1$ on the state $x(k)$ and the input sequence $u(k)$, $u(k+1)$. The inverse transformation is given by,

$$y_{11,k} = \omega_{0,k} + y_k^{ref} \tag{6.52}$$

then the transformed system is,

$$\begin{aligned} \omega_{0,k+1} &= \omega_{1,k} \\ &= \omega_{0,k} + \tau v_{1,k} + y_k^{ref} - y_{k+1}^{ref} \end{aligned} \tag{6.53}$$

It should be remarked that when the inputs and the initial state of (6.53) are properly set, the various components of the state of this system reproduce the output of the system and its next value,

$$\begin{aligned} v_{1,k} &= u_{k+1} \\ \omega_{0,k} &= y_k \end{aligned} \tag{6.54}$$

then

$$\omega_{1,k} = y_{k+1} \tag{6.55}$$

As the system model is described in controllable canonical form then a function,

$$s_k = \alpha_0\omega_{0,k} + \alpha_1\omega_{1,k} + \ldots + \alpha_{n-2}\omega_{n-2,k} + \omega_{n-1,k} \tag{6.56}$$

with the coefficients chosen in such a manner that the polynomial

$$p(\lambda) = \lambda^{n-1} + \alpha_{n-2}\lambda^{n-2} + \ldots + \alpha_0 \tag{6.57}$$

in the complex variables λ, is Hurwitz, defines a sliding surface as,

$$s_k \;=\; \omega_{0,k} \tag{6.58}$$

and a control u such that a sliding mode occurs on $s_k = 0$

$$\omega_{0,k} = 0$$

which define the equilibrium point $y_{11,k\to\infty} = y^{ref}$.
In the next instant of time the sliding mode is:

$$s_{k+1} \;=\; 0$$

then

$$s_{k+1} \;=\; \omega_{0,k+1} = 0$$

Incorporating this restriction in (6.53)

$$\omega_{0,k} + \tau v_{1,k} + y_k^{ref} - y_{k+1}^{ref} \;=\; 0$$

so that the control variable becomes,

$$\begin{aligned} v_{1,k} &= \frac{1}{\tau}\left(-\omega_{0,k} - y_k^{ref} + y_{k+1}^{ref}\right) \\ v_{1,k} &= \frac{1}{\tau}\left(-y_{11,k} + y_{k+1}^{ref}\right) \end{aligned} \tag{6.59}$$

It should be emphasized that the reactive current control depends only on the reference value in the next instant of time y_{k+1}^{ref}, and the reactive current measurement in the current instant of time $y_{11,k}$

- *dc voltage controller in the GSC:*

To keep the dc voltage constant in (6.48), the second output y_2 is to be used

$$\ddot{y}_2 = v_2$$

Representing the output function y_2 in controllable canonical form [146]

$$\begin{aligned} y_{21} &= y_2 \\ \dot{y}_{21} &= \dot{y}_2 = y_{22} \end{aligned}$$

which may be written in matrix form,

$$\begin{pmatrix} \dot{y}_{21} \\ \dot{y}_{22} \end{pmatrix} = \begin{pmatrix} 0 & 1 \\ 0 & 0 \end{pmatrix} \begin{pmatrix} y_{21} \\ y_{22} \end{pmatrix} + \begin{pmatrix} 0 \\ 1 \end{pmatrix} v_2 \tag{6.60}$$

In the same way that it was done for the output y_1, a discrete-time frame will be followed: Let us consider the Euler's discretization of the first derivative

$$\dot{x}(t) \approx \frac{x[k+1] - x[k]}{\tau}$$

where τ is the sampling time.

$$\begin{aligned} y_{21,k+1} &= y_{21,k} + \tau y_{22,k} \\ y_{22,k+1} &= y_{22,k} + \tau v_{2,k} \end{aligned} \tag{6.61}$$

In order to transform the system into the generalized observability canonical form (GOBCF) [147], the following sequence of maps are defined

$$\begin{aligned} \omega_{0,k} &= y_{21,k} - y_k^{ref} \\ \omega_{1,k} &= \omega_{0,k+1} = y_{21,k+1} - y_{k+1}^{ref} \\ &= y_{21,k} + \tau y_{22,k} - y_{k+1}^{ref} \\ \omega_{2,k} &= \omega_{1,k+1} = y_{21,k+1} + \tau y_{22,k+1} - y_{k+2}^{ref} \\ &= y_{21,k} + 2\tau y_{22,k} + \tau^2 v_{2,k} - y_{k+2}^{ref} \end{aligned} \tag{6.62}$$

with the inverse transformation given by

$$\begin{aligned} y_{21,k} &= \omega_{0,k} + y_k^{ref} \\ y_{22,k} &= \tau^{-1}\omega_{1,k} - \tau^{-1}\omega_{0,k} - \tau^{-1} y_k^{ref} + \tau^{-1} y_{k+1}^{ref} \end{aligned} \tag{6.63}$$

The transformed system then reads

$$\begin{aligned}\omega_{0,k+1} &= \omega_{1,k} \\ &= \omega_{0,k} + y_k^{ref} + \dots \\ &\dots + 2\tau\left(\tau^{-1}\omega_{1,k} - \tau^{-1}\omega_{0,k} - \tau^{-1}y_k^{ref} + \tau^{-1}y_{k+1}^{ref}\right) + \dots \\ &\dots + \tau^2 v_{2,k} - y_{k+2}^{ref} \\ &= -\omega_{0,k} + 2\omega_{1,k} + \tau^2 v_{2,k} - y_k^{ref} + 2y_{k+1}^{ref} - y_{k+2}^{ref} \end{aligned} \tag{6.64}$$

As aforementioned in the case of y_1 it should be clear that if

$$v_{2,k} = u_{k+1}$$

$$\omega_{0,k} = y_k \tag{6.65}$$

then

$$\omega_{1,k} = y_{k+1} \tag{6.66}$$

The sliding surface, defined by function (6.56), may be expressed in terms of the transformed coordinates

$$s_k = \alpha_o\omega_{0,k} + \omega_{1,k} \tag{6.67}$$

Incorporating the sliding condition $s_k = 0$, gives

$$0 = \alpha_o\omega_{0,k} + \omega_{1,k} = \alpha_o\omega_{0,k} + \omega_{0,k+1}$$

or

$$\omega_{0,k+1} + \alpha_o\omega_{0,k} = 0$$

which is stable at the equilibrium point $\omega_{0,k\to\infty} = 0$; that is,

$$y_{21,k\to\infty} = y^{ref}$$

In the next instant of time, the sliding motion is required to stay at the equilibrium point, which means

$$s_{k+1} \;=\; 0$$

then

$$s_{k+1} \;=\; \alpha_o \omega_{0,k+1} + \omega_{1,k+1} = 0$$

Incorporating this restriction in (6.53)

$$\alpha_o \omega_{1,k} + \left(-\omega_{0,k} + 2\omega_{1,k} + \tau^2 v_{2,k} - y_k^{ref} + 2y_{k+1}^{ref} - y_{k+2}^{ref}\right) = 0$$

the control for v_{dc} is given by

$$v_{2,k} \;=\; \frac{1}{\tau^2}\left(\omega_{0,k} - (\alpha_o - 2)\,\omega_{1,k} + y_k^{ref} - 2y_{k+1}^{ref} + y_{k+2}^{ref}\right)$$

where

$$\begin{aligned}
\omega_{0,k} \;&=\; y_{21,k} - y_k^{ref} \\
\omega_{1,k} \;&=\; \omega_{0,k+1} \;=\; y_{21,k} + \tau y_{22,k} - y_{k+1}^{ref} \\
\omega_{2,k} \;&=\; \omega_{1,k+1} \;=\; y_{21,k} + 2\tau y_{22,k} + \tau^2 v_{2,k} - y_{k+2}^{ref}
\end{aligned}$$

Hence,

$$\begin{aligned}
v_{2,k} \;=\; &\frac{1}{\tau^2}\left(y_{21,k} - y_k^{ref} - (\alpha_o - 2)\,(y_{21,k} + \tau y_{22,k} - y_{k+1}^{ref}) + y_k^{ref}\right) - \ldots \\
&\ldots - \frac{1}{\tau^2}\left(2y_{k+1}^{ref} + y_{k+2}^{ref}\right)
\end{aligned} \tag{6.68}$$

If measurements of $v_{dc,k}$, $e_{gd,k}$, $i_{fd,k}$, $P_{R,k}$ are available, then the value of $y_{21,k}$ and $y_{22,k}$ can be obtained from

$$y_{21,k} \;=\; v_{dc,k} \tag{6.69}$$

$$y_{22,k} \;=\; \frac{\omega}{C_{dc} v_{dc,k}}(-e_{gd,k} i_{fd,k} - P_{R,k}) \tag{6.70}$$

Alternatively, these quantities can be estimated by using an observer.

With the values of $v_{1,k}$,$v_{2,k}$ given by (6.59),(6.68), the values of v_{fd}, v_{fq} according to (6.49) are obtained.

Notice that, if the control voltage of the converter is limited to a maximum value u_{lim}, it should verified that

$$\|u_{k,eq}\| = \left\| \begin{pmatrix} v_{fd} \\ v_{fq} \end{pmatrix} \right\| < u_{lim}$$

Otherwise, the control signal should be limited to a maximum value according to the expression:

$$u_k = \begin{cases} u_{k,eq} & \text{for } \|u_{k,eq}\| \leq u_{lim} \\ u_{lim} \dfrac{u_{k,eq}}{\|u_{k,eq}\|} & \text{for } \|u_{k,eq}\| > u_{lim} \end{cases}$$

Example

In this section, the transient response of the GSC control is assessed in connection with voltage and current set point step changes. The wind turbine is represented by a generic model which incorporates features of wind turbine electrical controls relevant to transient stability studies.

Simulations of the grid side converter were carried out with the following parameters:

- The filter parameters: $L_f = 0.2$, $R_f = 0.002$, $C_{dc} = 3.5$
- For the proposed controller, the design parameter $\alpha_o = 0.9$ and the sampling interval was chosen to be $\tau = 0.1$ms
- The dc voltage and reactive power references are $v_{dc}^{ref} = 2.1$, $Q_{GSC} = 0.3$

The control performance is shown in Figs. 6.10 - 6.14. It is observed in Figs. 6.10 and 6.11 that dc voltage and reactive current at the stator side of the DFIG match rather well their respective reference signals.

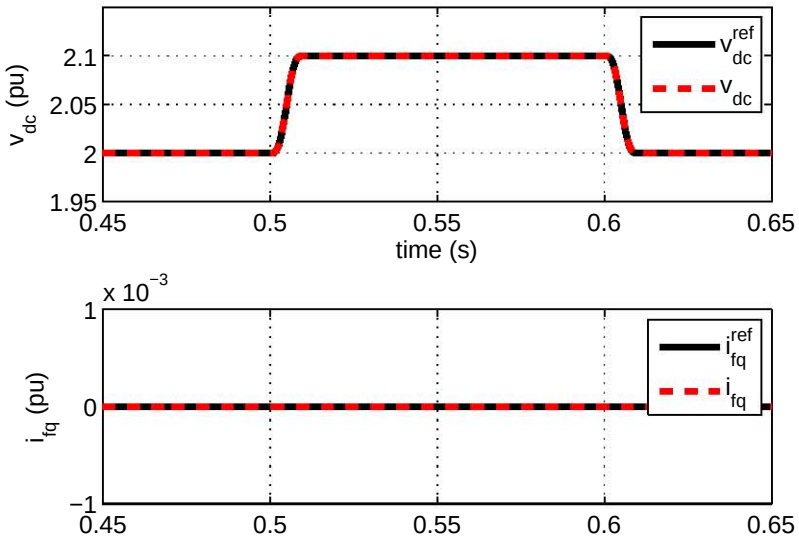

Figure 6.10: u_{dc} control in the GSC

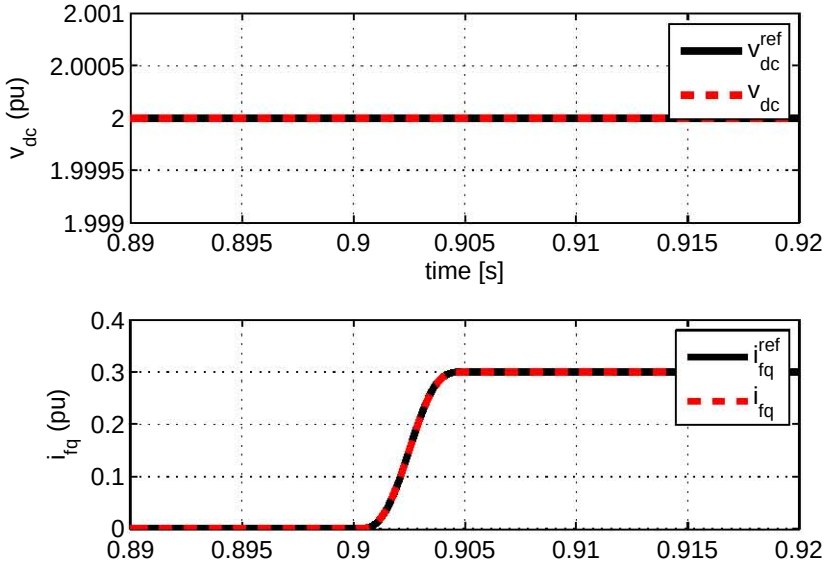

Figure 6.11: i_{fq} response to a change in the reactive current of the GSC

Fig. 6.12 depicts the *dq* axis components of the output voltage at the GSC. On the other hand, if the rotor active power is varied, i.e., disturbed, the GSC control acts to maintain the dc-link voltage at the specified voltage level, as shown Fig. 6.13.

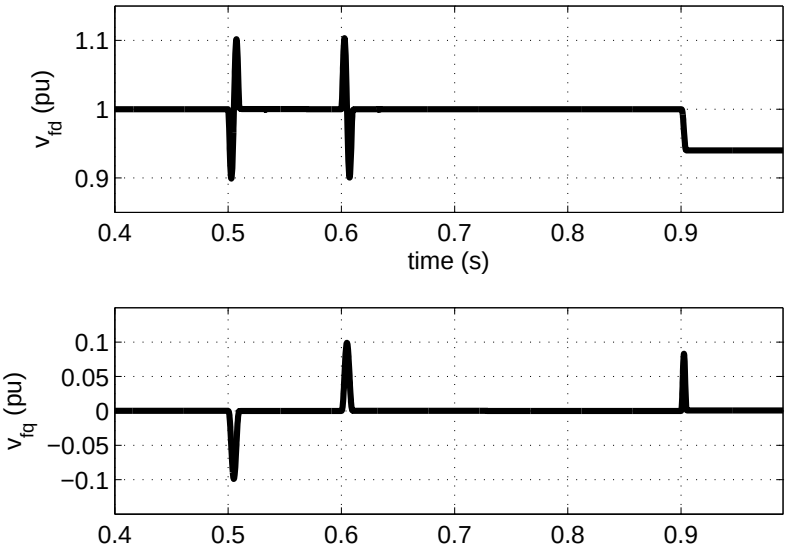

Figure 6.12: Control variable *d*-*q*

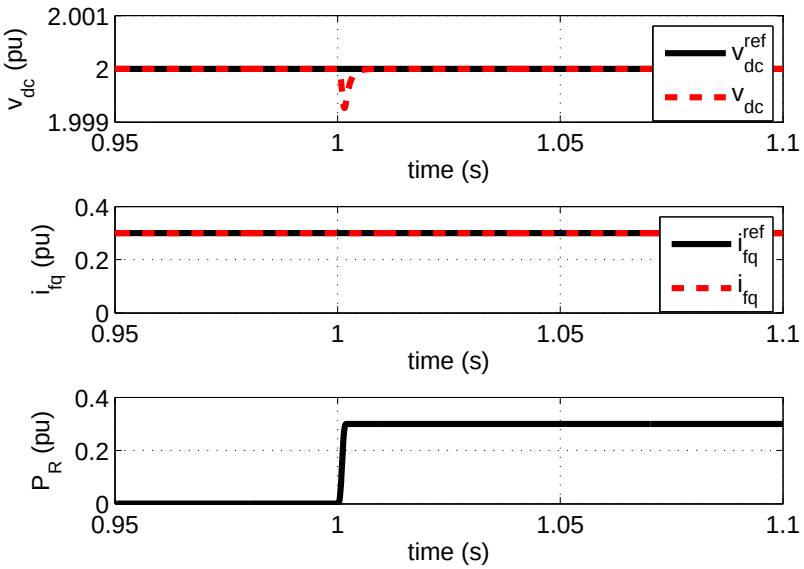

Figure 6.13: Response to a change in the active power flow from the MSC.

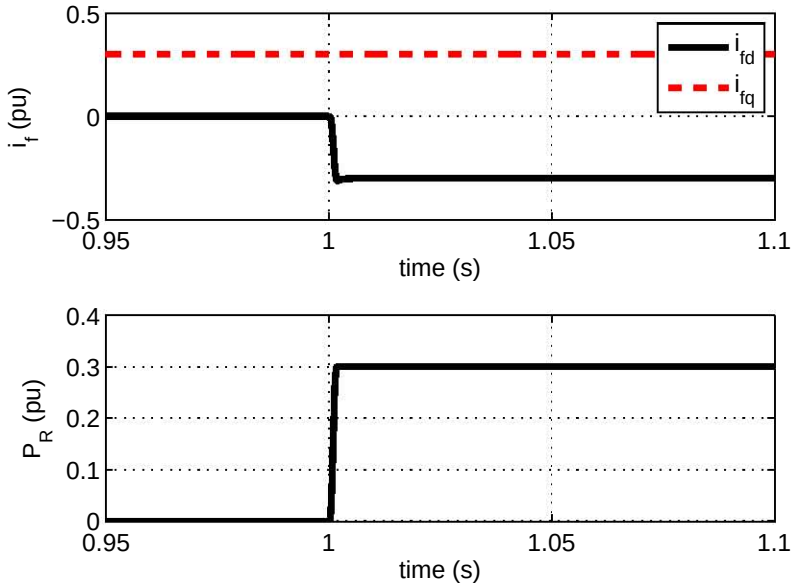

Figure 6.14: Detailed dq axis i_f with P_R change

The GSC q-axis component is not affected by variations of rotor active power. This result confirms the decoupled operation of the DFIG converter, as shown Fig. 6.14. Moreover, the response of the other variables that are not directly controlled in the system are governed by the dynamic equations; for example, the d-axis current i_{fd} is directly linked to the active power supplied to the network.

6.4 Sliding Mode Control for Damping Inter-area Oscillations in Power Systems

The Sliding Mode Control strategies shown in previous sections for the MSC and GSC, are now applied to a multi-area power system with wind generation. The GSC is in charge of damping power oscillations in the multi-area power system, by making use of its reactive power capabilities.

The dynamic model of a multi-machine power system comprising

N machines may be described by the classical swing equation [21, 148, 149, 150]

$$\begin{aligned} \dot{\delta}_i &= \omega_i - \omega_0 \\ \dot{\omega}_i &= \frac{1}{2H_i}\left(-D_i(\omega_i - \omega_0) + P_{mi} - P_{ei}\right) \\ &\quad \text{for } i = 1, \ldots, N \end{aligned} \tag{6.71}$$

where the state variables δ_i, ω_i are the relative generator power angle and the relative rotor speed of machine i, respectively. H_i is the inertia constant, D_i is the per unit damping constant, ω_0 is the system speed, P_{mi} is the mechanical input power, and P_{ei} is the electrical power.

A power network comprising two dynamic areas and one wind farm is depicted in Fig. 6.15. The transmission power network can be expressed as an admittance matrix $\underline{Y}$ of size $(N + m, N + m)$ where N is the number of generator buses and m is the number of wind farms with reactive current injection capability, as schematically shown in Fig. 6.16. The power network is taken to have L load buses.

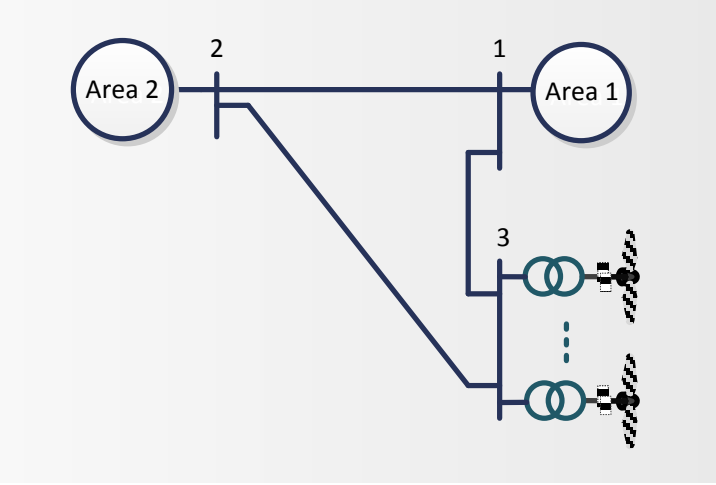

Figure 6.15: Two areas system with wind power generation

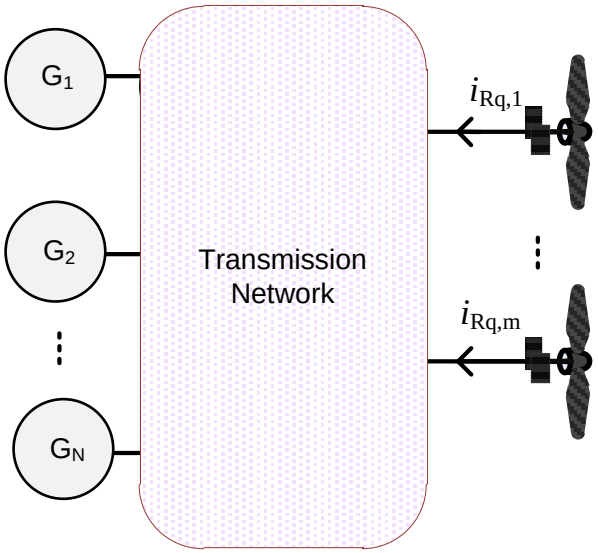

Figure 6.16: Equivalent Power System for SMC control design

The active power delivered to the system is given by

$$P_{ei} = \Re\left\{\sum_{j=1}^{N} \underline{V}_i \, \underline{I}_i^*\right\} \tag{6.72}$$

with

$$I_i = \sum_{j=1}^{N} \underline{Y}_{ij}\underline{V}_j = \sum_{j=1}^{N} \left[G_{ij}\cos\left(\delta_i - \delta_j\right) + B_{ij}\sin\left(\delta_i - \delta_j\right)\right] V_j \tag{6.73}$$

where G_{ij} the conductance and B_{ij} the susceptance between nodes i and j in per unit.

In the particular case of $N = 2$ generators and $m = 1$ wind farms, the power injected by generators is given by

$$P_{e1} = \Re\left\{\underline{V}_1 \underline{I}_1^*\right\} = \Re\left\{\sum_{j=1}^{2} V_1 Y_{1j}^* V_j^* + V_1 Y_{13}^* V_3^*\right\} \tag{6.74}$$

$$P_{e2} = \Re\left\{\underline{V}_2\underline{I}_2^*\right\} = \Re\left\{\sum_{j=1}^{2} V_2 Y_{2j}^* V_j^* + V_2 Y_{23}^* V_3^*\right\} \tag{6.75}$$

Defining $\delta_{12} = \delta_1 - \delta_2$, and $\omega_{12} = \omega_1 - \omega_2$, the relative power swing dynamics between the two areas is described by

$$\begin{aligned} \dot{\delta}_{12} &= \omega_{12} \\ \dot{\omega}_{12} &= f_{ij} + bV_3^* \end{aligned} \tag{6.76}$$

where

$$\begin{aligned} f_{ij} =& \frac{1}{2H_i}\left[-D_i\omega_i + P_{mi} - \sum_{k=1}^{2} V_i V_k \left[G_{ik}\cos(\delta_i - \delta_k) + B_{ik}\sin(\delta_i - \delta_k)\right]\right] - \dots \\ & \dots - \frac{1}{2H_j}\left[-D_j\omega_j + P_{mj} - \sum_{k=1}^{2} V_j V_k \left[G_{jk}\cos(\delta_j - \delta_k) + B_{jk}\sin(\delta_j - \delta_k)\right]\right] \end{aligned}$$

$$\begin{aligned} b =& -\frac{1}{2H_i} V_i \left[G_{i3}\cos(\delta_i - \delta_3) + B_{i3}\sin(\delta_i - \delta_3)\right] - \dots \\ & \dots - \frac{1}{2H_j} V_j \left[G_{j3}\cos(\delta_j - \delta_3) + B_{j3}\sin(\delta_j - \delta_3)\right] \end{aligned}$$

for $i = 1;\ j = 2$

get express $\dot{\omega} = f + bu$, where the indexes i, j have been omitted for brevity; δ and ω are the system's state variables, f represents the balance between mechanical power input (P_m) and electrical power output (P_e) and bu defines the control objective which force the relative rotor speed to zero. All terms involved in this equation arise from (6.71).

The current injection from the wind farm at bus 3 is

$$\underline{I}_3 = \sum_{k=1}^{2} Y_{3k} V_k + Y_{33} V_3 \tag{6.77}$$

Thus, the electrical active and reactive power output delivered by the

wind farm is given by [151]

$$\begin{aligned} P_{e3} &= \Re\left(\underline{V}_3 \underline{I}_3^*\right) \\ &= V_3^2 G_{33} - V_3 \sum_{k=1}^{2} V_k \left[G_{3k}\cos\left(\delta_3 - \delta_k\right) + B_{3k}\sin\left(\delta_3 - \delta_k\right)\right] \\ Q_3 &= \Im\left(\underline{V}_3 \underline{I}_3^*\right) \\ &= -V_3^2 B_{33} + V_3 \sum_{k=1}^{2} V_k \left[G_{3k}\sin\left(\delta_3 - \delta_k\right) - B_{3k}\cos\left(\delta_3 - \delta_k\right)\right] \end{aligned}$$

Consider the two-machine equivalent of a two-area power system, given in Fig. 6.17. Each coherent area is represented by a single equivalent machine which is connected to at buses 1 and 2 through power transformers.

The synchronous generators are represented by the classical model so that the internal voltage is denoted as $\underline{E}_{qi} = E_{qi}\angle\delta_i$, $i = 1, 2$. The voltages at buses 1, 2 and 3 correspond to nodal voltage at the point of connection of each machine, $\underline{V}_i = V_i\angle\delta_i$, $i = 1, 2, 3$. The reactance X_d consists of the sum of machine's transient reactance and the transformer reactance. The line's reactances are X_1 and X_2. The current I is the current injected by the wind farm.

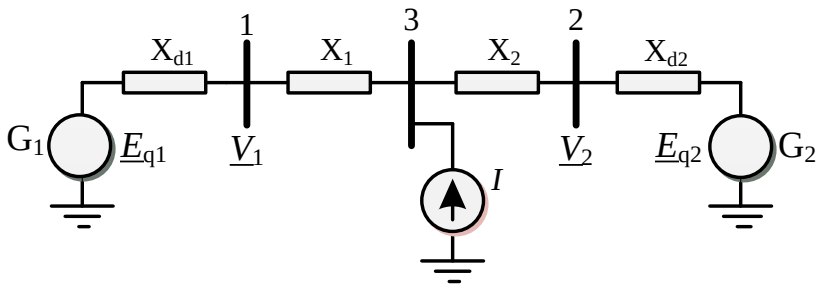

Figure 6.17: Classical two-machine power system model with wind generation

Taking voltage $\underline{V}_2 = V_2\angle 0$ as reference then voltage $\underline{V}_1$ can be expressed as

$$\underline{V}_1 = \underline{V_3} + jX_1\underline{I}_1 \tag{6.78}$$

with

$$\underline{I}_1 = \frac{E_{q1}\angle\delta_1 - V_1\angle\theta_1}{j\,X_{d1}} \tag{6.79}$$

and

$$\underline{V}_3 = \underline{V_2} + jX_2\left(\underline{I} + \underline{I}_1\right) \tag{6.80}$$

Substituting (6.79) and (6.80) into (6.78), gives,

$$\underline{V}_1 \;=\; \underline{V_2} + jX_2\underline{I} + j\left(X_1 + X_2\right)\frac{E_{q1}\angle\delta_1 - V_1\angle\theta_1}{j\,X_{d1}} \tag{6.81}$$

Further manipulation yields,

$$\underline{V}_1 \;=\; \left(\frac{X_{d1}}{X_{d1}+X_1+X_2}\right)\left(\underline{V}_2 + \frac{X_1+X_2}{X_{d1}}\underline{E}_{q1}\right) + \left(\frac{X_{d1}}{X_{d1}+X_1+X_2}\right)jX_2\underline{I}$$

When the current $\underline{I}$ injected by the wind farm is in quadrature with the voltage at PCC, it would only yield reactive power injection, i.e., no active power component,

$$\underline{I} = I\angle\left(\theta_1 + \frac{\pi}{2}\right) = jI\angle\theta_1$$

Therefore

$$V_1\angle\theta_1 = \left(\frac{X_{d1}}{X_{d1}+X_1+X_2}\right)\left(\underline{V}_2 + \frac{X_1+X_2}{X_{d1}}E_{q1}\angle\delta_1\right) - \left(\frac{X_{d1}}{X_{d1}+X_1+X_2}\right)X_2I\angle\theta_1$$

Where separate expressions for magnitude and phase angle are given as:

$$V_1 = \left|\left(\frac{X_{d_1}}{X_{d_1}+X_1+X_2}\right)\left(\underline{V}_2 + \frac{X_1+X_2}{X_{d1}}E_{q1}\angle\delta_1\right)\right| - \left(\frac{X_{d1}}{X_{d1}+X_1+X_2}\right)X_2I$$

$$\theta_1 = \angle\left(\frac{X_{d1}}{X_{d1}+X_1+X_2}\right)\left(\underline{V}_2 + \frac{X_1+X_2}{X_{d1}}E_{q1}\angle\delta_1\right)$$

Alternatively,

$$V_1 = c_1 + c_2 I \tag{6.82}$$

where

$$c_1 = \left| \left(\frac{X_{d1}}{X_{d1} + X_1 + X_2} \right) \left(\underline{V}_2 + \frac{X_1 + X_2}{X_{d1}} E_{q1} \angle \delta_1 \right) \right|$$

$$c_2 = - \left(\frac{X_{d1}}{X_{d1} + X_1 + X_2} \right) X_2$$

These expressions may be incorporated into the power equation,

$$P_{e1} \;=\; \frac{1}{X_{d1}} V_1 E_{q1} \sin\left(\delta_1 - \theta_1\right) = \frac{1}{X_{d1}} \left(c_1 + c_2 I\right) E_{q1} \sin\left(\delta_1 - \theta_1\right)$$

and into the dynamical equation

$$\begin{aligned} \dot{\delta}_1 &= \omega_1 - \omega_0 \\ \dot{\omega}_1 &= \frac{1}{2H} \left(-D_1 \left(\omega_1 - \omega_0\right) + P_{m1} - \frac{1}{X_{d1}} \left(c_1 + c_2 I\right) E_{q1} \sin\left(\delta_1 - \theta_1\right) \right) \end{aligned}$$

which can also be written down as:

$$\begin{aligned} \dot{\delta}_1 &= \omega_1 - \omega_0 \\ \dot{\omega}_1 &= d_1\left(\delta, \omega\right) + d_2\left(\delta\right) I \end{aligned} \tag{6.83}$$

where

$$\begin{aligned} d_1 &= \frac{1}{2H_1} \left(-D_1 \left(\omega_1 - \omega_0\right) + P_{m_1} - \frac{1}{X_{d1}} c_1 E_{q1} \sin\left(\delta_1 - \theta_1\right) \right) \\ d_2 &= \frac{1}{2H_1} \left(-\frac{1}{X_{d1}} c_2 E_{q1} \sin\left(\delta_1 - \theta_1\right) \right) \end{aligned}$$

In discrete-time form,

$$\begin{aligned} \delta_{k+1} &= \delta_k + \tau\omega_k - \tau\omega_0 \\ \omega_{k+1} &= \omega_k + \tau d_{1k}\left(\delta_k, \omega_k\right) + \tau d_{2k}\left(\delta_k\right) I_k \end{aligned} \tag{6.84}$$

Lyapunov theory may be used to determine both the solutions of the controller and its associated stability properties. A Lyapunov function candidate is selected to find out the control that enforces the sliding mode into the sliding surfaces [6]. For proved stability, the Lyapunov function candidate is of the form

$$\begin{aligned} 2V &= s^T s \\ &= s_1^2 + s_2^2 \\ &= (\omega_1 - \omega_0)^2 + (\omega_2 - \omega_0)^2 \end{aligned} \tag{6.85}$$

whose derivative is

$$\dot{V} = (\omega_1 - \omega_0)\,\dot{\omega}_1 + (\omega_2 - \omega_0)\,\dot{\omega}_2$$

where

$$\dot{\omega}_1 = f_1 + g_1 u$$

$$\dot{\omega}_2 = f_2 + g_2 u$$

For the purpose of control derivation, functions f_1, f_2, are very small and include terms with no control variables, and can therefore be neglected. Let us consider only terms with control variables, thus

$$\dot{\omega}_1 \simeq g_1 u$$

$$\dot{\omega}_2 \simeq g_2 u$$

such that

$$\dot{V} = [(\omega_1 - \omega_0)\, g_1 + (\omega_2 - \omega_0)\, g_2]\, u \tag{6.86}$$

Then, the control signal u can be selected as a discontinuous function as [6]

$$u = -k\,[(\omega_1 - \omega_0)\, g_1 + (\omega_2 - \omega_0)\, g_2] - M \text{sign}\,[(\omega_1 - \omega_0)\, g_1 + (\omega_2 - \omega_0)\, g_2] \tag{6.87}$$

with k and M being constant positive values.

Thus, the derivative of positive definite function (6.86) is of form

$$\dot{V} = -k\left(\left(\omega_1 - \omega_0\right) g_1 + \left(\omega_2 - \omega_0\right) g_2\right)^2 - M\left|\left(\omega_1 - \omega_0\right) g_1 + \left(\omega_2 - \omega_0\right) g_2\right|$$

which leads to the conclusion that $\dot{V} < 0$ and the system is asymptotically stable for k sufficiently high but finite and an arbitrary value of M .

Example

The dynamic analysis is carried out by applying the above SMC approach to the network used in [136]. The one-line diagram is given in Fig 6.18. It comprises a wind farm connected to bus 3 and conventional thermal generation connected to the main system through coupling transformers and transmission lines.

Generator 1 and Generator 3 represent steam turbine-driven synchronous generators; Generator 2 represents an equivalent DFIG-based wind farm. Synchronous generators are represented by their voltage-behind-transient-reactance model.

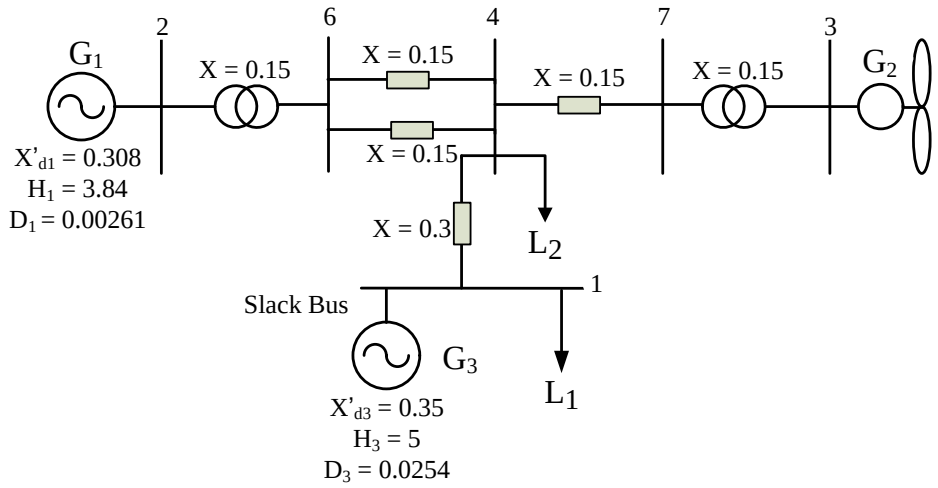

Figure 6.18: 3-machine

Table 6.2: Load Flow Results of the 3-machine system

Bus	**Bus Type**	**Voltage** (pu)	$\mathbf{P_G}$ (pu)	$\mathbf{Q_G}$ (pu)	$\mathbf{P_L}$ (pu)	$\mathbf{Q_L}$ (pu)
1	Swing	$1.0\angle 0°$	2.80	0.150	2.4	0.0
2	P-V	$1.0\angle 1.59°$	0.80	0.330	-	-
3	P-V	$1.0\angle 19.9°$	0.80	0.3142	-	-
4	P-Q	$0.93\angle -35.412°$	-	-	2.0	2.0

The generators rated power is: Generator 1 = 21000 MVA, Generator 2 = 2400 MVA, and Generator 3 = 2800 MVA. The system base MVA is 1000 and system frequency is 50 Hz. The system data are in per unit on the system MVA base and given in Fig. 6.18. The system state is described by the power flow results shown in Table 6.2.

The GSC is in charge of damping oscillations between machine 1 and machine 3. To assess the system behaviour when affected by a small disturbance in the form of a mechanical power reduction of 10% in G_1.

Figs. 6.19 and 6.20 illustrate the perturbed condition. The DFIG control strategy enhances the oscillatory behaviour by injecting dynamic reactive power to the system. The reactive current injection is depicted in 6.21. The four plots correspond to four values of gain factor $k = 0$, 2, 5, 10 in Eq. (6.87).

It is observed that the SMC applied to the GSC works very efficiently to damp out inter-area oscillations. It should be emphasized that the reactive current from the GSC is bounded between ± 0.2 pu, although the required value for this disturbance quite small (only 0.11 pu).

The chattering effect only appears when the system reaches the equilibrium point. This chattering effect is quite small, but it may be reduced even further by fine tuning the gain factor M used in equation (6.87).

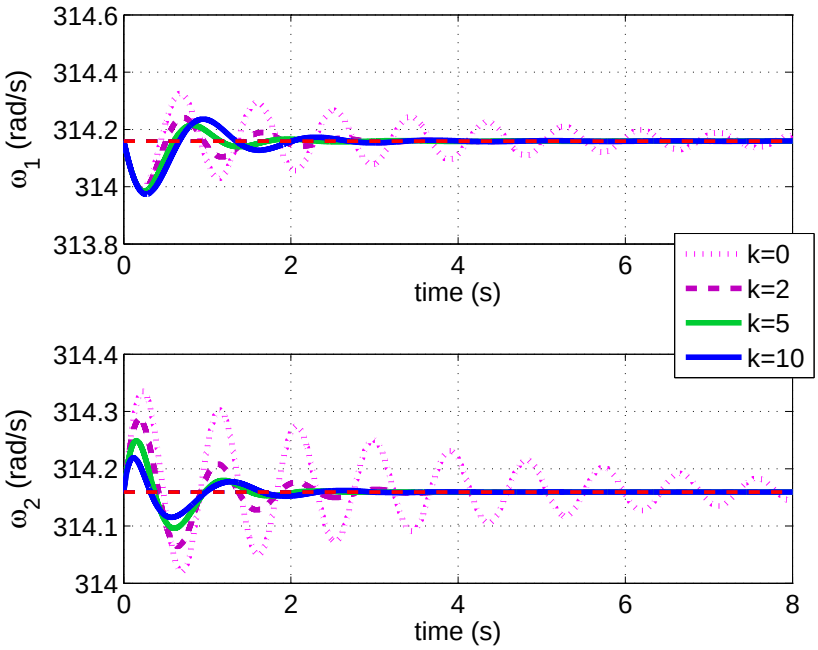

Figure 6.19: Generator rotor speed of area 1 and area 2

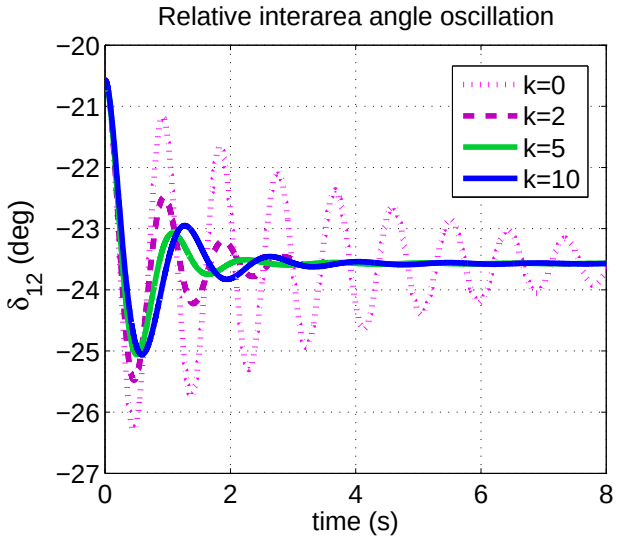

Figure 6.20: Inter-area angle

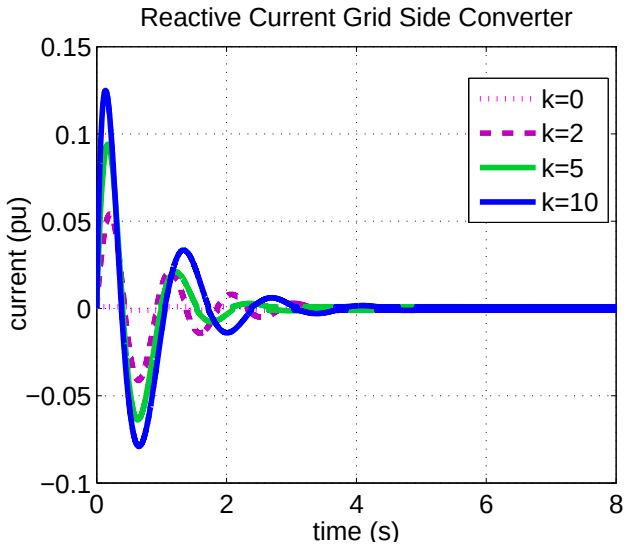

Figure 6.21: Reactive current from the GSC

6.5 Conclusions

The newly developed SMC control scheme demonstrates the importance of employing non-linear control algorithms since they yield good operational performances and network support. This is of the utmost important since in power systems with wind power generation is critically important to ensure the robust operation of the whole system with no interaction of controllers.

Sliding Mode Control based strategies applied in doubly fed induction generators have the potential to provide a superior dynamic and transient performance than that afforded by classical control methodologies. In mixed generation networks, bulk wind generation based on variable speed wind turbines, if suitably controlled, can be accommodated in the network without introducing transient or dynamic stability issues. Quite the contrary, the findings of this research seem to add further weight to those of other researchers that suitably controlled DFIGs can contribute positively to network operation and to an overall enhancement of the network dynamic characteristics.

Chapter 7

General Conclusions and Future Research Avenues

This research work has addressed the timely issue of the dynamic performance assessment of DFIG Wind Energy Conversion Systems, with particular reference to its control system and the impact of the wind power plant on the electrical power grid and vice-versa. The work has been carried out in connection with a DFIG-WECS connected to an equivalent strong system to investigate the issue of local oscillation modes within the wind power plant itself and in a combined multi-machine power system environment to investigate the issue of inter-area modes.

A non-linear DFIG controller based on Sliding Mode Control was proposed and its performance compared with that of a classical controller based on Field Oriented Control. Sliding Mode Control showed to be more robust and flexible than the classical controller, opening the door for a more widespread future participation of DFIG-WECS in the damping of power system oscillations. Modal analysis and time domain simulations were chosen to good effect as the study methods with which to interpret the responses of the dynamic models addressed in this research. They encompass both one DFIG-WECS connected to an equivalent strong system and the case of a multi-machine power system

including conventional generation and DFIG-WECS. In both cases the aim has been to assess the impact of wind turbine generator control in system stability, particularly in electromechanical oscillations damping. The assessment has been rather comprehensive, including different electrical grid topologies operating under a wide range of power generation scenarios.

The most significant findings and contributions of this thesis together with future avenues of research works in this area of electrical power systems research are given below:

It has been found rather useful in order to contextualize the importance of the research, to have started by examining the general aspects of power system stability and to have written down definitions and specific stability concepts in order to bring into the discussion, at a later stage in the thesis, the contribution that DFIG-WECS and SMC will make to power systems operation in the not too distant future. In the same tenor, it was also deemed important to outline the most relevant wind turbine components models available for power system dynamics, with reference to small-signal and transient stability analyses.

The new application of Sliding Mode Control has been comprehensive not only in the sense that it encompasses both the machine side converter and the grid side converter but also in the sense that it has been applied to cases of multi-machine power systems containing a combination of conventional synchronous generation and variable speed wind power generators. Moreover, a wide range of operating scenarios was considered and the new control strategy based on SMC, which is non-linear, showed a very robust performance. A case in point is the generator model and control strategies for the study of small-signal stability of a wind turbine generator connected to an equivalent grid, presented in Chapter 4. The modal analysis results for this simplified representation of the power grid correctly include the effects of oper-

ating conditions, machine parameters and models, grid strength and control system strategy. The results obtained corroborate that operating conditions, machine and system parameters affect markedly the location and nature of the oscillatory modes but also that the control approach adopted plays a major role. More specifically, it was found that stability of the DFIG-based wind turbine using FOC depends to a large extent on the tuning of the proportional-integral controllers and on having good knowledge of the machine parameters - a change in operating scenarios or system topology may require a re-tuning of the proportional-integral controllers. Conversely, it was found that SMC is a very convenient vehicle to improve on the DFIG stability; it showed to be very robust under machine parameter and network variations. It yields electro-mechanical coupling cancellation without introducing additional modes and provides extra-damping which, in turn, reduces local oscillations. In brief, SMC presents a far better performance than the classical controller FOC, in this application.

Since the integration of wind power generators in the power grid is on the increase, particularly the integration of wind power generation systems with double-fed induction generators, having a solid understanding of the impact that these generators will have on system stability, is a current issue of paramount importance. Comprehensive computer simulation studies have been carried out to gain a greater insight into the benefits or otherwise of using variable-speed wind turbine in mixed generation systems to improve on the stability of the overall power networks. FOC- and SMC-based strategies were used to evaluate the contribution that the controllers of the wind power generation units were able to exert on network damping. This showed the effectiveness that SMC has in enhancing the dynamic performance of the DFIG plant as well as the great potential that it has in drawing an even superior dynamic performance of grid connected wind turbines. This was further corroborated by carrying out transient studies using time domain simulations of multi-machine power systems with embedded wind power generation. It was found that the best control strategy

was: (i) to apply SMC in the machine side converter to control the rotor voltage in order to operate the wind turbine at optimum efficiency, at the desired power factor; (ii) to apply SMC in the grid side converter to maximize the damping of electromechanical oscillations by drawing on its reactive power capability - the control law was derived using a defined Lyapunov function. More punctually, the multi-machine power system studies carried out in this research indicate the following:

- That a double fed induction generator has the potential to provide a superior dynamic and transient performance than that of a conventional synchronous generator
- That in mixed generation networks, bulk wind generation based on variable speed wind turbines, if suitably controlled, can be accommodated on a network without introducing transient or dynamic stability issues and that they can contribute positively to network operation and contribute to an overall enhancement of the network dynamic characteristics
- That the newly developed SMC control scheme demonstrates the importance of employing non-linear control algorithms since they yield good operational performances and network support. This is the most important since in power systems with wind power generation is critically important to ensure the robust operation of the whole system with no interaction of controllers.

7.1 Future Research Avenues

Concerning recommendations for future research in this area of electrical power systems, the following topics seem a natural extension of this research:

- The proposed SMC control should be implemented in larger electrical power systems, including networks with a higher degree of complexity

- In order to test the performance of the sliding mode control approach in a real-time, a suitable laboratory environment and eventually a field-trial implementation ought to be carried out
- To take full advantage of the flexibility offered by the SMC, it looks a rather attractive proposition to apply it other wind power generation technologies such as the full power-converter system

Bibliography

[1] M. J. Novogradac, *Renewable Energy Tax Credit Handbook - 2010 Edition*. Novogradac & Company LLP.

[2] V. Climate Policy Initiative, U. Varadarajan, and C. Initiative, "A comparative Case-Study analysis of the effectiveness and efficiency of policies that influence the financing of renewable energy projects: US and europe,"

[3] "Global wind report 2010," tech. rep., Global WindEnergy Council - GWEC:, 2010.

[4] A. Mendonca and J. A. Lopes, "Impact of large scale wind power integration on small signal stability," in *2005 International Conference on Future Power Systems*, pp. 5 pp.–5, IEEE, Nov. 2005.

[5] O. Anaya-Lara, N. Jenkins, J. Ekanayake, P. Cartwright, and M. Hughes, *Wind Energy Generation: Modelling and Control*. Wiley, 1 ed., Sept. 2009.

[6] V. Utkin, J. Guldner, and J. Shi, *Sliding Mode Control in Electro-Mechanical Systems, Second Edition*. CRC Press, 2 ed., May 2009.

[7] A. Sabanovic, L. Fridman, S. K. Spurgeon, and I. o. E. Engineers, *Variable structure systems: from principles to implementation*. IET, 2004.

[8] W. Lee, M. Chen, J. Gim, K. Yoshimura, and S. Wang, "Dynamic stability analysis of an industrial power system," *IEEE Transactions on Industry Applications*, vol. 31, pp. 675–681, Aug. 1995.

[9] "Proposed terms & definitions for power system stability," *IEEE Transactions on Power Apparatus and Systems*, vol. PAS-101, pp. 1894–1898, July 1982.

[10] P. Kundur, J. Paserba, V. Ajjarapu, G. Andersson, A. Bose, C. Canizares, N. Hatziargyriou, D. Hill, A. Stankovic, C. Taylor, T. Van Cutsem, and V. Vittal, "Definition and classification of power system stability IEEE/CIGRE joint task force on stability terms and definitions," *IEEE Transactions on Power Systems*, vol. 19, pp. 1387– 1401, Aug. 2004.

[11] K. R. Padiyar, *Power System Dynamics: Stability and Control*. John Wiley & Sons Ltd (Import), Pap/Dsk ed., Apr. 1999.

[12] "Power oscillation protection," Nov. 2002.

[13] K. Prasertwong, N. Mithulananthan, and D. Thakur, "Understanding low-frequency oscillation in power systems," *International Journal of Electrical Engineering Education*, vol. 47, no. 3, pp. 248–262, 2010.

[14] Y. N. N. Tchokonte, *Real-time Identification and Monitoring of the Voltage Stability Margin in Electric Power Transmission Systems Using Synchronized Phasor Measurements*. PhD thesis, Kassel University, Germany, 2009.

[15] Taylor, *Power System Voltage Stability*. McGraw-Hill Education, Sept. 1994.

[16] T. v. Cutsem and C. Vournas, *Voltage Stability of Electric Power Systems*. Springer, 1 ed., Mar. 1998.

[17] N. R. Ullah, T. Thiringer, and D. Karlsson, "Voltage and transient stability support by wind farms complying with the E.ON netz grid code," *IEEE Transactions on Power Systems*, vol. 22, pp. 1647–1656, Nov. 2007.

[18] E. Vittal, M. O'Malley, and A. Keane, "A Steady-State voltage stability analysis of power systems with high penetrations of wind," *IEEE Transactions on Power Systems*, vol. 25, pp. 433–442, Feb. 2010.

[19] J. Morren, S. W. de Haan, W. L. Kling, and J. A. Ferreira, "Wind turbines emulating inertia and supporting primary frequency control," *IEEE Transactions on Power Systems*, vol. 21, pp. 433– 434, Feb. 2006.

[20] G. Ramtharan, J. B. Ekanayake, and N. Jenkins, "Frequency support from doubly fed induction generator wind turbines," *IET Renewable Power Generation*, vol. 1, pp. 3–9, Mar. 2007.

[21] P. Kundur, *Power System Stability and Control*. McGraw-Hill Professional, Jan. 1994.

[22] L. L. Grigsby, *The electric power engineering handbook*. CRC Press, 2001.

[23] J. Machowski, J. W. Bialek, and J. R. Bumby, *Power system dynamics and stability*. John Wiley & Sons, Oct. 1997.

[24] P. W. Sauer and M. A. Pai, *Power System Dynamics and Stability*. Prentice Hall, 1st ed., July 1997.

[25] L. Wang, F. Howell, P. Kundur, C. Y. Chung, and W. Xu, "A tool for small-signal security assessment of power systems," in *22nd IEEE Power Engineering Society International Conference on Power Industry Computer Applications, 2001. PICA 2001. Innovative Computing for Power - Electric Energy Meets the Market*, pp. 246–252, IEEE, 2001.

[26] U. Kerin, T. N. Tuan, E. Lerch, and G. Bizjak, "Small signal security index for contingency classification in dynamic security assessment," in *PowerTech, 2011 IEEE Trondheim*, pp. 1–6, IEEE, June 2011.

[27] S. Yang, F. Liu, D. Zhang, S. Mei, and G. He, "Polynomial approximation of the damping-ratio-based small-signal security region boundaries of power systems," in *2011 IEEE Power and Energy Society General Meeting*, pp. 1–8, IEEE, July 2011.

[28] J. Paserba *et al.*, "Analysis and control of power system oscillation," *CIGRE special publication*, vol. 38, no. 07, 1996.

[29] G. C. Verghese, I. J. Perez-Arriaga, and F. C. Schweppe, "Selective modal analysis with applications to electric power systems, part II: the dynamic stability problem," *IEEE Transactions on Power Apparatus and Systems*, vol. PAS-101, pp. 3126–3134, Sept. 1982.

[30] I. J. Perez-Arriaga, G. C. Verghese, and F. C. Schweppe, "Selective modal analysis with applications to electric power systems, PART i: Heuristic introduction," *IEEE Transactions on Power Apparatus and Systems*, vol. PAS-101, pp. 3117–3125, Sept. 1982.

[31] J. G. F. Francis, "The QR transformation a unitary analogue to the LR Transformation-Part 1," *The Computer Journal*, vol. 4, pp. 265 –271, Jan. 1961.

[32] J. G. F. Francis, "The QR Transformation-Part 2," *The Computer Journal*, vol. 4, pp. 332 –345, Jan. 1962.

[33] J. H. Wilkinson, *The algebraic eigenvalue problem.* Clarendon Press, 1988.

[34] R. T. Byerly, R. J. Bennon, and D. E. Sherman, "Eigenvalue analysis of synchronizing power flow oscillations in large electric

power systems," *IEEE Transactions on Power Apparatus and Systems*, vol. PAS-101, pp. 235–243, Jan. 1982.

[35] L. Wang and A. Semlyen, "Application of sparse eigenvalue techniques to the small signal stability analysis of large power systems," in *Power Industry Computer Application Conference, 1989. PICA '89, Conference Papers*, pp. 358–365, IEEE, May 1989.

[36] P. Kundur, G. J. Rogers, D. Y. Wong, L. Wang, and M. G. Lauby, "A comprehensive computer program package for small signal stability analysis of power systems," *IEEE Transactions on Power Systems*, vol. 5, pp. 1076–1083, Nov. 1990.

[37] J. I. Pérez Arriaga, "Selective modal analysis with applications to electric power systems," s, Fred C. Schweppe and George C. Verghese., Massachusetts Institute of Technology. Dept. of Electrical Engineering and Computer Science., Massachusetts Institute of Technology. Dept. of Electrical Engineering and Computer Science., 1981.

[38] M. Pai, *Energy Function Analysis for Power System Stability*. Springer, 1 ed., Aug. 1989.

[39] F. A. Rahimi, M. G. Lauby, J. N. Wrubel, and K. L. Lee, "Evaluation of the transient energy function method for on-line dynamic security analysis," *IEEE Transactions on Power Systems*, vol. 8, pp. 497–507, May 1993.

[40] A. D. Patton, "Assessment of the security of operating electric power systems using probability methods," *Proceedings of the IEEE*, vol. 62, pp. 892– 901, July 1974.

[41] Slootweg, *Wind Power: Modelling and Impact on Power System Dynamics*. PhD thesis, Electrical Engineering, Mathematics and Computer Science, Delft University of Technology, Dec. 2003.

[42] J. Ekanayake and N. Jenkins, "Comparison of the response of doubly fed and fixed-speed induction generator wind turbines to changes in network frequency," *IEEE Transactions on Energy Conversion*, vol. 19, pp. 800– 802, Dec. 2004.

[43] P. W. Carlin, A. S. Laxson, and E. B. Muljadi, "The history and state of the art of Variable-Speed wind turbine technology," tech. rep., NREL, National Renewable Energy Laboratory, February 2001.

[44] S. Muller, M. Deicke, and R. W. De Doncker, "Doubly fed induction generator systems for wind turbines," *IEEE Industry Applications Magazine*, vol. 8, pp. 26–33, June 2002.

[45] E. B. Muhando, T. Senjyu, E. Omine, T. Funabashi, and C. Kim, "Modelling-based approach for digital control design for nonlinear WECS in the power system," *Wind Energy*, vol. 13, pp. 543–557, Sept. 2010.

[46] T. Ackermann, *Wind power in power systems*. John Wiley and Sons, Mar. 2005.

[47] A. Hansen, P. Sorensen, F. Iov, and F. Blaabjerg, "Control of variable speed wind turbines with doubly-fed induction generators," *Wind Engineering*, vol. 28, pp. 411–432, June 2004.

[48] J. G. Slootweg, H. Polinder, and W. L. Kling, "Representing wind turbine electrical generating systems in fundamental frequency simulations," *IEEE Transactions on Energy Conversion*, vol. 18, pp. 516– 524, Dec. 2003.

[49] J. G. Slootweg, S. W. de Haan, H. Polinder, and W. L. Kling, "General model for representing variable speed wind turbines in power system dynamics simulations," *IEEE Transactions on Power Systems*, vol. 18, pp. 144– 151, Feb. 2003.

[50] B.O.E, "Procedimiento de operación PO 12.3. requisitos de respuesta frente a huecos de tensión de las instalaciones eléctricas (in spanish)," tech. rep., 2006.

[51] F. K. Lima, A. Luna, P. Rodriguez, E. H. Watanabe, and F. Blaabjerg, "Rotor voltage dynamics in the doubly fed induction generator during grid faults," *IEEE Transactions on Power Electronics*, vol. 25, pp. 118–130, Jan. 2010.

[52] J. Slootweg and W. Kling, "The impact of large scale wind power generation on power system oscillations," *Electric Power Systems Research*, vol. 67, pp. 9–20, Oct. 2003.

[53] L. Holdsworth, X. G. Wu, J. B. Ekanayake, and N. Jenkins, "Comparison of fixed speed and doubly-fed induction wind turbines during power system disturbances," *Generation, Transmission and Distribution, IEE Proceedings-*, vol. 150, pp. 343– 352, May 2003.

[54] J. J. Sanchez-Gasca, N. W. Miller, and W. W. Price, "A modal analysis of a two-area system with significant wind power penetration," in *Power Systems Conference and Exposition, 2004. IEEE PES*, pp. 1148– 1152 vol.2, IEEE, Oct. 2004.

[55] F. M. Hughes, O. Anaya-Lara, N. Jenkins, and G. Strbac, "A power system stabilizer for DFIG-based wind generation," *IEEE Transactions on Power Systems*, vol. 21, pp. 763– 772, May 2006.

[56] E. Muljadi, C. P. Butterfield, B. Parsons, and A. Ellis, "Effect of variable speed wind turbine generator on stability of a weak grid," *IEEE Transactions on Energy Conversion*, vol. 22, pp. 29–36, Mar. 2007.

[57] J. M. Rodriguez, J. L. Fernandez, D. Beato, R. Iturbe, J. Usaola, P. Ledesma, and J. R. Wilhelmi, "Incidence on power system dynamics of high penetration of fixed speed and doubly fed wind

energy systems: study of the spanish case," *IEEE Transactions on Power Systems*, vol. 17, pp. 1089– 1095, Nov. 2002.

[58] F. W. Koch, I. Erlich, F. Shewarega, and U. Bachmann, "Dynamic interaction of large offshore wind farms with the electric power system," in *Power Tech Conference Proceedings, 2003 IEEE Bologna*, vol. 3, IEEE, June 2003.

[59] P. Ledesma and J. Usaola, "Doubly fed induction generator model for transient stability analysis," *IEEE Transactions on Energy Conversion*, vol. 20, pp. 388– 397, June 2005.

[60] Y. Chi, Y. Liu, W. Wang, and H. Dai, "Voltage stability analysis of wind farm integration into transmission network," in *International Conference on Power System Technology, 2006. PowerCon 2006*, pp. 1–7, IEEE, Oct. 2006.

[61] A. D. Hansen and G. Michalke, "Fault ride-through capability of DFIG wind turbines," *Renewable Energy*, vol. 32, pp. 1594–1610, July 2007.

[62] V. Bufano, M. Dicorato, A. Minoia, and M. Trovato, "Embedding wind farm generation in power system transient stability analysis," in *Power Tech, 2005 IEEE Russia*, pp. 1–7, IEEE, June 2005.

[63] H. Gaztanaga, I. Etxeberria-Otadui, S. Bacha, and D. Roye, "Fixed-Speed wind farm operation improvement by using DVR devices," in *IEEE International Symposium on Industrial Electronics, 2007. ISIE 2007*, pp. 2679–2684, IEEE, June 2007.

[64] C. Alvarez, H. Amaris, O. Samuelsson, D. Florez, and L. Gonzalez, "Custom power systems and software platforms for wind farms under voltage dips situations," in *Universities Power Engineering Conference, 2008. UPEC 2008. 43rd International*, pp. 1–4, IEEE, Sept. 2008.

[65] C. Angeles-Camacho, E. Farinas-Wong, and F. Banuelos-Ruedas, "FACTS: its role in the connection of wind power to power networks," in *Modern Electric Power Systems (MEPS), 2010 Proceedings of the International Symposium*, pp. 1–7, IEEE, Sept. 2010.

[66] L. Holdsworth, J. B. Ekanayake, and N. Jenkins, "Power system frequency response from fixed speed and doubly fed induction generator-based wind turbines," *Wind Energy*, vol. 7, pp. 21–35, Jan. 2004.

[67] G. Lalor, A. Mullane, and M. O'Malley, "Frequency control and wind turbine technologies," *IEEE Transactions on Power Systems*, vol. 20, pp. 1905– 1913, Nov. 2005.

[68] R. Doherty, A. Mullane, G. Nolan, D. J. Burke, A. Bryson, and M. O'Malley, "An assessment of the impact of wind generation on system frequency control," *IEEE Transactions on Power Systems*, vol. 25, pp. 452–460, Feb. 2010.

[69] N. R. Ullah, T. Thiringer, and D. Karlsson, "Temporary primary frequency control support by variable speed wind turbines-potential and applications," *IEEE Transactions on Power Systems*, vol. 23, pp. 601–612, May 2008.

[70] N. R. Ullah, *Wind Power - Added Value for Network Operation*. PhD thesis, Chalmers University Of Technology, Göteborg, Sweden, 2008.

[71] A. Mullane and M. O'Malley, "The inertial response of Induction-Machine-Based wind turbines," *IEEE Transactions on Power Systems*, vol. 20, pp. 1496– 1503, Aug. 2005.

[72] R. G. de Almeida and J. A. Lopes, "Participation of doubly fed induction wind generators in system frequency regulation," *IEEE Transactions on Power Systems*, vol. 22, pp. 944–950, Aug. 2007.

[73] E. Vittal, J. D. McCalley, V. Ajjarapu, and T. Harbour, "Wind penetration limited by thermal constraints and frequency stability," in *Power Symposium, 2007. NAPS '07. 39th North American*, pp. 353–359, IEEE, Oct. 2007.

[74] R. Fernández, R. Mantz, and P. Battaiotto, "Impact of wind farms on a power system. an eigenvalue analysis approach," *Renewable Energy*, vol. 32, pp. 1676–1688, Aug. 2007.

[75] J. M. Mauricio, A. Marano, A. Gomez-Exposito, and J. L. Martinez Ramos, "Frequency regulation contribution through Variable-Speed wind energy conversion systems," *IEEE Transactions on Power Systems*, vol. 24, pp. 173–180, Feb. 2009.

[76] O. Anaya-Lara, F. M. Hughes, N. Jenkins, and G. Strbac, "Contribution of DFIG-based wind farms to power system short-term frequency regulation," *Generation, Transmission and Distribution, IEE Proceedings-*, vol. 153, pp. 164– 170, Mar. 2006.

[77] D. A. Spera, *Wind turbine technology: fundamental concepts of wind turbine engineering*. ASME Press, May 2009.

[78] E. Hau, *Wind Turbines: Fundamentals, Technologies, Application, Economics*. Springer, 2nd ed., Oct. 2005.

[79] J. Zhou, E. Erdem, G. Li, and J. Shi, "Comprehensive evaluation of wind speed distribution models: A case study for north dakota sites," *Energy Conversion and Management*, vol. 51, pp. 1449–1458, July 2010.

[80] M. Mohanpurkar and R. G. Ramakumar, "Probability density functions for power output of wind electric conversion systems," in *2010 IEEE Power and Energy Society General Meeting*, pp. 1–7, IEEE, July 2010.

[81] A. Ouammi, V. Ghigliotti, M. Robba, A. Mimet, and R. Sacile, "A decision support system for the optimal exploitation of wind

energy on regional scale," *Renewable Energy*, vol. 37, pp. 299–309, Jan. 2012.

[82] R. Bansal, T. Bhatti, and D. Kothari, "On some of the design aspects of wind energy conversion systems," *Energy Conversion and Management*, vol. 43, pp. 2175–2187, Nov. 2002.

[83] J. L. R. Amenedo, *Análisis Dinámico y Diseño del Sistema de Control de Aeroturbinas de Velocidad Variable con Generador Asíncrono de Doble Alimentación (in spanish)*. PhD thesis, Carlos III de Madrid, Leganés, Madrid, 2000.

[84] C. Vilar Moreno, *Fluctuaciones de tensión producidas por los aerogeneradores de velocidad fija (in spanish)*. PhD thesis, Carlos III de Madrid, Leganés, Madrid, 2002.

[85] L. Helle, *Modeling and Comparison of Power Converters for Doubly Fed Induction Generators in Wind Turbines*. Institut for Energiteknik, Aalborg Universitet, 2007.

[86] T. Burton, *Wind energy: handbook*. John Wiley and Sons, Dec. 2001.

[87] M. O. L. Hansen, *Aerodynamics of wind turbines*. Earthscan, Feb. 2008.

[88] S. K. Salman and A. L. Teo, "Windmill modeling consideration and factors influencing the stability of a grid-connected wind power-based embedded generator," *IEEE Transactions on Power Systems*, vol. 18, pp. 793– 802, May 2003.

[89] S. K. Salman, A. L. Teo, and I. M. Rida, "The effect of shaft modelling on the assessment of fault CCT and the power quality of a wind farm," in *Ninth International Conference on Harmonics and Quality of Power, 2000. Proceedings*, vol. 3, pp. 994–998 vol.3, IEEE, 2000.

[90] E. N. Hinrichsen and P. J. Nolan, "Dynamics and stability of wind turbine generators," *IEEE Transactions on Power Apparatus and Systems*, vol. PAS-101, pp. 2640–2648, Aug. 1982.

[91] R. Pena, J. C. Clare, and G. M. Asher, "Doubly fed induction generator using back-to-back PWM converters and its application to variable-speed wind-energy generation," *Electric Power Applications, IEE Proceedings* -, vol. 143, pp. 231–241, May 1996.

[92] I. Takahashi and T. Noguchi, "A new Quick-Response and High-Efficiency control strategy of an induction motor," *IEEE Transactions on Industry Applications*, vol. IA-22, pp. 820–827, Sept. 1986.

[93] L. Xu and P. Cartwright, "Direct active and reactive power control of DFIG for wind energy generation," *IEEE Transactions on Energy Conversion*, vol. 21, pp. 750–758, Sept. 2006.

[94] L. Holdsworth, X. G. Wu, J. B. Ekanayake, and N. Jenkins, "Direct solution method for initialising doubly-fed induction wind turbines in power system dynamic models," *Generation, Transmission and Distribution, IEE Proceedings*-, vol. 150, pp. 334–342, May 2003.

[95] W. Leonhard, *Control of Electrical Drives*. Springer, 3nd ed., Sept. 2001.

[96] F. Valenciaga, P. F. Puleston, and S. K. Spurgeon, "A geometric approach for the design of MIMO sliding controllers. application to a wind driven double output induction generator," in *International Workshop on Variable Structure Systems, 2006. VSS'06*, pp. 115–120, IEEE, June 2006.

[97] T. Lund, P. Sorensen, and J. Eek, "Reactive power capability of a wind turbine with doubly fed induction generator," *Wind Energy*, vol. 10, pp. 379–394, July 2007.

[98] L. Fernandez, C. Garcia, and F. Jurado, "Comparative study on the performance of control systems for doubly fed induction generator (DFIG) wind turbines operating with power regulation," *Energy*, vol. 33, pp. 1438–1452, Sept. 2008.

[99] Y. Tang and L. Xu, "A flexible active and reactive power control strategy for a variable speed constant frequency generating system," *IEEE Transactions on Power Electronics*, vol. 10, pp. 472–478, July 1995.

[100] M. V. Nunes, J. A. Lopes, H. H. Zurn, U. H. Bezerra, and R. G. Almeida, "Influence of the variable-speed wind generators in transient stability margin of the conventional generators integrated in electrical grids," *IEEE Transactions on Energy Conversion*, vol. 19, pp. 692– 701, Dec. 2004.

[101] J. Hu, H. Nian, B. Hu, Y. He, and Z. Q. Zhu, "Direct active and reactive power regulation of DFIG using Sliding-Mode control approach," *IEEE Transactions on Energy Conversion*, vol. 25, pp. 1028–1039, Dec. 2010.

[102] X. Zheng, L. Li, D. Xu, and J. Platts, "Sliding mode MPPT control of variable speed wind power system," in *Power and Energy Engineering Conference, 2009. APPEEC 2009. Asia-Pacific*, pp. 1–4, IEEE, Mar. 2009.

[103] S. Z. Chen, N. C. Cheung, K. C. Wong, and J. Wu, "Integral Sliding-Mode direct torque control of Doubly-Fed induction generators under unbalanced grid voltage," *IEEE Transactions on Energy Conversion*, vol. 25, pp. 356–368, June 2010.

[104] M. I. Martinez, G. Tapia, A. Susperregui, and H. Camblong, "Sliding-Mode control for DFIG rotor- and Grid-Side converters under unbalanced and harmonically distorted grid voltage," *IEEE Transactions on Energy Conversion*, vol. PP, no. 99, pp. 1–12.

[105] "World wind energy association, wwea 2010, http://www.wwindea.org."

[106] N. Jenkins, R. Allan, P. Crossley, D. Kirschen, and G. Strbac, *Embedded Generation (IEE Power)PBPO0310*. Institution of Engineering and Technology, July 2000.

[107] D. Gautam, L. Goel, R. Ayyanar, V. Vittal, and T. Harbour, "Control strategy to mitigate the impact of reduced inertia due to doubly fed induction generators on large power systems," *IEEE Transactions on Power Systems*, vol. 26, pp. 214–224, Feb. 2011.

[108] M. Klein, G. Rogers, and P. Kundur, "A fundamental study of inter-area oscillations in power systems," *IEEE Transactions on Power Systems*, vol. 6, pp. 914–921, Aug. 1991.

[109] T. Petru and T. Thiringer, "Modeling of wind turbines for power system studies," *IEEE Transactions on Power Systems*, vol. 17, pp. 1132– 1139, Nov. 2002.

[110] Y. Lei, A. Mullane, G. Lightbody, and R. Yacamini, "Modeling of the wind turbine with a doubly fed induction generator for grid integration studies," *IEEE Transactions on Energy Conversion*, vol. 21, pp. 257– 264, Mar. 2006.

[111] J. B. Ekanayake, L. Holdsworth, X. Wu, and N. Jenkins, "Dynamic modeling of doubly fed induction generator wind turbines," *IEEE Transactions on Power Systems*, vol. 18, pp. 803–809, May 2003.

[112] M. Rahimi and M. Parniani, "Transient performance improvement of wind turbines with doubly fed induction generators using nonlinear control strategy," *IEEE Transactions on Energy Conversion*, vol. 25, pp. 514–525, June 2010.

[113] B. Beltran, T. Ahmed-Ali, and M. E. Benbouzid, "Sliding mode power control of variable speed wind energy conversion systems,"

in *Electric Machines & Drives Conference, 2007. IEMDC '07. IEEE International*, vol. 2, pp. 943–948, IEEE, May 2007.

[114] F. Valenciaga, P. F. Puleston, and P. E. Battaiotto, "Variable structure system control design method based on a differential geometric approach: application to a wind energy conversion subsystem," *Control Theory and Applications, IEE Proceedings -*, vol. 151, pp. 6– 12, Jan. 2004.

[115] F. Wu, X. P. Zhang, K. Godfrey, and P. Ju, "Small signal stability analysis and optimal control of a wind turbine with doubly fed induction generator," *IET Generation, Transmission & Distribution*, vol. 1, pp. 751–760, Sept. 2007.

[116] M. Al-Biati, M. El-Kady, and A. Al-Ohaly, "Dynamic stability improvement via coordination of static var compensator and power system stabilizer control actions," *Electric Power Systems Research*, vol. 58, pp. 37–44, May 2001.

[117] Z. Elrazaz and A. A. Al-Ohaly, "Optimal coordination of shunt reactors to enhance system performance at light load operation," *Generation, Transmission and Distribution, IEE Proceedings C*, vol. 140, pp. 293–298, July 1993.

[118] E. Z. Zhou, "Application of static VAr compensators to increase power system damping," *IEEE Transactions on Power Systems*, vol. 8, pp. 655–661, May 1993.

[119] C. Wang, L. Shi, L. Wang, and Y. Ni, "Small signal stability analysis considering grid-connected wind farms of DFIG type," in *2008 IEEE Power and Energy Society General Meeting - Conversion and Delivery of Electrical Energy in the 21st Century*, pp. 1–6, IEEE, July 2008.

[120] G. Tsourakis, B. Nomikos, and C. Vournas, "Effect of wind parks with doubly fed asynchronous generators on small-signal stabil-

ity," *Electric Power Systems Research*, vol. 79, pp. 190–200, Jan. 2009.

[121] D. Gautam, V. Vittal, and T. Harbour, "Impact of increased penetration of DFIG-Based wind turbine generators on transient and small signal stability of power systems," *IEEE Transactions on Power Systems*, vol. 24, pp. 1426–1434, Aug. 2009. cc.

[122] Y. Mishra, S. Mishra, F. Li, Z. Y. Dong, and R. C. Bansal, "Small-Signal stability analysis of a DFIG-Based wind power system under different modes of operation," *IEEE Transactions on Energy Conversion*, vol. 24, pp. 972–982, Dec. 2009.

[123] S. Yuanzhang, W. Lixin, L. Guojie, and L. Jin, "A review on analysis and control of small signal stability of power systems with large scale integration of wind power," in *2010 International Conference on Power System Technology (POWERCON)*, pp. 1–6, IEEE, Oct. 2010.

[124] J. L. Rueda and I. Erlich, "Impacts of large scale integration of wind power on power system small-signal stability," in *2011 4th International Conference on Electric Utility Deregulation and Restructuring and Power Technologies (DRPT)*, pp. 673–681, IEEE, July 2011.

[125] Z. Miao, L. Fan, D. Osborn, and S. Yuvarajan, "Control of DFIG-Based wind generation to improve interarea oscillation damping," *IEEE Transactions on Energy Conversion*, vol. 24, pp. 415–422, June 2009.

[126] L. Fan, H. Yin, and Z. Miao, "On Active/Reactive power modulation of DFIG-Based wind generation for interarea oscillation damping," *IEEE Transactions on Energy Conversion*, vol. 26, pp. 513–521, June 2011.

[127] N. Kshatriya, U. D. Annakkage, F. M. Hughes, and A. M. Gole, "Optimized partial eigenstructure Assignment-Based design of a

combined PSS and active damping controller for a DFIG," *IEEE Transactions on Power Systems*, vol. 25, pp. 866–876, May 2010.

[128] K. Elkington, M. Ghandhari, and L. Soder, "Using power system stabilisers in doubly fed induction generators," in *Power Engineering Conference, 2008. AUPEC '08. Australasian Universities*, pp. 1–6, IEEE, Dec. 2008.

[129] L. Fan, Z. Miao, and D. Osborn, "Impact of doubly fed wind turbine generation on inter-area oscillation damping," in *2008 IEEE Power and Energy Society General Meeting - Conversion and Delivery of Electrical Energy in the 21st Century*, pp. 1–8, IEEE, July 2008.

[130] C. Martinez, G. Joos, and B. T. Ooi, "Power system stabilizers in variable speed wind farms," in *IEEE Power & Energy Society General Meeting, 2009. PES '09*, pp. 1–7, IEEE, July 2009.

[131] N. R. Ullah and T. Thiringer, "Effect of operational modes of a wind farm on the transient stability of nearby generators and on power oscillations: a nordic grid study," *Wind Energy*, vol. 11, pp. 63–73, Jan. 2008.

[132] W. Qiao and R. G. Harley, "Effect of grid-connected DFIG wind turbines on power system transient stability," in *2008 IEEE Power and Energy Society General Meeting - Conversion and Delivery of Electrical Energy in the 21st Century*, pp. 1–7, IEEE, July 2008.

[133] J. Slootweg and W. Kling, "Modelling and analysing impacts of wind power on transient stability of power systems," *Wind Engineering*, vol. 26, pp. 3–20, Jan. 2002.

[134] K. Elkington, V. Knazkins, and M. Ghandhari, "On the stability of power systems containing doubly fed induction generator-based generation," *Electric Power Systems Research*, vol. 78, pp. 1477–1484, Sept. 2008.

[135] M. Rahimi and M. Parniani, "Dynamic behavior analysis of doubly-fed induction generator wind turbines -the influence of rotor and speed controller parameters," *International Journal of Electrical Power & Energy Systems*, vol. 32, pp. 464–477, June 2010.

[136] F. M. Hughes, O. Anaya-Lara, N. Jenkins, and G. Strbac, "Control of DFIG-based wind generation for power network support," *IEEE Transactions on Power Systems*, vol. 20, pp. 1958– 1966, Nov. 2005.

[137] A. Luna, F. K. de Araujo Lima, D. Santos, P. Rodriguez, E. H. Watanabe, and S. Arnaltes, "Simplified modeling of a DFIG for transient studies in wind power applications," *IEEE Transactions on Industrial Electronics*, vol. 58, pp. 9–20, Jan. 2011.

[138] H. A. Pulgar-Painemal and P. W. Sauer, "Reduced-order model of Type-C wind turbine generators," *Electric Power Systems Research*, vol. 81, pp. 840–845, Apr. 2011.

[139] S. Foster, L. Xu, and B. Fox, "Coordinated reactive power control for facilitating fault ride through of doubly fed induction generator- and fixed speed induction generator-based wind farms," *IET Renewable Power Generation*, vol. 4, pp. 128–138, Mar. 2010.

[140] I. Erlich, J. Kretschmann, J. Fortmann, S. Mueller-Engelhardt, and H. Wrede, "Modeling of wind turbines based on Doubly-Fed induction generators for power system stability studies," *IEEE Transactions on Power Systems*, vol. 22, pp. 909–919, Aug. 2007.

[141] S. Engelhardt, J. Kretschmann, J. Fortmann, F. Shewarega, I. Erlich, and C. Feltes, "Negative sequence control of DFG based wind turbines," in *2011 IEEE Power and Energy Society General Meeting*, pp. 1–8, IEEE, July 2011.

[142] G. Monsees, *Discrete-Time Sliding Mode Control*. PhD thesis, Delft University of Technology, 2002.

[143] V. Utkin and A. Zinober, "Variable structure and lyapunov control," vol. 193 of *Lecture Notes in Control and Information Sciences*, pp. 87–107, Springer Berlin / Heidelberg, 1994.

[144] A. Isidori, *Nonlinear Control Systems*. Birkhäuser, Aug. 1995.

[145] P. Kachroo and K. Ozbay, "Sliding mode for user equilibrium dynamic traffic routing control," in *Intelligent Transportation System, 1997. ITSC '97., IEEE Conference on*, pp. 70 –75, Nov. 1997.

[146] Q. Khan, A. I. Bhatti, S. Iqbal, and M. Iqbal, "Dynamic integral sliding mode for MIMO uncertain nonlinear systems," *International Journal of Control, Automation and Systems*, vol. 9, pp. 151–160, Feb. 2011.

[147] M. Fliess, "Nonlinear control theory and differential algebra," in *Modelling and Adaptive Control* (C. Byrnes and A. Kurzhanski, eds.), vol. 105 of *Lecture Notes in Control and Information Sciences*, pp. 134–145, Springer Berlin / Heidelberg, 1988.

[148] X. Yan, C. Edwards, S. Spurgeon, and J. Bleijs, "Decentralised sliding-mode control for multimachine power systems using only output information," *Control Theory and Applications, IEE Proceedings* -, vol. 151, pp. 627 – 635, Sept. 2004.

[149] L. Jiang, Q. Wu, and J. Wen, "Decentralized nonlinear adaptive control for multimachine power systems via high-gain perturbation observer," *Circuits and Systems I: Regular Papers, IEEE Transactions on*, vol. 51, pp. 2052 – 2059, Oct. 2004.

[150] F. Pourboghrat, F. Farid, C. Hatziadoniu, M. Daneshdoost, F. Mehdian, and M. Lotfalian, "Local sliding control for damping

interarea power oscillations," *Power Systems, IEEE Transactions on*, vol. 19, pp. 1123 – 1134, May 2004.

[151] P. M. Anderson and A. A. Fouad, *Power System Control and Stability*. Wiley-IEEE Press, 2 ed., Oct. 2002.